ScuDo
Scuola di Dottorato ~ Doctoral School
WHAT YOU ARE, TAKES YOU FAR

Doctoral Dissertation
Doctoral Program in Chemical Engineering (30th Cycle)

DEVELOPMENT OF UV-BASED POLYMERIZATION TECHNIQUES FOR THE PRODUCTION OF DRUG DELIVERY DEVICES

Marco Bazzano
******

Supervisors:
Prof. R. Pisano, Supervisor
Prof. M. Sangermano, Co-Supervisor

Politecnico di Torino
2017

Declaration

I hereby declare that, the contents and organization of this dissertation constitute my own original work and does not compromise in any way the rights of third parties, including those relating to the security of personal data.

Marco Bazzano

2017

* This dissertation is presented in partial fulfillment of the requirements for **Ph.D. degree** in the Graduate School of Politecnico di Torino (ScuDo).

"A famous bon mot asserts that opinions are like arse-holes, in that everyone has one. There is great wisdom in this, but I would add that opinions differ significantly from arse-holes, in that yours should be constantly and thoroughly examined.

We must think critically, and not just about the ideas of others. Be hard on your beliefs. Take them out onto the veranda and beat them with a cricket bat. Be intellectually rigorous. Identify your biases, your prejudices, your privileges."

Tim Minchin

Acknowledgment

Ai miei supervisori Roberto e Marco, grazie per avermi dato questa possibilità di crescita.

Ai professori che mi hanno aiutato nel lavoro del dottorato: Giancarlo che mi ha ospitato a Parigi, Daniele che mi ha introdotto alla dinamica molecolare e a Michael che mi ha accolto a Karlsruhe (vielen dank!)

Ai compagni di questi tre anni, Irene e Tereza perché mi avete insegnato tutto agli inizi, Luigi col quale ho gioito, litigato e discusso a lungo e Nicolò che si è sempre dimostrato un saggio ed intelligente pagliaccio.

Ai nuovi arrivati nel girone, ad Andrea, Fiora e Luca che ho imparato a conoscere durante i patimenti del loro lavoro di tesi e che, nonostante tutto, hanno voluto continuare. Buona fortuna!

Alla mia hermana colombiana Cata, you've been here for 6 months but you brought us joy, laughs and some latin spice :) miss you!

Ai "miei" tesisti, Lucas, Tyani, Francesca, Donato, Kliton e Martina, poichè con il loro lavoro hanno avuto un ruolo fondamentale nel completamento di questa ricerca. Grazie mille!

Al compagno di mille corse Mirko, nonostante i tanti pacchi, se mi sono scaricato dalle noie del lavoro è stato anche grazie a te. Sempre cazzuto e cattivo!

Al giramondo Christophe-sama, maestro di nerdismo e discreto giocatore di basket con cui siamo sempre rimasti in contatto.

A Miriam, mi sei stata vicina in questi anni; grazie della tua presenza e pazienza nel farmi crescere e superare molti momenti bui.

A Gabriele, con cui ho condiviso tanti interessi, serate e birre in questi 13 anni di amicizia… da quando, al primo allenamento a basket mi hai guardato e detto: "e tu che ci

fai qui, formichina?" (lo so, è imbarazzante e senza senso… ma oramai ho smesso di cercare un senso in quello che dici).

Ad Andrea, 13 anni come sopra, premesse alquanto instabili e piene di richieste irragionevoli (comprati un orologio!). 2 Wacken, 3 Fosch, mille vacanze e tantissimi concerti… quasi metà vita a so(/u)pportarsi… ma poteva andare peggio!

Ai miei genitori, ovviamente (e biologicamente) non sarei qui se non fosse per voi. Maghi della sopportazione, nella mia mancanza di dialogo, e abili a far fruttare e aiutarmi nelle rare occasioni di apertura. Questa è per voi…

Abstract

Production of particles with dimension in the submicron scale underwent a significant increase in the last decades. The idea to exploit these devices to actively target a wide range of applications drove many important efforts in the development of such particles. In particular, the possibility to encapsulate and release active ingredients with desired rates, as well as to specifically target certain areas of the human body, is of huge importance in therapeutic treatments.

Among the broad spectrum of micro and submicron particles, polymeric particles represent an extremely versatile class of devices. Their high biocompatibility and possibility to swell or degrade to enhance release once in contact with body fluid are particularly interesting in drug administration.

This work was focused on the development of new techniques to produce structured polymeric particles in the micro and nano regions. Two rather different polymerization techniques were investigated and modified in order to pursue this goal: miniemulsion and aerosol polymerization. In both cases, polymerization triggering was achieved by UV light in presence of photo-initiator compounds and two reaction mechanisms were investigated: radical and cationic.

Miniemulsion polymerization was studied as a case study of a well-known technique for production of polymeric particles. One major modification was applied to the standard experimental setup: polymerization was confined at the interface between dispersed and continuous phase, thus producing capsules with a polymeric shell and a liquid core. The product was characterized and the impact of process conditions on size and morphology of capsules was evaluated. In particular, ultrasound exposure time was used to design capsules size. After optimization of process parameters, an active ingredient was encapsulated. Its controlled release was evaluated in case of different polymeric shells. Differences were observed using different degrees of crosslinking in the polymeric material, thus showing the possibility to design release rate by varying the ratio between monomer and crosslinker.

Aerosol polymerization was studied as a rather new technique for production of polymeric particles. It is a continuous process that does not require a liquid medium nor, usually, surfactants. For these reasons, it does not imply a cumbersome downstream work of purification. One major drawback of this technique is the challenging particles

structuring process. In our work, phase separation was induced within aerosol droplets to obtain structured particles. Mixtures of “good” and “bad” solvents were used to carefully design solubility of the monomer and its oligomers in the sprayed solution. Thus, it was possible to obtain different porous particles morphologies simply by varying the ratio between the two solvents. Capsules structures were obtained using different approaches in cationic and radical mechanism. Chain transfer mechanism was applied in cationic polymerization by adding an alcohol in the sprayed solution, while the addition of a soft-maker was crucial for the production of polymeric shells in radical polymerization. In both cases, the goal was to delay gelation of the polymeric structure, thus providing more time for the structuring process. Once the particles morphology was designed, an active ingredient was encapsulated within different types of particles and its release was monitored.

Molecular dynamic simulations were carried out to study the mechanisms that control the structuring process in aerosol cationic polymerization. Diffusion of the oligomer in the solvent mixture, as well as its interactions with the solvents, were calculated and the results confirmed the strong impact of solvent composition on the macromolecules transport parameters and, therefore, on their morphology.

Contents

Chapter 1

Introduction

Polymer technology has gone through a huge development in the last decades. An increased attention to new materials and to cheaper ways to obtain them is at the basis of this leap. Under this strain, different techniques to produce polymeric devices got through some big improvement in order to tackle both economic and environmental issues in the production of polymers (Ebewele, 2000). Each technique differentiate itself from others for peculiar characteristics and drawbacks and it is focused on the fabrication of materials for a specific application.

In this work, we present an extensive study on two polymerization techniques and the development of new features to improve their flexibility.

1.1 Nanotechnologies: the concept

The term technology derives from the ancient greek words *τέχνη*, tékhne, indicating "crafting skills" and *λογία,* loghìa, a suffix that indicates "study" and is, thus, commonly referred as the study or collection of skills or capabilities that can generate outputs (Crabb, 1823). Technology is strictly related to human activities, although it is not a privilege of human beings, and throughout history it has been developed by humans to high complexity degrees. The ambitious aim of this work is to go further on, to expand a little bit the range of technology by developing production techniques, which bring some new interesting features in their fields of application.

Human history is often divided using milestones such as giant technology leaps, i.e. Stone Age, Bronze Age, industrial revolution, etc. One of those latest leaps began in the XX century when the focus was shifted towards the development of technologies able to

operate in the micro and nano-scale. These technologies were called nanotechnologies and are capable to manipulate materials which have at least one dimension in the 1 to 100 nm scale.

The first seeds of this revolution are commonly attributed to one Richard Feynman's most famous lectures (Feynman, 1960). However, as some studies pointed out in the last years (Toumey, 2008), the impact of this lecture has been overestimated during the early 1990s thanks to citations of Feynman's speech in well-established books on nanotechnology (Drexler, 1986). Research on this subject was fueled by some crucial inventions such as the scanning tunneling microscope, in 1981, that enabled the visualization at the atomic scale. An important theoretical work on the purposes and applications of nanotechnology was carried on by Drexler in the middle 1980s (Drexler, 1986). In his books, Drexler theorized the development of tiny machines able to "build nanocircuits and nanomachines" (Drexler, 1986). In a subsequent book, he tackled some of the new challenges and issues introduced by the use of nanotechnology, such as the importance of molecular dynamics and molecular architecture (Drexler, 1992).

1.2 Nano and micro particles

With the terms "nanoparticle" (NP) or "microparticle" (MP) one usually refers to small objects with various shapes and characteristic dimension below 10^{-4} m. The International Union of Pure and Applied Chemistry (IUPAC) defines microparticles as "particles with dimensions between 1×10^{-7} and 1×10^{-4} m", while it defines nanoparticles as "particles with dimensions between 1×10^{-9} and 1×10^{-7} m" (Vert *et al.*, 2012). The common limit between the two ranges, 100 nm, is still a matter of debate. In fact, based on certain type of physical features, such as transparency, the limit is sometimes shifted towards 500 nm, see Figure 1.

Nano and microparticles can be divided, on the nature of their components, in organic and inorganic. Organic examples of NP and MP are liposomes, organic inclusion complexes or polymeric particles. On the other hand, NP and MP can be synthetized with different types of oxides materials (iron oxide, zinc oxide, etc…) or salts.

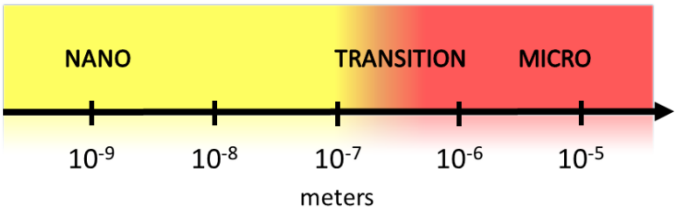

Figure 1. Schematics of the division between nano and micro-scale.

Particles in this length-scale are interesting in different applications for their characteristic features, such as high specific surface, high colloidal stability, possibility of functionalization and possibility to exploit peculiar physical phenomena, e.g. plasmonic effect. Their dimension and morphology can be also designed to allow an easy penetration of tissues or specific cell targeting.

1.3 Polymeric particles

A specific type of organic particles is represented by the class of polymeric particles. Polymers are a class of macromolecules characterized by the repetition of a relatively small building block throughout the entire molecule. Polymers are produced via a reaction, called polymerization, in which the reagent, called monomer, is used to build the macromolecule. Physical and chemical features of polymers are consequences of the monomer used and of the reaction type. In particular, polymers can be divided in two groups: thermoplastic and thermosetting (Ebewele, 2000).

Thermoplastic materials consist of macromolecules interacting with one another by simple electrostatic interactions. Thus, when the temperature rises and the mobility of the polymeric chains increases, melting of the material occurs. Polymeric chains can be linear or branched and this plays an important role in the properties of the material, since a linear polymer is able to arrange into crystals and to create interactions that result in higher mechanical properties. Interactions between chains can be also improved by the presence of dipoles inside the macromolecules, this is common in polymers with oxygen atoms. Another important feature, that has a strong impact on the properties of the materials, is the average degree of polymerization. It is defined as the average number of building blocks that constitute the macromolecule (Ebewele, 2000).

On the other hand, thermosetting materials consist of a polymeric crosslinked network. In this case, there are no distinct macromolecules but only one extensive three-dimensional matrix. Because of that, when the temperature is increased, the covalent

bonds hinder the melting of the material. Thus, it is not possible to reshape thermosetting polymer.

The same distinct behavior between thermoplastic and thermosetting materials can be seen in case of solvent addition. Good solvents can decrease the strength of electronic interactions between polymeric chains and solvate the thermoplastic materials while, in case of thermosetting network, a good solvent is only able to swell the matrix by filling the void volume inside the structure. Another important and tunable characteristic of polymer material is the chemical nature. Although usually the main component of the backbone is carbon, the presence of other elements such as oxygen, chlorine or fluorine is able to change dramatically the chemical behavior of the material in terms of solvent resistance, wettability, polarity and presence of surface charge (Ebewele, 2000).

Biocompatibility of the material is a further crucial issue in some types of applications. Some polymeric materials give the possibility to obtain particles that are both biocompatible and biodegradable. This can happen not only in polymeric-based particles but also in composites particles, where the polymer is added to mask the inorganic component and to avoid the immunogenic response (Gaucher *et al.*, 2009).

For all this reasons, polymeric materials drew the interest of many researchers in order to develop new processes and new materials for different purposes.

1.3.1 Applications

Polymeric particles in the nano and micro scale, as we previously discussed, are suitable for an extensive variety of applications because of their wide range of adjustable characteristics. The chemistry of polymers is in continuous development and it enables the production of materials with interesting properties. In the following section, we will briefly discuss some of the most important applications of these devices.

1.3.1.1 Therapeutic treatments

Application of polymeric nano and microparticles for medical treatment is crucial for the design of some medicine. The use of particles, in fact, enables the control of the release rate and enhances the solubility of many drugs (LaVan *et al.*, 2002).

In the last decades, there has been a strong interest in the development of drug releasing devices that are suitable for specific treatments (Sinha *et al.*, 2003). There are many characteristics that are needed for the design of such devices. The most important

are: average dimension, dimension polydispersity, biocompatibility and toxicity of the material, amount of drug loading within the particle and its release rate. Average dimension is crucial for the availability of particles inside human body, it defines which barriers particles are going to cross and which not (Lin *et al.*, 2005). Moreover, dimension affects the response of the immune system (Champion *et al.*, 2008). Opsonization is the process that enables the removal of foreign particles from blood stream and it is one of the main issues that hinder the feasibility of drug release from particles. This process involves the attachment of markers (e.g., opsonin) to the foreign particle or the pathogen, thus dramatically shortening the lifetime of particles in the human body by selecting the targets for phagocytosis (Owens *et al.*, 2006). Opsonization is dependent on the size of the particles, although the relationship between them is still under debate and it seems also to be linked with superficial properties of the particles. Polydispersity of population is an essential parameter in the application of polymeric particles to therapeutic treatments (Owens *et al.*, 2006). For the reasons that we previously discussed, it is crucial to know precisely the dimension of the particles that are inserted inside the human body to avoid side effects.

Biocompatibility of the material is a key issue in the development of new particles for therapeutic treatments. Several polymeric materials are characterized by the absence of immunogenic response when inserted in human body. However, opsonization can occur, reducing the effectiveness of the devices. There are some polymeric materials, which are capable of masking particles, such as polyethylene glycol (PEG), and prevent opsonization. Particles utilized in therapeutic treatments can be made of or covered with PEG in order to obtain a longer time for the drug release. To tackle this problem, PEG was widely used to mask inorganic particles for body imaging or treatments (Gaucher *et al.*, 2009; Owens *et al.*, 2006).

A further issue in pharmacological applications of polymeric particles is to promote the removal of particles when the treatment is completed. In some cases, for prolonged treatments, it is crucial to avoid the accumulation of foreign material inside human tissues. Biodegradable polymer where designed to solve this problem, such as poly-d,l-lactide-co-glycolide (PLGA), polylactic acid (PLA), chitosan and poly-ε-caprolactone (PCL) (Kumari *et al.*, 2010).

As to the drug loading and the release kinetics, polymeric material are quite versatile because of the different techniques that can be used to prepare particles and also because of the tunable chemical properties of the polymer which can be chosen similar to the drug.

1.3.1.2 Environmental treatments

Use of polymeric particles is also common in environmental treatments such as water treatments or intelligent nanopesticides release. In these fields of application, the key issue is the low, or preferably negligible, environmental impact of the polymers used. In water treatments, polymer based particles can be functionalized to entrap impurities or used to disperse inorganic nanoparticles able to convert toxic substances into safer ones. Thus, the effectiveness of the inorganic particles is increased, while the filtering process is simplified (Carpenter *et al.*, 2015).

In the agricultural sector, polymeric particles can be used to entrap pesticides or micronutrients on the surface of fields, thus increasing their effectiveness and avoiding problems related to the leaching caused by rain (Kumar *et al.*, 2014). Slowing down the release of pesticides over long time is able to prevent multiple administrations or overdose which might be dangerous for other species, e.g. pollinating insects or the crop itself (Liu *et al.*, 2008; dos Santos Silva *et al.*, 2011). Due to the impossibility to recover particles, polymer biodegradability is crucial in these applications (Liu *et al.*, 2016).

1.3.1.3 Textile industry

Textile application of polymeric particles is mainly focused on the coating of fabrics for antibacterial purposes. Different studies aimed at developing polymer based materials for the encapsulation of active compounds (Ye *et al.*, 2005; Ye *et al.*, 2006). In this field, the use of particles as storage or disperser of antibacterial compounds can be crucial for the long-term bacterial reduction activity of the fabrics. In particular, chitosan containing polymeric core-shell latexes are interesting for their ability to stick to the fabric and endure washing cycles without losing their activity. Moreover, no dramatic modifications are induced in the tensile strength nor in the air permeability of the fabrics (Ye *et al.*, 2006).

1.3.1.4 Catalyst

Polymeric particles can be used also to disperse catalytic materials enhancing, thus, their effectiveness. It is possible, in fact, to cover the surface of particles with inorganic catalyst as well as enzymatic ones (Jia *et al.*, 2003; Tamai *et al.*, 2009). Studies have shown high activities in reacting systems catalyzed using enzymes attached to nanoparticles compared with the ones of enzymes attached to thin films. Thus, they highlighted the importance of mobility of the catalytic system (Jia *et al.*, 2003). This

application of the particles is useful, in addition to the increased specific surface, also in the downstream filtration for the recovery of the catalytic material. In fact, in large-scale applications, purification is often a limiting factor of the process (Jia *et al.*, 2003). The main drawback of the use of polymeric material for catalyst dispersion is the maximum temperature that the polymer can withstand, which is usually in the 400-500 °C range (Mittal, 2005).

1.3.2 Synthesis techniques

Production of polymeric particles can be achieved by many different synthesis techniques, each of them developed, throughout the years, to tackle one or more specific issues in particles synthesis. Some of them are focused on the capability to tailor the dimension and morphology of particles with excellent precision. Others are meant to solve problems related to purification in the downstream processes, which can be a major problem if the application needs a highly purified material, e.g. medicine treatments.

In the following sections, we will briefly discuss the features of the most common available techniques to obtain polymeric particles. Pros and cons of each technique will be reported and discussed in order to identify unaddressed issues that are worth solving.

1.3.2.1 Emulsion

One of the most common technique to produce polymeric particles is the polymerization in emulsion. Emulsion polymerization is actually a wide class of techniques that exploit the presence of a continuous and a dispersed phase to produce material with controlled dimension and morphology (Landfester, 2001; Asua, 2002; Schork *et al.*, 2005). Emulsion is commonly defined as a dispersion of a liquid into another immiscible one (Schork *et al.*, 2005), see Figure 2. In such systems, one can identify a continuous and a dispersed phase.

Emulsions can be divided in two classes: oil-in-water and water-in-oil, based on whether a polar or a non-polar solvent constitutes the continuous phase. In this type of techniques, usually a surfactant is added to help stabilize the emulsion which is achieved by mechanical stirring or sonication (Asua, 2002). Both the type of surfactant and its amount are crucial for the dispersed phase droplet dimensions. Emulsion polymerization can be subdivided based on where the activation of the reacting species takes place (Schork *et al.*, 2005).

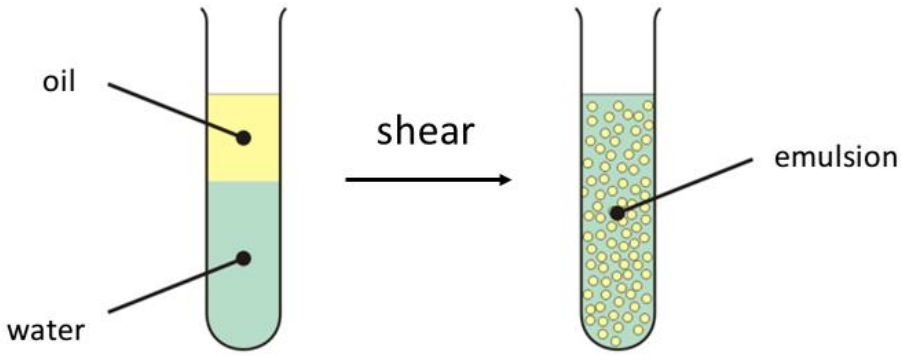

Figure 2. Schematics of an emulsion production.

A common division is the one between microemulsion and miniemulsion. In microemulsion, the concentration of surfactant is significantly above the critical micellar concentration (CMC) and, thus, the dispersed phase is confined within micelles or free droplets. In such conditions, the reaction starts preferably in the micelles volume, whereas the polymerization is usually controlled by the diffusion of monomer from the bigger droplets (reservoir) to the micelles. Micelles are thermodynamically stable and, thus, a slow polymerization step does not hinder the possibility to obtain a monodisperse production. The dimension of the product can be designed by choosing the type of surfactant that will lead to a certain micelles dimension (Schork *et al.*, 2005; Capek, 2001).

In miniemulsion, the surfactant concentration is below the CMC and, thus, the dispersed phase is in form of partially stabilized submicron droplets. High energy devices, such as ultrasound baths, are used to obtain the dispersion and, thus, dimension of droplets is comparable to the one of micelles. In such conditions, the reaction starts inside the droplets, which act as independent mini-reactors, without the need for external monomer feed (Schork *et al.*, 2005). However, the lack of thermodynamic stability results, in case of miniemulsion, in coalescence of the formed droplets over a long period. Thus, it is crucial to exploit a rapid polymerization mechanism in order to avoid the production of a polydispersed population with higher average size. Usually, the droplets dimension control is achieved by choosing a sonication time (Schork *et al.*, 2005). In fact, an increase in sonication results in lower dimensions of the droplets. Decrease in dimensions stops after a threshold value in sonication time, as explained in Figure 3.

Miniemulsion technique presents some advantages if compared with microemulsion. The presence of a lower concentration of surfactant is crucial to obtain a product, which is more pure, thus avoiding a troublesome purification. On the other hand, the less stabilized miniemulsion dispersion needs faster reaction rate in order to obtain a full conversion before coalescence. To solve this problem, UV light triggering of the

polymerization is frequently adopted for its ability to get a quick conversion (Chicoma *et al.*, 2013).

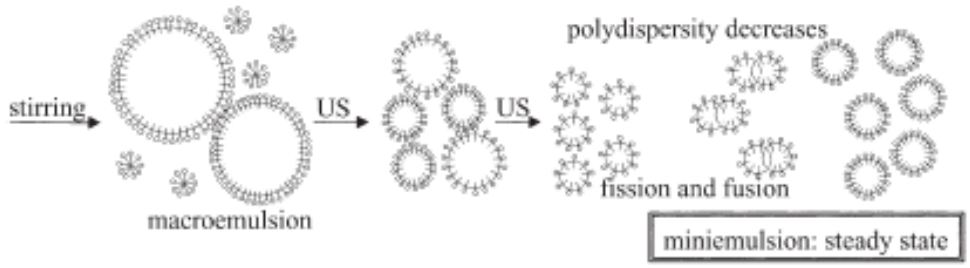

Figure 3. Schematic of droplets breakage by ultrasounds and achievement of the steady state in miniemulsion. Figure taken from Landfester (2003) with modifications.

In general, emulsion techniques have proven to be flexible ways to produce polymeric micro and nano particles. By designing the correct formulation for both the continuous and dispersed phase, it is possible to obtain particles with interesting features, such as porosity, core-shell structure or surface functionalization. The main drawbacks of these techniques are represented by the need for surfactants and for a liquid medium, a dispersant that implies some purification issues. The batch nature of this technique can also be a limiting factor for process scalability.

1.3.2.2 Spray-drying

Spray-drying is a continuous technique that consists of a solution atomization in an environment where the solvent is removed by quick evaporation (Eerikäinen & Kauppinen, 2003; Sastre *et al.*, 2007; Raula *et al.*, 2004). The solution is usually composed by a preformed polymer solubilized in an appropriate solvent. Removal of the solvent, or mixture of solvents, results in the precipitation of the polymeric material and, thus, in the production of particles. This technique has been widely used for the production of drug delivery devices (Sastre *et al.*, 2007). In this type of application, two crucial issues are the interactions between the active ingredient and the solvent and the effect of high temperature that is required to induce a rapid solvent evaporation. Morphology can be adjusted varying the rate of evaporation of the solvent. Some studies showed the feasibility of the production of core-shell structures by quick removal of the solvent (Raula *et al.*, 2004). It results in the precipitation of a polymeric layer at the droplets surface, thus producing particles with a thin solid shell and hollow core, see Figure 4-b.

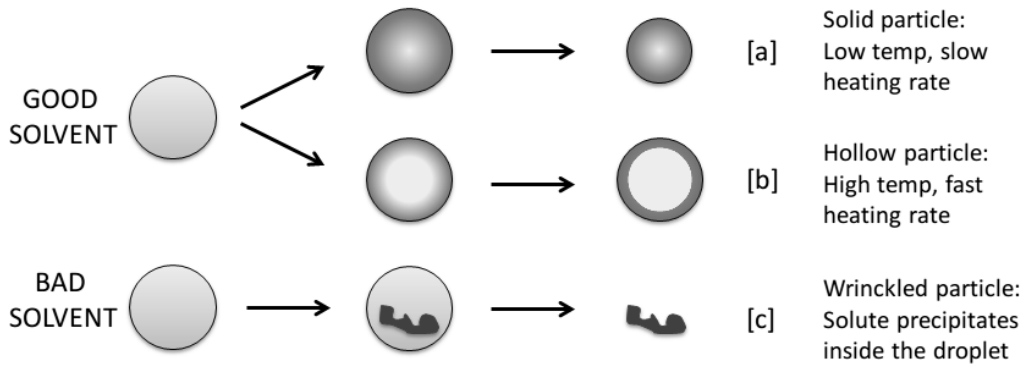

Figure 4. Schematics of spray-drying process. Figure taken from Eerikäinen & Kauppinen (2003) with modifications.

1.3.2.3 Aerosol

Aerosol synthesis of polymeric particles consists of a continuous process that can be divided into two steps: atomization of a monomer solution and reaction triggering inside each solution droplet (Akgün *et al.*, 2013), see Figure 5. This technique differs from spray-drying because of the presence of reaction, which is achieved usually by UV light exposure. UV light triggering of the polymerization is preferred to thermal triggering for its rapid curing. Indeed, residence time in the aerosol reactor is low, usually less than 60 s, and a rapid curing is crucial for the production of individual particles (Akgün *et al.*, 2013).

This aerosol process proved feasible in both radical and cationic polymerization. Moreover, it is also possible to incorporate inorganic materials within the polymeric matrix by simple dispersion of these in the sprayed solution (Akgün *et al.*, 2014a; Akgün *et al.*, 2015). Finally, production of porous particles can be obtained by an accurate design of the sprayed formulation (Akgün *et al.*, 2014b).

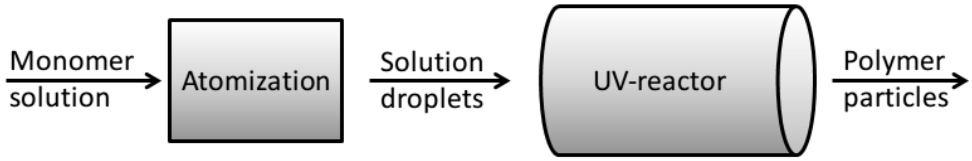

Figure 5. Schematics of an aerosol photo-induced polymerization process.

Different types of atomization systems can be used to achieve a monodisperse aerosol dimension; the most common are pneumatic, ultrasonic and electrospray atomizers, since they are able to produce rather monodisperse population with average size below 10 µm. Another important feature of atomizers is the rate of aerosol production, which is crucial for the process scale-up (Biskos et al, 2008).

1.3.2.4 Microfluidics

The use of microfluidics in polymeric particles synthesis has been widely studied in the last two decades. This techniques is mainly used to produce highly monodisperse droplets of polymerizable compounds exploiting channels junctions with different geometries (Dendukuri *et al.*, 2009). Dispersion is then polymerized during the passage in a coil, usually by UV light triggering of the reaction. Similarly as the emulsion technique, microfluidics uses two non-miscible streams that are referred as continuous and dispersed phase (Dendukuri *et al.*, 2009). These two streams are fed into a junction that creates the dispersion. There are three main different junction types: T-junction, flow-focusing and co-flow (Figure 6) (Zhao *et al.*, 2013). Many studies are present on the use of different types of junctions specific for each process. By designing the geometry of the junction, in fact, it is possible to control accurately the fluid dynamics and thus the features of the droplets. For example, Y-shaped junction with a double feed for the dispersed phase were proposed to achieve the production of janus particles, namely non-symmetric particles (Dendukuri *et al.*, 2009). Many studies have been carried out on the fluid dynamics within the microchannels using computational fluid dynamic (CFD) (Kobayashi *et al.*, 2011).

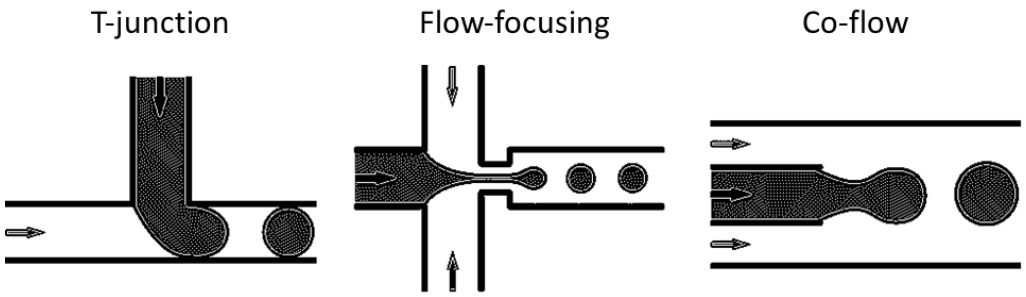

Figure 6. Schematics of the three main types of microfluidics junctions.

Droplets dimension is mainly dependent on the fluid dynamic regime in the microfluidic device. Possible regimes are divided into dripping, jetting and squeezing. Varying two fluid dynamic parameters, such as capillary number (*Ca*) and flow ratio, it is

possible to change the regime and, thus, change the dispersion size (Dendukuri *et al.*, 2005).

In polymeric particles production, microfluidics presents two crucial advantages if compared to other techniques: it is a continuous process and it enables the production of highly monodisperse particles population. On the other hand, the main drawbacks are the low production rates, the presence of a liquid medium in which the product is dispersed, the need for surfactants and the relatively high dimensions which rarely can go below 400 nm (Dendukuri *et al.*, 2009).

1.3.2.5 Photo-lithography

Photo-lithography is one of the most flexible technique to design polymeric particles. It takes advantage of masking devices to delimit UV light irradiation, and thus the reaction triggering, within a small volume (Levenson *et al.*, 1982), see Figure 7.

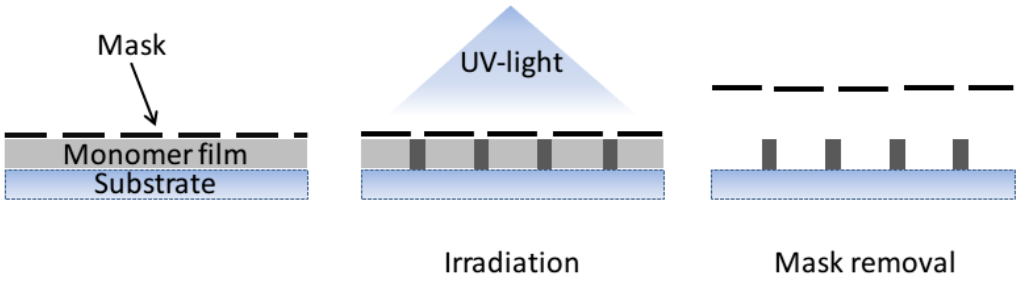

Figure 7. Schematics of photo-lithography method.

With this technique, it is possible to design particles with different geometries, as well as growing polymeric material on well-defined surface portions (Prucker *et al.*, 1998). The shape of the mask is one of the most important parameter and it can be a limiting factor since it must be prepared with extreme precision (Levenson *et al.*, 1982). Thus, developing of masks is crucial for the flexibility of the technique and masks can be expensive. Another drawback of the technique is its inherent batch nature that hinders the production of high amount of polymeric material. To solve this problem, continuous flow lithography has been developed in order to get a non-stop production of particles (Dendukuri *et al.*, 2009).

Another limiting factor of the lithography method is the fact that the particles have a 2D extruded shape. To tackle this issue, interference lithography is used. Phase masks are used to induce phase differences that creates non-curing volumes and, thus, an actual 3D structuring of the particle (Dendukuri *et al.*, 2009).

1.4 Polymeric particles via miniemulsion or aerosol

In these studies, the attention was focused on two polymerization techniques: miniemulsion and aerosol polymerization. These are examples of a batch and a continuous process and are interesting for different reasons.

Miniemulsion is a well-known technique that falls into the broad category of emulsion polymerizations. It is characterized by a low concentration of surfactants in order to be more eco-friendly and for this reason it has some issues related to the stability the emulsion (Schork *et al.*, 2005). Our aim is to develop a modified version of the technique in order to get an easier control over the morphology of the produced particles. On the other hand, aerosol polymerization is a technique relatively new that has some promising features such as being a continuous process, avoiding the use of surfactant and avoiding the use of a liquid medium (Akgün *et al.*, 2013). For all these reasons, it is an interesting and eco-friendly process that is worth developing in order to obtain a structured product with different morphologies.

In both cases, the reaction triggering is achieved by UV light exposure and, in the following paragraphs, we will discuss the reasons behind this choice, evaluating pros and cons of the different triggering options.

1.4.1 Photo-induced polymerization

Polymerization triggering is a key issue in the design of a polymerization process. In certain conditions, molecules of monomer become reactive and are able to polymerize. However, it is more frequent that a further compound is added inside the reacting volume to gain a better control over the reaction and to simplify the triggering (Ebewele, 2000). This molecule is able to decompose and form a reactive specie, see Figure 8. Usually, two techniques, based on the type of initiator, can be used to start a polymerization reaction: thermal triggering or UV triggering. Both ways lead to the formation of a reactive specie that interacts with the monomer causing the polymerization to start (Ebewele, 2000; Fouassier, 2012).

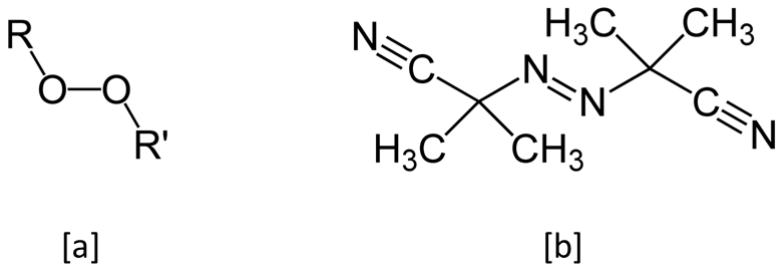

[a] [b]

Figure 8. Examples of commonly used initiators: (a) peroxides and (b) azobisisobutyronitrile (AIBN).

Thermal triggering is achieved applying high temperatures to the reacting volume. This additional energy leads to the decomposition of the initiator that results in a radical or ionic compound that enables the activation of the monomer by interacting with the functionality of that molecule. One advantage of the thermal triggering is the fact that the mixture of monomer and initiator are inert at room temperature and thus can be stored and manipulated without risks. Moreover, when the temperature in increased to start the reaction, viscosity initially decreases and is easier to handle the formulation (Ebewele, 2000). One of the major drawbacks of this technique is its slowness; characteristic times of a complete thermal curing are in the range of hours. Moreover, if the polymer is filled with a thermo-sensitive material, the use of high temperature for a long period can damage the filler, causing its decomposition or deactivation. This is particularly true when the polymerization is highly exothermic and the heat produced results in a further increase in temperature inside the reacting volume (Ebewele, 2000).

Photo triggering, on the other hand, exploits the ability of some compounds, hereafter referred as photo-initiators, to decompose in presence of a specific radiation source. The most common radiation is UV light, as it is easy to produce and relatively safe if compared with other high energetic types of irradiation. Photo-initiators have two main tasks: to absorb energy through UV light at a precise wavelength and to decompose into reacting species able to attack the monomer functionality. To fulfill those requirements, photo-initiators frequently present a segment, most of the time an aromatic ring, able to absorb UV light and a bond able to break via homolysis or heterolysis (Fouassier, 2012). This technique presents many advantages if compared with the previous one: it requires lower energy, it is possible to limit the irradiation within a small volume, it avoids the need for high temperatures, which might damage thermally sensitive chemicals, it has characteristic curing times in the range of seconds or minutes. Efforts have been devoted to the development of eco-friendlier systems. Sunlight triggering is the final goal, although a limited number of sun-triggered systems have been studied. Less energetic emitting sources, such as light emitting diodes (LEDs), are also under study for their ability to initiate the reaction (Fouassier, 2012).

On the other hand, photo-induced polymerization has some drawbacks that must be taken into account when designing a polymerization process. Formulations can sometimes be triggered simply by exposure to sunlight since a fraction of that radiation falls into the UV spectrum. Thus, it is crucial to shade the monomer solution until production step. Moreover, UV light can create some issues to chemicals present in the formulation, so it is fundamental to keep in mind the possibility to get decomposition or deactivation due to UV exposure. Another key issue is the possibility, for example in thick samples, to incur in non-homogeneous UV irradiation. Since photo-initiators are designed to absorb UV light with high yields, in case of high concentration of these compounds after few micrometers within the reacting volume the radiation is almost completely absorbed. This phenomenon leads to the presence of the so-called frontal polymerization, a process in which the reaction is not triggered at the same time throughout the whole formulation volume but it propagates with a reaction front (Fouassier, 2012).

1.4.1.1 Different types of mechanism

Photo-induced polymerization can occur via three different mechanisms: radical, cationic and anionic. The type of mechanism is linked with the photo-initiator that is added to the formulation. If the compound dissociates in a homolytic way, two radicals are generated and a propagation of a radical growing polymer will start. If, alternatively, the compound dissociates in a heterolytic way, such as salts do, it will result in a cationic or anionic triggering of the polymerization and in the propagation of a charged polymer. Both ionic and non-ionic mechanisms have some peculiarities that make them attractive in certain applications. In the following lines, we will briefly discuss about the features of these mechanisms and how they can be exploited to produce polymeric material (Fouassier, 2012).

Radical photo-induced polymerization is characterized by the non-ionic nature of the reacting species. Thus, it does not interact with polar solvents but it can be hindered by the presence of radical subtracting substances. In fact, molecular oxygen is able to inhibit the radical polymerization, which is usually conducted under nitrogen gas atmosphere. Radical photo-initiators are generally organic molecules characterized by the presence of aryl groups and heteroatoms like oxygen or phosphorus, see Figure 9. This reaction pathway is characterized by a quick curing and by the need for continuous irradiation throughout the curing time since radicals have short lifetime and must be continuously generated to achieve a complete conversion (Allen, 1996).

Ionic photo-induced polymerization can be divided based on the nature of the charge of the propagating specie. Throughout the years, both anionic and cationic pathways were studied, with particular focus on the photo-initiators nature. However, the majority of the

industrial applications that exploits a ionic mechanism are focused on the cationic pathway (Fouassier, 2012). Because of the covalent nature and low polarity of the bonds in monomers, it is not easy to charge these compounds and special photo-initiators must be applied. The most common photo-initiators for cationic triggering are diazonium salts, onium salts and organometallic complexes (Fouassier, 2012; Crivello, 1984).

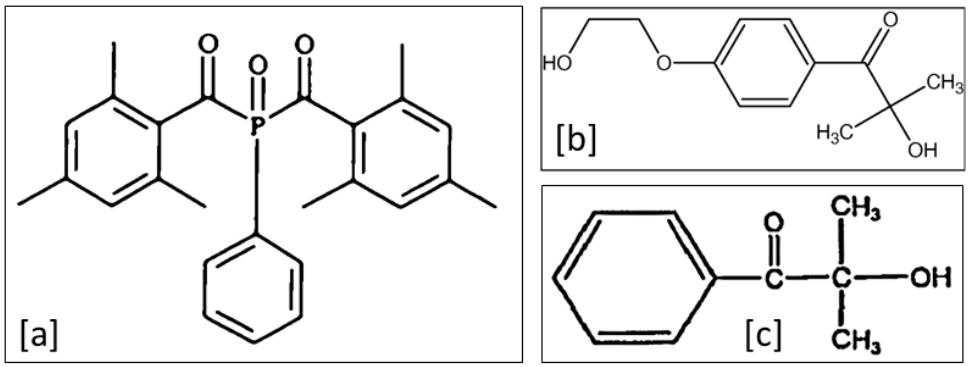

Figure 9. Examples of radical photo-initiators, (a) Irgacure 819, (b) Irgacure 2959 and (c) Darocur 1173.

We will focus our attention on the second class, which can be further divided into iodonium and sulfonium salts, see Figure 10, both characterized by the ability to form a super acid upon UV irradiation.

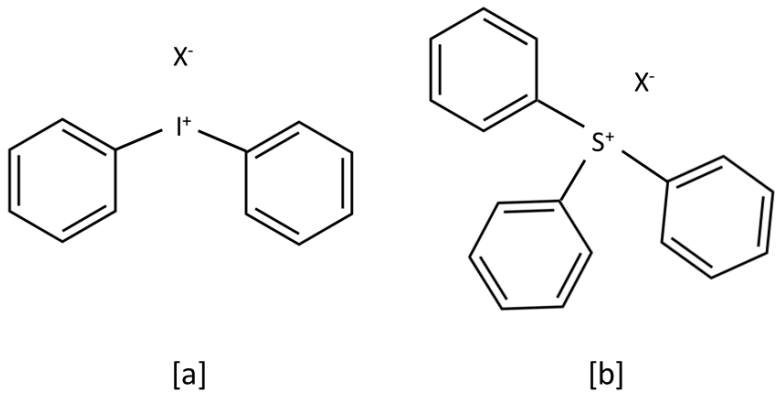

Figure 10. Molecular structure of (a) iodonium and (b) sulfonium salts.

These Lewis acids are able to attack the functionalities of the monomer creating a carbocation on the monomer and, therefore, a reactive specie. Onium photo-initiators consist of a positively charged atom (I^+ or S^+) surrounded by aryl groups and a

nucleophile counter ion (X^- in Figure 10) (Fouassier, 2012). The nature of the counter ion is crucial for the reactivity of the photo-initiator that decreases following the order:

$$SbF_6^- >> AsF_6^- > PF_6^- >> BF_4^-$$

Antimonium based salts are the ones that give the stronger acid and, thus, quicker triggering of the polymerization. Cationic polymerization, due to the lack of radicals, is not affected by the presence of molecular oxygen or other radical impurities. On the other hand, the presence of ions in the chemical mechanism leads to interaction of the reaction with proton acceptor substances. In particular, the presence of bases, water and alcohols have an effect on the reaction and are worth mentioning. Water and alcohols have been studied for their ability to promote the conversion of some epoxy resins (Sangermano, 2012). This can be explained by a mechanism in which the proton acceptor transfers the positive charge from a propagating chain to another one. Thus, the presence of low amount of these compounds increases the velocity of the reaction, whereas experimental evidence showed that at higher concentration the effect is opposite (Fouassier, 2012).

Another characteristic of the cationic mechanism is the possibility to have a living chain polymerization, namely a propagation step that does not stop when UV irradiation ends. This is due to the fact that, compared to the radical mechanism, the carbocations have longer lifetime and are able to sustain the propagation step (Fouassier, 2012).

1.4.1.2 The reasons behind our choice

After this brief introduction to the features of photo polymerization, let us discuss why we chose photo triggering over thermal triggering. As we already stated, thermal triggering is a slow process that requires high amounts of energy. On the other hand, photo triggering is almost instantaneous and not so energy demanding. These consideration, all alone should be already a good explanation, but if we apply them to the features of the two polymerization techniques, the choice is straightforward.

In miniemulsion polymerization, one of the main issues is the lack of stability of the emulsion after its creation. Since coalescence of the emulsion may start in few minutes, it is crucial to obtain the polymeric material in the quickest possible way. Photo triggering, although in the liquid medium scattering and absorption phenomena occur, can ensure a polymerization in few minutes and thus is preferable to a thermal triggering. Moreover, in order to heat the whole emulsion volume, high amounts of energy would be wasted to heat the liquid medium, which is inert. Besides, an increase in temperature might be able to change the equilibrium of the two-phase system. For all these reasons, photo triggering is preferable to the thermal one. As to the reaction mechanism, emulsion techniques have some problems related to the need for polar solvents, which can interact with the cationic reaction. Thus, we focused our attention on the radical mechanism, whereas feasibility

tests were conducted on the cationic system before carrying out a complete study of the reaction and production process.

There again, aerosol polymerization presents somehow similar issues. Reaction rate is still a key to the success of the process, due to the very low residence times in the reactor, and photo-induced polymerization is the only way to obtain cured material at the reactor outlet. Moreover, heat transfer in the aerosol system is not easy to design. The gaseous medium can be pre-heated but then reaction could start before the reactor and obstruct the atomization nozzle. Furthermore, in the rarefied aerosol stream, absorption and scattering phenomena, which might hinder the yield of the UV radiation, are less problematic than in the emulsion environment. As to the reaction mechanism, in this case the choice between cationic and radical is free from relevant technological issues. Using nitrogen as gas carrier it is possible to avoid oxygen inhibition of the radical mechanism, while the absence of water or polar solvents, unless in cases in which they are specifically requested, ensure the feasibility of the cationic photo polymerization. Additionally, the cationic mechanism has another advantage compared to the radical one, due to its living character it can be carried out also after the reactor passage and thus it can be used, with some restrictions, in high flow conditions. For these reasons, the cationic mechanism will be favored over the radical one in the aerosol process. However, a study on radical mechanism in aerosol polymerization will follow the cationic one, as comparison between the two polymerization types.

1.5 Aim of the study

In this work, we aim at developing pre-existing polymerization techniques in order to easily produce structured micro and nano-particles and gain a better control over their morphology. The selected application of these polymeric devices is drug release and, thus, design of dimension, morphology and chemical structure is crucial. Capsules structure will be favored over the porous one, for its ability to store an active compound within its core. For this purpose, we will select two polymerization processes and modify them accordingly.

Poly ethylene glycol based monomers will be investigated in order to produce devices able to avoid opsonization (Owens *et al.*, 2006). In miniemulsion, fast reacting monomers, such as acrylic and methacrylic compounds, will be used with the radical mechanism, see Figure 11, while divinyl ethers will be used in the cationic one, see Figure 12.

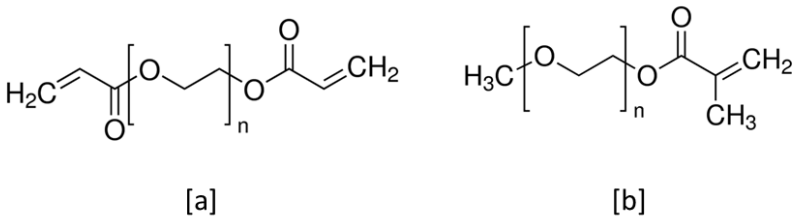

Figure 11. Molecular structure of (a) poly(ethylene glycol) diacrylate and (b) poly(ethylene glycol) methyl methacrylate.

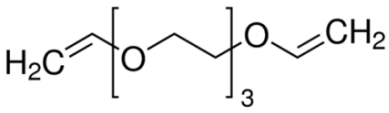

Figure 12. Molecular structure of divinyl ether tri(ethylene glycol).

In cationic aerosol polymerization, on the other hand, we will use divinyl ethers, in some experiments coupled with vinyl ethers, dissolved in a mixture of solvents, see Figure 13.

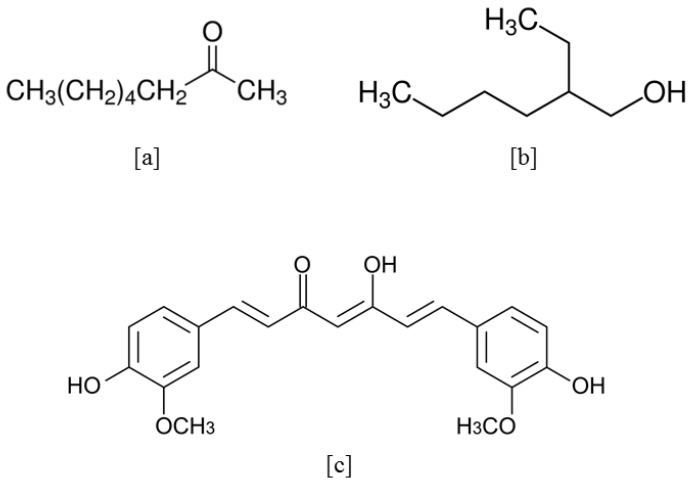

Figure 13. Molecular structure of (a) 2-octanone, (b) 2-ethylhexanol and (c) curcumin.

As a model drug, curcumin will be selected, see Figure 13c. Curcumin is an antioxidant and anti-inflammatory compound, which is extracted from turmeric. It is gaining interest in drug delivery research because of various issues related to its low water solubility and, therefore, to its low bioavailability (Tønnesen, 1992). Our aim is to produce devices which can entrap curcumin and release it in a controlled way, thus avoiding the immune response of the human body, that would quickly remove solid curcumin, and enhancing its bioavailability.

1.5.1 Polymeric particles with tunable dimension and morphology

Tunable particles dimension is a key issue in polymeric particles production, especially in case of medical applications. In both miniemulsion and aerosol technique we will tackle this problem adjusting some of the processes parameters. In miniemulsion, we will discuss the effect of different parameters, such as time of sonication, time of UV irradiation and surfactant concentration, on particles dimension and polydispersity. In aerosol polymerization, on the other hand, we will study the effect of nitrogen pressure and formulation composition on morphology, dimension and polydispersity of the product. In both cases, process parameters will be optimized in order to obtain monodisperse samples.

Structure of the particles, e.g. porosity or core-shell structure, is another crucial topic in the production of drug releasing devices. In fact, it changes both the loading and releasing characteristics of the polymeric particles. Tunable morphology is, thus, a goal in the development of the two techniques. In miniemulsion, it will be taken on by limiting the reaction within a specific volume, whereas in aerosol polymerization a phase separation will be induced to obtain a nanostructure within particles.

1.5.2 Tunable release characteristics

Among the different parameters that have an impact on the release characteristics of polymeric devices, we can find the molecular structure of the thermosetting polymeric network. This feature is critical for the diffusion of compounds through the matrix since it defines the mobility of the chains and the possibility of swelling in presence of solvents.

In miniemulsion, studies will be focused on the differences in behavior between a polymer obtained from a bi-functional monomer and one obtained from a mono-functional one, namely between a thermosetting and a thermoplastic material. A mixture of the two monomer will be also investigated and its effects on the release evaluated.

Similarly, in the case of aerosol polymerization a study on the effect of the network structure will be carried out with the addition of a solvent to the initial monomer formulation. This solvent is able to interact with the reaction mechanism and modify the final structure, lowering the gel content. Moreover, the network structure will be studied by co-polymerizing two monomers using different ratios.

Chapter 2

Particles characterization

In the following paragraphs, all characterization techniques that were used will be described. The procedures will be defined in general and, then, the differences for each type of sample will be highlighted.

2.1 Dimension and morphology

Particles size was evaluated using three different analyses: dynamic light scattering (DLS), field emission scanning electron microscopy (FESEM) and transmission electron microscopy (TEM). These analyses are different in both samples preparation and type of results.

DLS was performed using a Zetasizer Nano ZS90 (Malvern Instruments, Worcestershire, UK). Temperature of analyses was 25 °C. Suspensions from emulsion were diluted accordingly to the optimum particles count of the instrument. Usually, the applied dilution was 1 to 10 and the analyzed volume was 1 mL. Only samples from miniemulsion were analyzed with this technique, due to the larger dimensions of the aerosol particles. In fact, it is not possible to use DLS to obtain accurate sizing of particles larger than few hundreds nanometers.

FESEM analyses were performed using two different instruments: a Zeiss Supra 40 (Carl Zeiss NTS, Oberkochen, Germany) and a Leo Gemini 1530 (Carl Zeiss NTS, Oberkochen, Germany). Samples from miniemulsion and from aerosol polymerization were prepared in different way. Miniemulsion samples were freeze-dried to avoid agglomeration of particles during the drying step. Mannitol was added (2% w/w) to the aqueous suspension as bulking agent to avoid collapse of the lyophilized product. No cryoprotectants were added. The freezing step was conducted with a ramp from ambient temperature to -50 °C in 1.5 h. Temperature was held at -50 °C for 2 h and then primary drying was conducted for 20 h at -10 °C and 10 Pa. Secondary drying was carried out to remove bound water in three steps: 2 h at 5 °C and 10 Pa, 0.5 h at 15 °C and 10 Pa and, as a final step, 25 °C overnight. Lyophilized samples were then loaded on the sample holder and directly analyzed without metallization.

Aerosol samples were collected in dry powder form and, thus, freeze-drying was not necessary. Small amounts of polymeric powder (~2 mg) were dispersed in ultrapure water by intense mechanical stirring and by ultrasounds, if necessary, to break the macroscopic agglomerates. Few microliters of suspension were dropped on a membrane (Whatman, Nucleopore Track-Etch Membrane, 200 nm pore width) or a silicium wafer, then dried and coated. Platinum or a mixture of platinum and palladium was used to coat the samples.

TEM analyses were performed using a JEM-2010F (JEOL, Tokyo, Japan). Samples suspension were dropped on a microscopy grid (carbon film on HF15 Cu grid, Agar Scientific, Stansted, UK) and let dry for few minutes. Chamber vacuum during the analyses was approximately $3*10^{-5}$ Pa and voltage 200 keV. TEM micrographs were acquired by a slow scan CCD camera (Orius Camera, Gatan, Pleasanton, CA, USA). Miniemulsion samples were directly deposited on the microscopy grid, whereas samples from aerosol were dispersed in ultrapure water, with a procedure similar to the one used for the FESEM analyses.

2.2 Zeta-potential evaluation

Particles suspensions were analyzed to evaluate their stability. In order to access this feature, zeta-potential measurement were conducted. Zeta-potential is, in fact, a measure of the electrostatic repulsive strength between particles. High values of zeta-potential usually lead to high suspension stability. The instrument used was a Zetasizer Nano ZS90 (Malvern Instrument, Worcestershire, UK). The particles suspension was diluted to get a proper particle count during the analysis and then transferred into a capillary cuvette (DTS1070, Malvern Instrument). Three measurements for each samples were conducted.

Dried samples were dispersed in ultrapure water by intense mechanical stirring. After a proper dilution, the analyses were performed with the same experimental setup.

2.3 Thermal behavior

Thermal behavior of product was evaluated using differential scanning calorimetry (DSC). The instrument used was a Q200 DSC (TA Instrument, New Castle, USA). The analyses were conducted in a temperature range within -80 °C to 250 °C, using a ramp of 5 °C/min. This type of analysis was applied for the detection of unreacted monomer as well as for detection of T_g shifts from the usual values. In fact, these shifts might suggest changes in the polymerization outcome due to the peculiar environment in which it was performed.

2.4 Process conversion

Fourier transform infrared spectroscopy (FT-IR) was adopted to study monomer conversion. Two different instruments were used to study this aspect: a Nicolet 5700 (Thermo Scientific, Waltham, USA) and an Equinox 55 (Bruker Optics, Billerica, USA). In both cases, for each sample multiple spectrum were acquired from 500 to 4000 cm^{-1}. The absence of carbon-carbon double bond (C=C, at ~1640 cm^{-1}) was used as a proof of the complete conversion. Reference peaks were chosen in each system depending upon the chemicals that were present and did not participate to the reaction. Examples of reference peaks are: C=O stretching at ~1740 cm^{-1} and ether groups stretching at ~1100 cm^{-1}.

Samples produced with aerosol technique were analyzed in attenuated total reflectance mode (FT-IR/ATR) using the Equinox 55. Both the starting monomer solution and the final product were analyzed in order to evaluate the conversion during reactor passage.

2.5 Active ingredient controlled release

Release of encapsulated active ingredient was followed by UV-visible spectroscopy. Samples of 3 mL volume were prepared and analyzed using a Jenway 6850 (Bibby Scientific, Stone, UK). Depending upon the active ingredient, the scanned wavelength range was within 200 to 500 nm with a step of 1 nm. A calibration curve was used to correlate the absorbance with the active ingredient concentration. The evolution of released active ingredient was followed using the Weibull equation, see Eq. 1 (Morales *et al.*, 2004). This empiric model, even if it lacks physical meaning, has been extensively used to fit data from release of encapsulated compounds:

$$\varphi = 1 - e^{-kt^{\theta}} \quad \text{(Eq.1)}$$

where φ is the released fraction, t is the release time, k and θ are release parameters. In particular, some studies have been carried out in order to find a physical meaning for the θ parameter, often correlated to the release mechanism (Papadopoulou *et al.*, 2006). However, in this study, k and θ will be used solely as fitting parameters. The choice is due to the complexity of the system, which is not only non-homogeneous, but it is also characterized by different particles geometries.

Release experiments were performed using dialysis tubing to confine a concentrated suspension of nanoparticles loaded with curcumin. Dialysis membrane was made of cellulose with a molecular cut-off of 14000 daltons. The sealed membrane, containing 12 mL of suspension, was immersed in phosphate buffer saline (PBS), pH 7.4, which was gently mechanically stirred, see Figure 14. Release sampling was achieved withdrawing 3 mL of the external buffer solution and analyzing it by UV-vis spectrophotometer. Absorbance of the solution was evaluated at wavelength of 420-430 nm.

Figure 14. Schematic of the dialysis experimental setup.

PART I

MINIEMULSION INTERFACIAL PHOTO-INDUCED POLYMERIZATION

Chapter 3

Photo-induced interfacial polymerization in miniemulsion

In the first part of our study, the attention was focused on the development of a single step polymerization to produce nanocapsules for drug delivery. The starting technique was a miniemulsion polymerization of oil in water. Some modifications were applied to the standard method in order to easily design a hollow structure. Once the feasibility of the new method was confirmed, studies on the effects of the different process parameters were conducted. Moreover, the effects of the type of monomer were studied using both mono-functional and bi-functional ones.

Encapsulation of an active ingredient was then achieved by simple solvation of the molecule in the solvent of the dispersed phase. Release tests were conducted to access the different release rates of the materials.

In the following sections, the state of the art of the emulsion techniques will be discussed; attention will be then given to the new ideas and developments achieved.

3.1 Overview on the emulsion polymerization techniques

Emulsion polymerization is a well-established technique since the first works on this topic were published around 1940-50 (Hauser *et al.*, 1948, Reynolds, 1949). As shown in Figure 15, number of publications on emulsion polymerization exponentially increased over the last 50 years. One of the first thoroughly studied polymerizing system was styrene. In these preliminary studies, emulsions of monomer in water was achieved by mechanical stirring and subsequently polymerized by thermal triggering. At this stage, attention was focused on the interfacial phenomena that control this system with high specific surface (Hauser *et al.*, 1948).

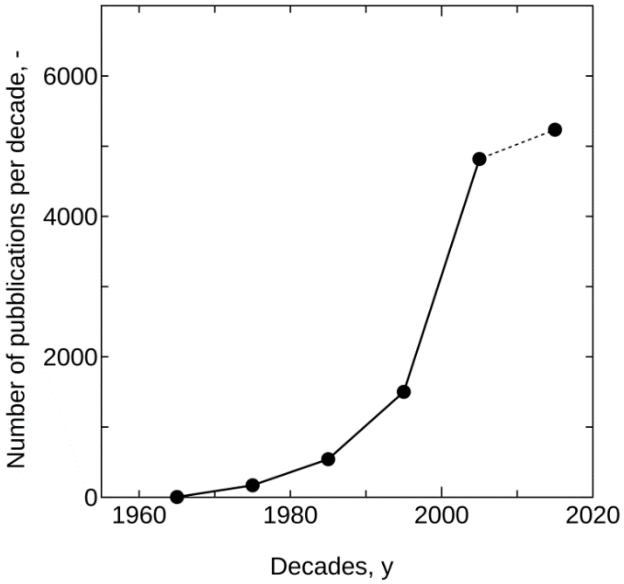

Figure 15. Trend in publications with keyword "emulsion polymerization" throughout the last 50 years. The decade 2010-2019 is obviously not complete. Source: www.scopus.com.

Throughout the years, focus shifted towards different polymerizing systems. Methyl methacrylate was successfully polymerized in water-in-oil emulsion exploiting its non-miscibility with water (Tsunooka *et al.*, 1978). The attention was, then, gradually drawn by the problem of particles nucleation in the emulsion: what are the preferred loci and how is it possible to control them? Thus, were introduced other polymerization methods developed from the initial standard emulsion: microemulsion and miniemulsion, that we described earlier (Schork *et al.*, 2005). Furthermore, in order to solve some issues of the thermal triggering, photo triggering in emulsion was proposed.

3.1.1 Photo-induced polymerization in emulsion techniques

The use of photons to trigger polymerization in emulsion had the task to overcome some of the major problems related to thermal triggering. First works and patents on this topic were published in the ’50 (Steven *et al.*, 1962; Jhon *et al.*, 1952). Ethylenic compounds were polymerized in presence of a catalyst, both suspended in emulsion (Jhon *et al.*, 1951). Emulsion photo-polymerization was applied also to nanocomposites production. In fact, it is possible to confine inorganic material within the dispersed phase, which will be polymerized. Moreover, the light absorption abilities of some inorganic materials can be exploited in the process (Luan *et al.*, 2012). Coupling of polymerization in emulsion and photo triggering went through a robust increase in the last 30 years, see Figure 16.

Photo-induced polymerization is characterized by high reaction rates that enables a rapid conversion and it is, thus, attractive from an industrial point of view. It avoids problems related to long-term stability of the emulsion; therefore, stabilizing compounds are sometimes not necessary in order to extend the stabilization over longer time. Moreover, as we already discussed, photo triggering is eco-friendly if compared with thermal triggering because of the lower energies involved (Fouassier, 2012).

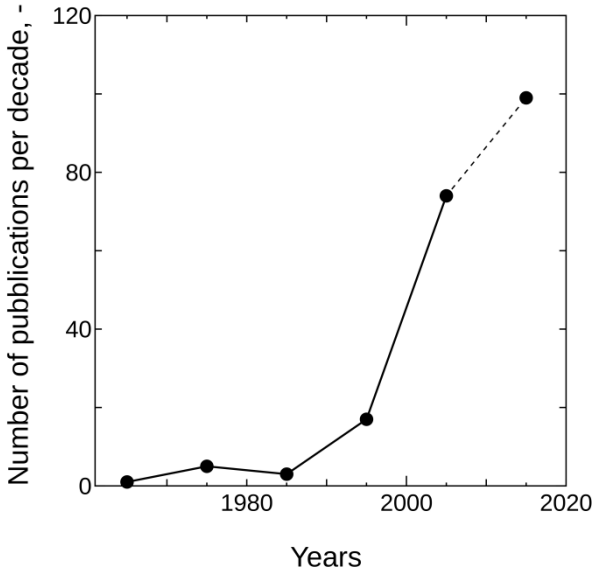

Figure 16. Trend in publications with keyword “emulsion photo-polymerization” throughout the last 50 years. The decade 2010-2019 is obviously not complete. Source: www.scopus.com.

In order to get a better control over particles dimensions, microemulsions have been extensively studied. Microemulsion is a thermodynamically stable dispersion that, because of the typical droplets dimensions, does not suffer from UV scattering. For these reasons, it is a promising technique in the photo-polymerization field (Chemtob *et al.*,

2010). However, it suffers from other problems such as low concentration of particles, that results in low production rate per volume. In addition, the high surfactant concentrations needed can hinder the range of application (Chemtob *et al.*, 2010).

3.2 Photo-induced polymerization via oil-in-water miniemulsion

Miniemulsion techniques consists in the production of a submicron dispersion, for example of monomer in water, able to avoid coagulation for a certain amount of time. A low amount of surfactant is present to stabilize partially the droplets without forming micelles. Ostwald ripening, which boosts droplets coagulation, is countered by addition of a co-stabilizer. Usually the co-stabilizer is a compound non-miscible with the continuous phase that is able to block the dissolution of the main compound of the dispersed phase in the continuous one. In these conditions, nucleation is confined within the monomer droplets and each of them can be considered as a mini batch reactor (Asua, 2002).

Photo triggering in miniemulsion has been studied in the last 10 years in order to solve problems related to the well-known photo-polymerizations in microemulsions. Droplets size is higher than the one obtainable from microemulsions but still in the nano-region, moreover, lower amounts of surfactant result in easier purification of the product (Chemtob *et al.*, 2010; Hoijemberg *et al.*, 2011).

3.2.1 General ideas and modifications

In this study, we started from the concept of miniemulsion and modified the procedure in order to grow a polymeric shell on the surface of emulsion droplets. Interfacial polymerization is not a new concept in material science, but it is frequently limited to these two types: grafting on a solid surface or copolymerization at the interface of two liquids (Minko, 2008; Gaudin *et al.*, 2008). Recently, confinement of the initiator at droplets surface was exploited to achieve interfacial thermally induced polymerization (Piradashvili *et al.*, 2015)

The goal of this new method is to exploit the physical separation of photo-initiator and monomer to induce a reaction confined at the surface between the two phases of the miniemulsion. A dispersion of oil in water is produced. In the oil phase a hydrophobic photo-initiator is dissolved, while a hydrophilic monomer is dissolved in the aqueous phase along with the surfactant. Using these experimental conditions, the idea is to exploit the oil droplets as template and to grow a polymeric shell on their surface in such

a way to completely engulf them in capsules. A schematic of the ideal physical setup is provided in Figure 17.

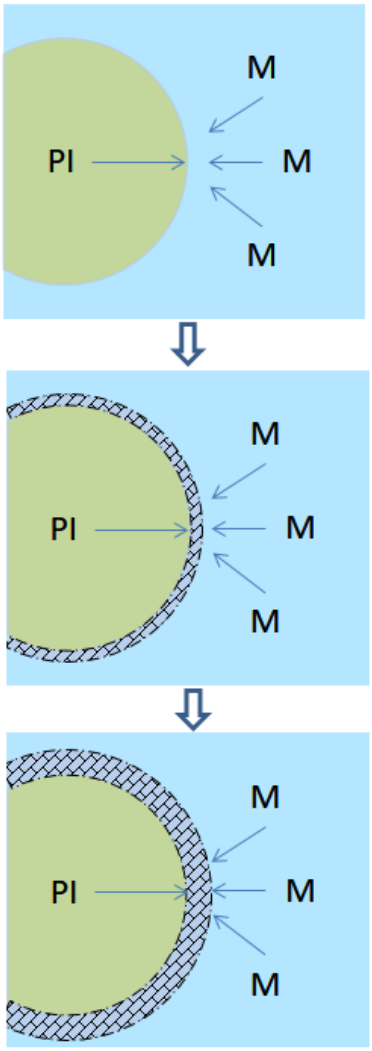

Figure 17. Schematics of the nanocapsules production. The monomer (M) reacts with the photo-initiator (PI) on the droplet surface.

Both radical and cationic polymerization mechanisms were studied in this experimental setup. Studies on the two mechanisms were treated separately, since the issues that needed to be overcome are different. In the following paragraphs, the study using the radical polymerization mechanism will be accurately described and the results discussed. In a further section, a similar discussion will be presented for the cationic mechanism of polymerization.

3.2.2 Materials and Methods

In the next section, we will list all the chemicals used in the particles synthesis. Methods for the production of the different polymeric capsules will be also discussed.

3.2.2.1 Materials

All reagents, if not specifically indicated, were purchased from Sigma Aldrich. Monomers used for the synthesis were: poly(ethylene glycol) diacrylate (PEGDA) and poly(ethylene glycol) methyl ether methacrylate (PEGMEMA), see Figure 11. Photo-initiator was bis(2,4,6-trimethylbenzoyl)-phenylphosphineoxide (commercially known as Irgacure 819), purchased from BASF, see Figure 9. A brief description of the monomers used is reported in Table 1.

Table 1. List of monomers used in the synthesis.

Code	Name	Avg. Mol. Weight, Da	Avg. number of repetition units, -
Resin A	PEGDA 700	700	13
Resin B	PEGMEMA 300	300	5
Resin C	PEGMEMA 950	950	20

Continuous phase in the emulsion mainly consists of deionized water, obtained from a filtering system (Visio, ELGA LabWater), while the dispersed phase was hexadecane (purity > 99%). The surfactant used to stabilize the emulsion was sodium dodecyl sulfate (SDS, purity > 99%).

Curcumin, see figure 13c, was chosen as active ingredient for the encapsulation and purchased in powder form with purity > 65%. The reagent was then extracted using pure ethanol (purity > 99.8%) and subsequently dried at room temperature.

3.2.2.2 Particles synthesis

Synthesis of particles can be divided into three steps: preparation of the two phases, production of the emulsion and reaction.

The two phases were prepared separately and mixed afterwards. The continuous one was prepared adding a given amount of SDS into 50 g of deionized water. The solution was, then, gently stirred to promote the dissolution of SDS without the production of bubbles on the liquid surface. The water soluble monomer, 1 g ($1.4*10^{-3}$ mol), was added to the aqueous solution and dissolved by gentle stirring. The dispersed phase was

prepared using hexadecane as main component. Irgacure 819 was added until saturation of the solution (~5.5 mg/mL). If present, curcumin was added in this step. In that case, a curcumin saturated solution in hexadecane/Irgacure was prepared (~1 $mg_{curcumin}/mL_{solution}$).

To prepare the miniemulsion, 0.4 g of the oil phase were added to the becher containing the continuous solution. The liquid was then exposed to an intense mechanical stirring (>4000 rpm) for 2 min and rapidly transferred in the ultrasonic bath (Sonorex, Bandelin, Berlin, Germany). Ultrasounds were applied for a certain amount of time, varying from 5 up to 30 min. The initial mechanical stirring was crucial for the breakage of the dispersed phase into droplets that will be further broken by the action of ultrasounds.

Once the ultrasound step was completed, the dispersion was transferred into a 3-necks round bottom flask. In case of radical polymerization, in order to avoid oxygen inhibition of the reaction, a nitrogen gas flow was provided. A pipe fed nitrogen with overpressure of 0.3 bars directly in one of the side necks, see Figure 18. Nitrogen supply was carried out for 30 s before switching on the mercury lamp to start the reaction. While irradiation was conducted, the liquid was stirred to obtain a continuous circulation and, thus, an homogeneous irradiation of the droplets. The dispersion was exposed to UV for a time interval that varied from 5 to 20 min. The UV source was a mercury lamp (LC8 lightingcure, Hamamatsu Photonics, Hamamatsu, Japan) equipped with optical fiber, which was positioned at ~40 mm from the liquid surface.

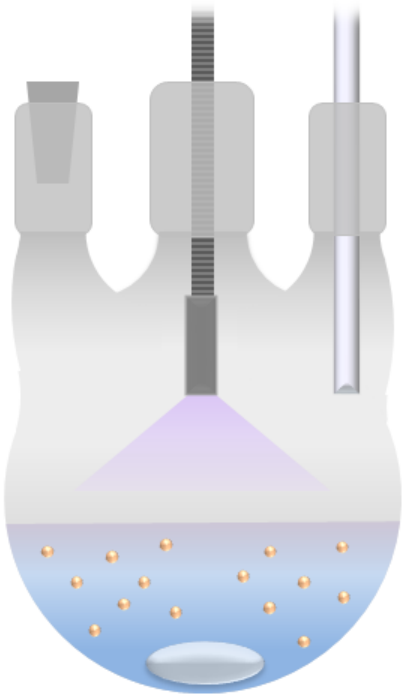

Figure 18. Schematic of the miniemulsion setup.

After irradiation, the samples were stored in three different ways: suspended in water in a 5 mL flask, dried at room temperature or freeze-dried. Suspended sample were used in DLS and TEM analyses, dried samples were used in the DSC and the freeze-dried ones were analyzed using SEM.

3.2.3 Results

In the following paragraphs are summarized the results obtained in the study on photo-induced interfacial polymerization in miniemulsion. Process conditions were optimized in order to reduce process time and obtain a well-defined product capable of releasing an active ingredient. A "one-variable-at-a-time" approach (OVAT) was adopted in the experimental study. The reason behind this choice is related to the presence of variables which, at least from a theoretical point of view, do not effect one another. Design of the formulation and of process conditions were ,therefore, studied separately. Most of the methods and results reported in this section were already published in a paper (Bazzano *et al.*, 2016).

3.2.3.1 Dimension and morphology

In the initial part of the study, the attention was focused on the bi-functional resin (Resin A) for its ability to produce a thermosetting material, more resistant than a thermoplastic one, especially within the aqueous environment of the miniemulsion process. Thus, the first results that will be shown are the ones obtained using PEGDA.

The effect of different process parameters was evaluated in order to optimize the particles production. In particular, UV light exposure time was varied between 5 and 17.5 minutes to study its impact on the reaction outcome. Results are shown in Figure 19.

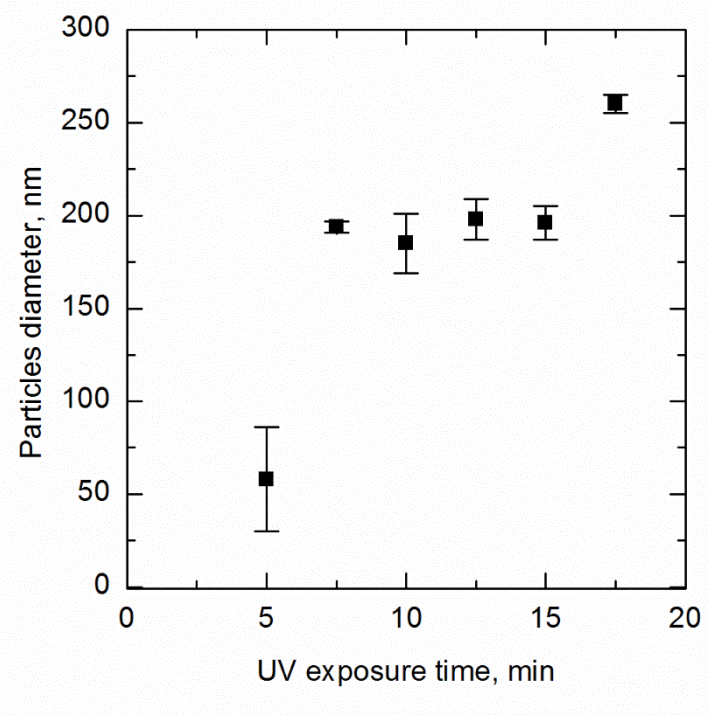

Figure 19. DLS evaluation of the nanocapsules diameter vs UV exposure time. Samples were prepared from Resin A and sonicated for 10 min. Markers refer to the mean values and error bars refer to the standard deviations.

DLS evaluation was conducted on samples prepared with 10 minutes of sonication and different UV exposure time. Results showed the presence of a plateau value in the particles dimensions. This began at 7.5 minutes of UV exposure and ended at 15 minutes. For exposure time lower than 7.5 the average size was significantly lower, probably because time was not sufficient to complete the reaction and, thus, the product consisted of polymeric shell shards. In the range within 7.5 to 15 minutes, the average dimension was almost constant, indicating that the shell production was complete and no other size affecting phenomena occurred. For irradiation time above 15 minutes, the average dimension of nanocapsules started to increase. This could be linked to a further reaction of the monomer in the aqueous phase, which caused agglomeration of particles or a further increase in their dimensions. For the following productions, UV exposure time was fixed at 10 min, in order to remain on the plateau while avoiding long process time.

After the optimization of the UV irradiation time, a study was conducted to evaluate the optimum concentration of surfactant, see Figure 20. In particular, the tests were meant to estimate the change in particles size and polydispersity index (PDI) while decreasing to 0 the concentration of SDS.

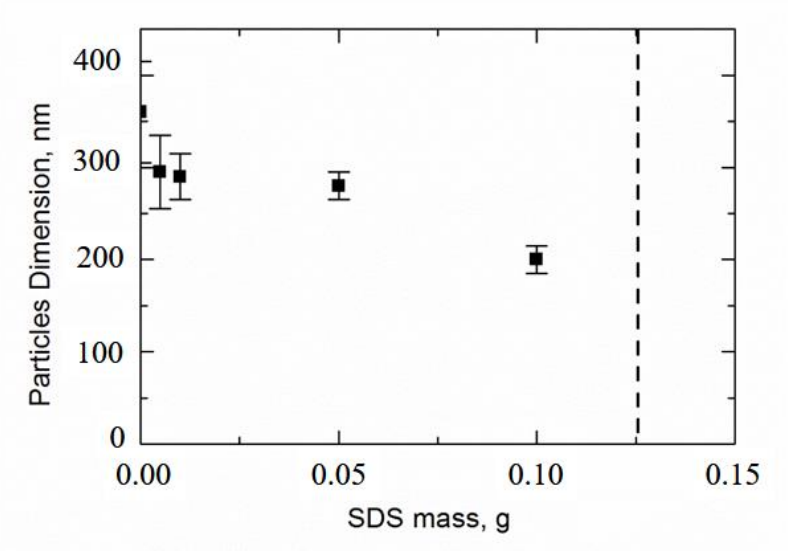

Figure 20. DLS evaluation of nanocapsules diameter vs SDS concentration. Vertical dashed line represent CMC of SDS in water at 25 °C. Samples were prepared with Resin A, sonicated for 10 min and exposed to UV light for 10 min. Markers refer to the mean values and error bars refer to the standard deviations.

SDS concentration in the continuous phase was varied from 0 up to 0.100 g/50mL$_{water}$. Results showed that a lower concentration of surfactant affected the particles dimension. Thus, the highest concentration was used in the following synthesis. Moreover, it must be taken into account that the concentration must be held at values lower than the CMC in order to obtain a polymer nucleation within the droplets.

Once the UV light exposure time and SDS concentration were optimized, a study on the effect of the sonication time was conducted. Empirical evidence reported in literature, indeed, suggested that sonication time has a strong impact on the droplets dimensions and, thus, on the particles size (Ramisetty *et al.*, 2015). Results are summarized in Figure 21.

Sonication time greatly affected particles dimension. In particular, an increase in sonication time initially led to a decrease in nanocapsules diameter. Results, however, showed the presence of a threshold value above which particles dimension was not affected by an increase in sonication time. This behavior had already been showed in emulsion technology and it is due to the instauration of a steady state, in which droplets breakage due to ultrasounds and droplets coalescence are in equilibrium (Ramisetty *et al.*, 2015; Gaudin & Sintes-Zydowicz, 2008). As shown in Figure 21, samples prepared without active ingredient presented a threshold value at 15 min of sonication. Above this value the particles dimensions were almost constant at ~ 90 nm. The *p*-value analysis conducted on data obtained after 15 min sonication showed values higher than 0.05,

confirming the loss of dependence after the threshold time. In samples prepared with curcumin, on the other hand, dimensions were generally higher and the threshold values was identified at 20 min.

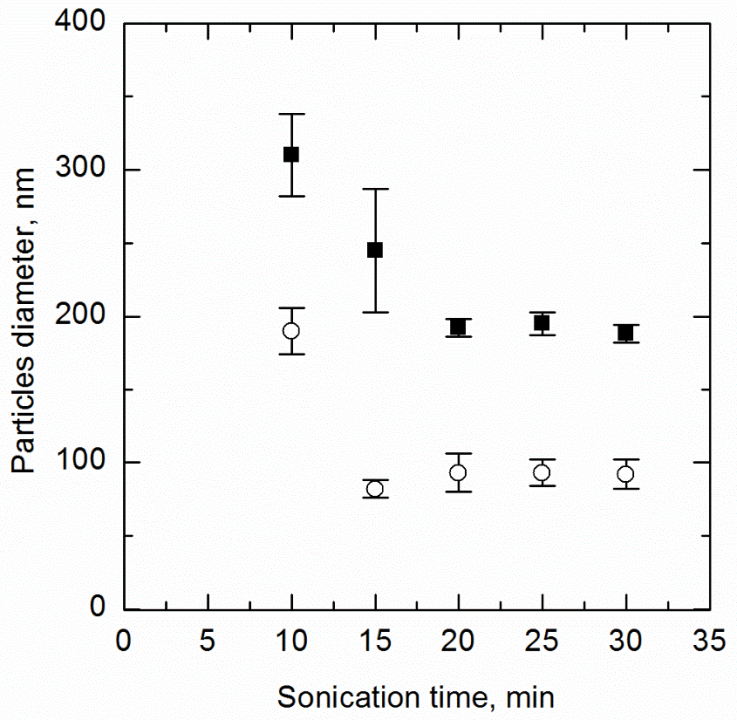

Figure 21. The average size of the NCs (as observed by DLS) as a function of sonication time. Results refer to the NCs with (■) and without (○)curcumin. Samples were prepared from Resin A and irradiated for 10 minutes. Markers refer to the mean values and error bars refer to the standard deviations.

This seemed to suggest that curcumin dissolved in hexadecane promotes coalescence or hinders breakage of droplet. The hypothesis is also supported by the higher average size of curcumin loaded particles. The presence of the threshold time was confirmed by *p*-value analysis, which provided values above 0.05 for data sets beyond the threshold value.

Particles dimensions and morphology was also evaluated by FESEM and TEM analysis, see Figure 22. Results confirmed the production of polymeric shell wrapping the dispersed phase. In Figure 22b, it is possible to see many particles stuck on the sugar surface of the freeze-dried sample. Thus, for some sample, dimensions were evaluated from FESEM and the results showed a good agreement with the ones obtained from both DLS and TEM. Using TEM analyses, dimension evaluation was conducted measuring the

average size of a population of 40 up to 50 nanocapsules. Results were plotted and compared with the ones obtained by DLS analyses, see Figure 23.

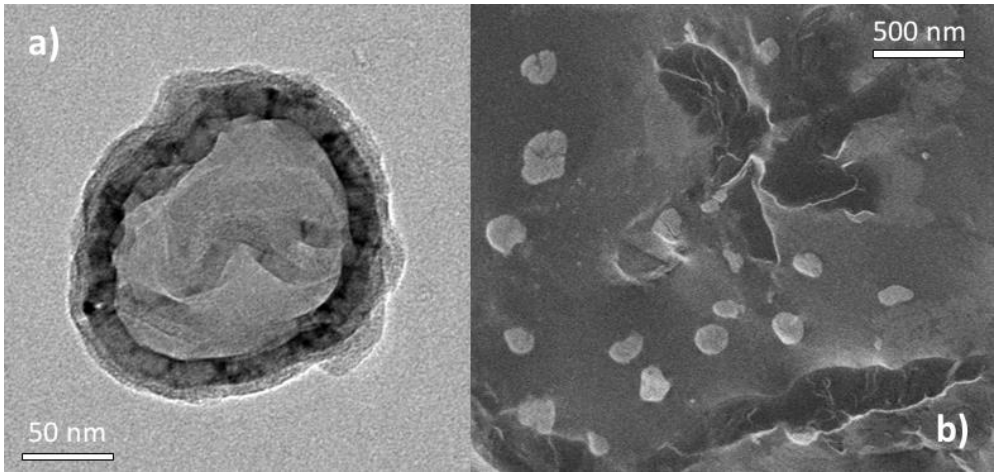

Figure 22. (a) TEM micrograph and (b) FESEM image of nanocapsules prepared with 15 min sonication, 10 min UV exposure and Resin A. The sample was prepared with curcumin.

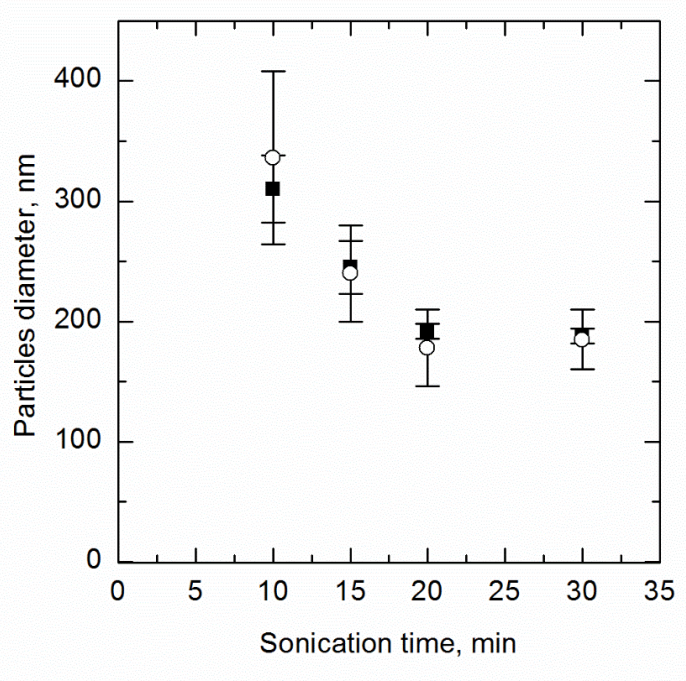

Figure 23. Nanocapsules dimensions vs sonication time as observed by (■) DLS and (○) TEM. Samples were prepare with Resin A, using 10 min of UV exposure and curcumin in the dispersed phase. Markers refer to the mean values and error bars refer to the standard deviations.

It is possible to appreciate a correspondence between DLS and TEM results. TEM standard deviations were significantly higher than the DLS ones. This is linked to a difference in the number of particles analyzed with the two technique. While DLS provided an average value over tenths of thousands particles, TEM evaluation was conducted with ~50 particles. Thus, the different size distribution is not due to an actual difference in the samples.

TEM micrographs were also analyzed to evaluate the mean shell thickness of the nanocapsules. For each sample, from 30 up to 50 capsules were analyzed and for each capsule shell thickness was measured three times and averaged. Mean values and standard deviations are reported in Table 2.

Table 2. Shell thickness vs sonication time, as evaluated by TEM micrographs. Samples prepared with Resin A, using 10 min of UV exposure and curcumin in the dispersed phase.

Sonication time, min	10	15	20	30
Shell thickness, nm	27.52	23.38	18.73	18.74
Std. Deviation, nm	7.73	4.81	4.48	4.56
Particle count, -	32	30	38	41

In Table 2, it is possible to see that the shell mean thickness decreases while increasing the sonication time. This might be because the mean droplets dimension decreases while increasing the sonication time. Thus, the specific oil/water interfacial surface in the system is increased and the monomer, which was held constant, has to cover a wider surface. However, the high standard deviation values, reported in Table 2, hinder an accurate evaluation of this phenomenon. The *p*-value analyses performed between these samples, indeed, did not show a statistically significant difference in the data sets.

In order to study the shape of nanocapsules and the effect of sonication time on that feature, a new parameter was defined. For each capsule, the maximum diameter (D_{max}, nm) and the minimum diameter (D_{min}, nm) were measured. The shape factor, Ω, was defined as the ratio between the difference between the two diameters and the D_{max}:

$$\Omega = \frac{D_{\max} - D_{\min}}{D_{\max}} * 100 \qquad \text{(Eq. 2)}$$

Results were, then, expressed as a percentage of nanocapsules non-sphericity. Data are shown in Figure 24.

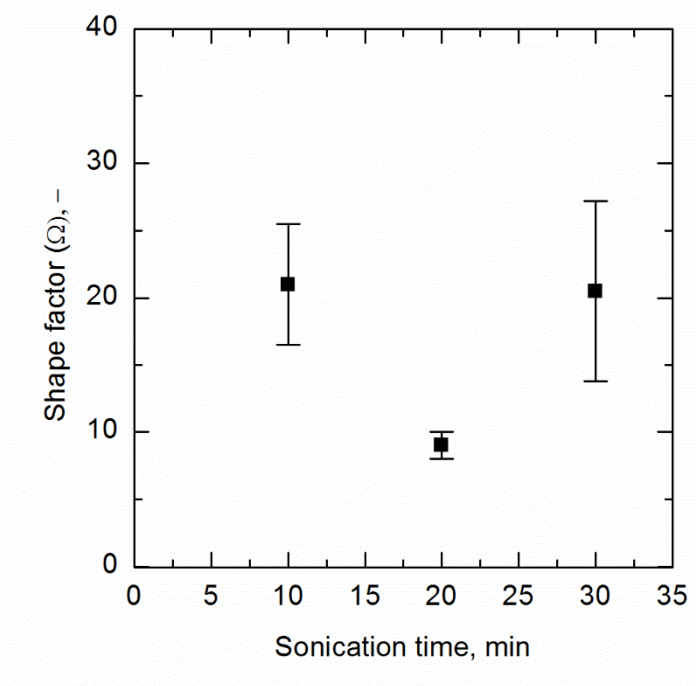

Figure 24. Nanocapsules shape factor vs sonication time. Samples prepared with Resin A, using 10 min of UV exposure and curcumin in the dispersed phase. Markers refer to the mean values and error bars refer to the standard deviations.

Results showed an initial decrease in the Ω value and its standard deviation, followed by an increase in both. The *p*-value tests, however, did not show a strong statistical difference between the data sets. Values of Ω are comprised within 10 to 25, indicating a modest non-sphericity of the product, which is almost constant while varying the sonication time.

As a further step, Resin B and C were introduced and a similar study was conducted. These two resins are mono-functional and, thus, the polymeric material will have thermoplastic behavior. Initial tests were used as a confirmation of the process parameters such as UV exposure time and SDS concentration. These values were held constant in the following tests. The effect of sonication time on the particles dimension was followed by TEM analyses, which were also useful to prove the actual production of nanocapsules, see Figure 25 and Figure 26.

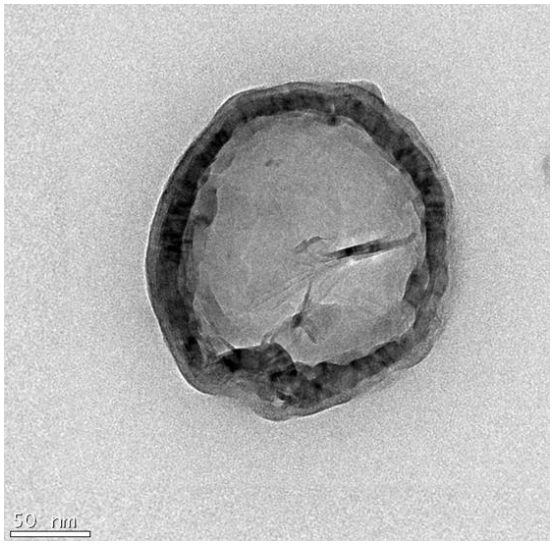

Figure 25. TEM micrograph of nanocapsule prepared with 15 min sonication, 10 min UV exposure and Resin B. The sample was prepared with curcumin.

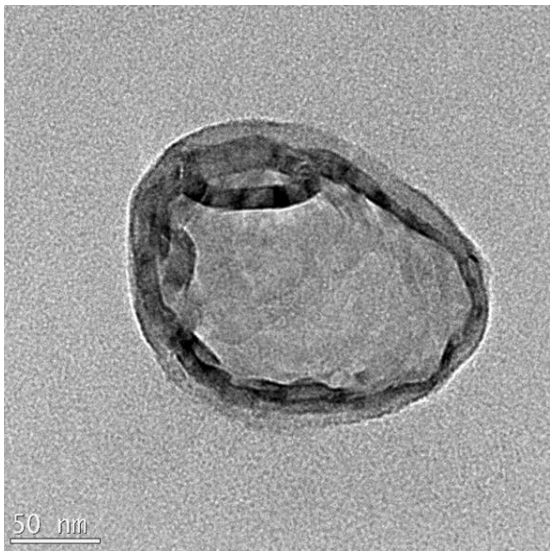

Figure 26. TEM micrograph of nanocapsule prepared with 15 min sonication, 10 min UV exposure and Resin C. The sample was prepared with curcumin.

In Figure 27 are reported the results on the study on the impact of sonication on particles dimension, for both Resin B and Resin C. It can be seen that in both cases the particles dimension decreased when increasing sonication time. Differently from the Resin A case, for sonication times longer than 15 min dimensions decreased almost linearly and did not reach a steady state value. Longer sonication times were not studied

because the energy dissipation of the ultrasound bath led to a significant increase in water temperature. Moreover, for the aim of this study, 100 nm nanocapsules were judged small enough.

Dimensions were significantly lower than the ones obtained with Resin A and this might be due to a lower viscosity of the continuous media or a droplet stabilizing effect of the monomer molecules. In fact, especially Resin C was not easily solubilized in water and, thus, it might preferentially positioned itself at the interface between oil and water and acted as a stabilizer.

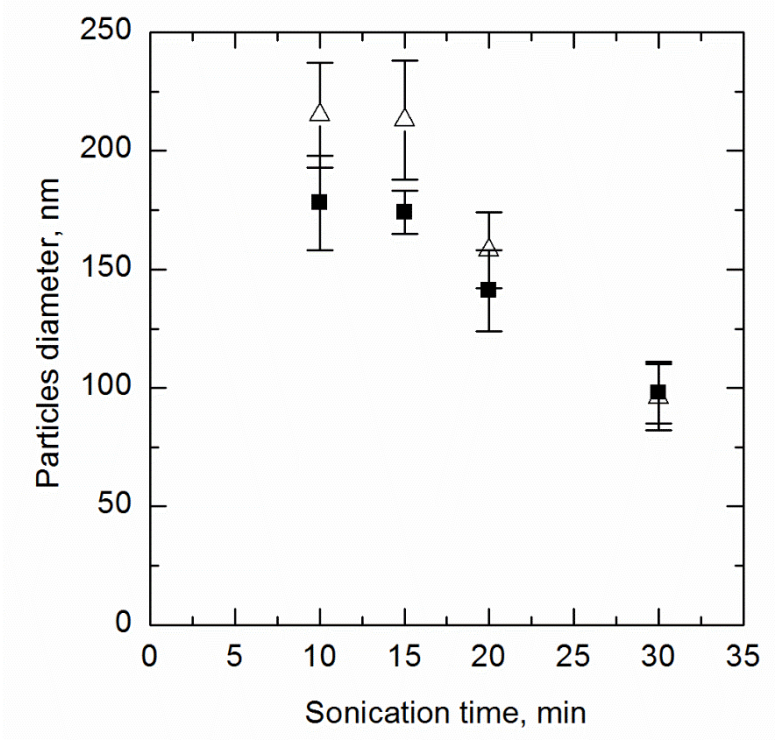

Figure 27. The average size of the NCs (as observed by TEM) as a function of the time of sonication. Results refer to the NCs prepared with (Δ) Resin B and with (■) Resin C. Samples were irradiated for 10 minutes. Markers refer to the mean values and error bars refer to the standard deviations.

Shell thickness was evaluated from TEM micrographs using a methodology similar to the one used in the previous samples. Results, reported in Table 3, showed a general decrease in shell thickness while increasing sonication time. Values are mostly lower if compared with the ones obtained with Resin A. This can be explained tacking into account two differences between the bi-functional and the mono-functional monomer. In fact, mono-functional monomer are generally less reactive and, thus, a lower fraction of the total monomer might reacts and produce the shell. On the other hand, crosslinked polymers have a more rigid structure. Therefore, a once swollen thermosetting material

have a lower tendency to collapse under vacuum, if compared with a thermoplastic one. Thus, an artifact might also explain the differences in shell thickness.

Samples prepared with Resin B and C were analyzed to access their sphericity. Shape factors were evaluated and plotted against sonication time in Figure 28. Results show a slight improvement in sphericity, decreased Ω, while increasing the sonication time with both Resin B and C. Samples prepared with Resin B showed lower Ω values compared with Resin C. Standard deviation were also lower, indicating a better homogeneity of the sample.

Table 3. Shell thickness vs sonication time, as evaluated by TEM micrographs. Samples prepared with Resin B and C, using 10 min of UV exposure and curcumin in the dispersed phase.

	Sonication time, min	10	20	30
B	*Shell thickness, nm*	19.80	18.07	13.73
	Std. Deviation, nm	4.27	3.93	2.74
	Particle count, -	43	39	39
C	*Shell thickness, nm*	17.97	13.47	12.85
	Std. Deviation, nm	4.09	4.02	3.12
	Particle count, -	37	41	40

In order to exploit some good features of both thermosetting and thermoplastic materials, a study was conducted mixing two monomers: Resin A and Resin B. Resin B was chosen as mono-functional monomer for its good results in the previous evaluations, especially in the shape factor. Moreover, the choice was driven by the fact that a low molecular weight monomer was considered more suitable to move towards a less crosslinked material. TEM analyses were performed in order to confirm the production of nanocapsules, see Figure 29.

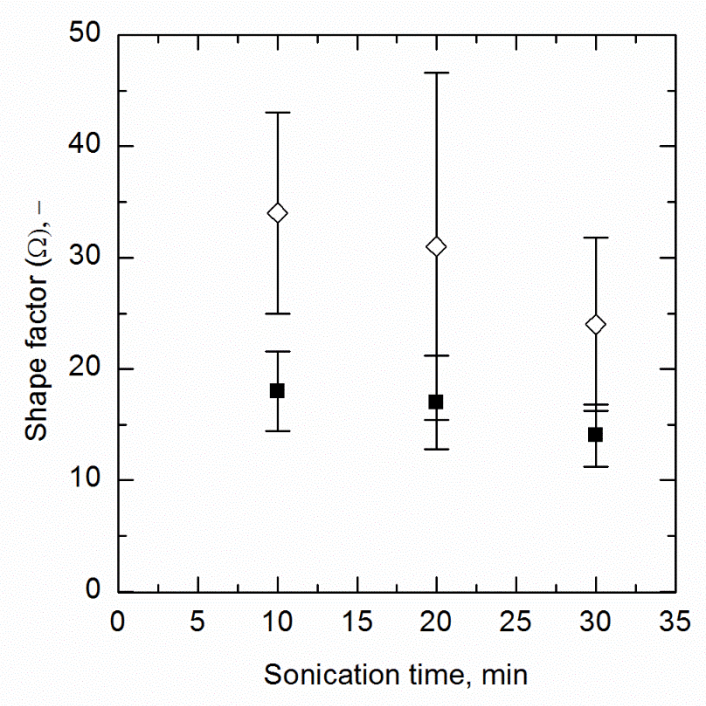

Figure 28. Nanocapsules shape factor vs sonication time. Samples prepared with Resin (■) B and (◊) C, using 10 min of UV exposure and curcumin in the dispersed phase. Markers refer to the mean values and error bars refer to the standard deviations.

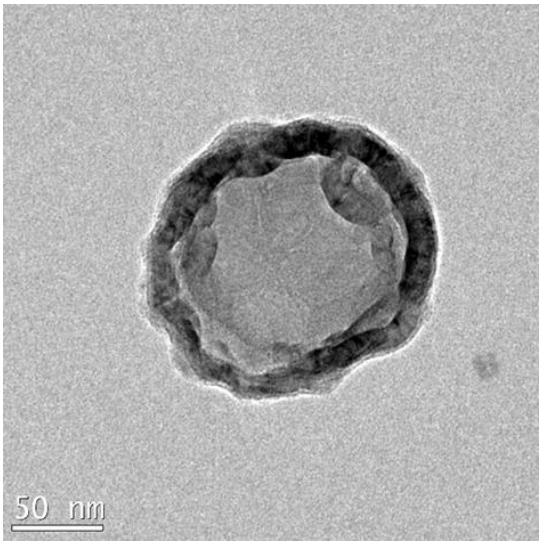

Figure 29. TEM micrograph of nanocapsule prepared with 15 min sonication, 10 min UV exposure and mixture of resins: 20% Resin A and 80% Resin B. The sample was prepared with curcumin.

Experiments were carried out varying the ratio between the two resins and evaluating the impact of sonication time on particles dimensions, see Figure 30. The complete list of experiments and their composition is provided in Table 4.

Table 4. List of experiments carried out on the effect of monomer composition.

Exp. Code	% Resin A	% Resin B
M1	100	0
M2	90	10
M3	80	20
M4	70	30
M5	50	50
M6	30	70
M7	20	80
M8	10	90
M9	0	100

Results reported in Figure 30 showed a continuous decrease in particles dimensions while increasing the percentage of Resin B in the initial solution. The trend is almost linear and confirmed the possibility to design easily nanocapsules dimensions by varying the ratio between the two initial monomers. Once the study on monomer ratios was completed, the evaluation of behavior under different manufacturing conditions, namely sonication time, and using various monomer mixtures was carried out, see Figure 31.

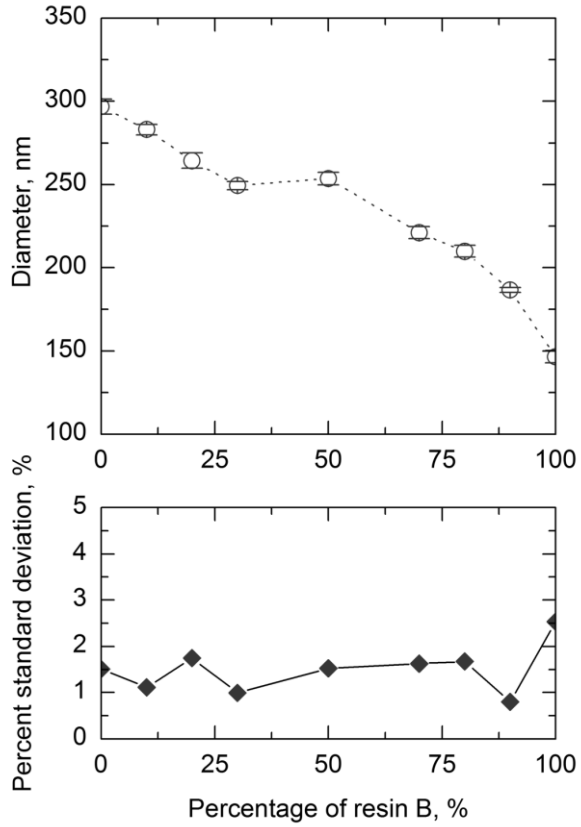

Figure 30. Upper graph: nanocapsules dimensions vs. percentage of Resin B as observed by TEM. Lower graph: Percent standard deviation of nanocapsules dimensions vs percentage of Resin B. Samples were prepare with Resin A and B, using 15 min sonication, 10 min of UV exposure and curcumin in the dispersed phase.

In Figure 31, it is possible to appreciate the gradual change of behavior from the total bi-functional monomer towards the total mono-functional one. In particular, in data series M1 and M3, dimensions did not decrease while increasing sonication time above 20 min. For data sets M1 and M3, the p-value tests conducted on data obtained at 20 min and at 30 min did not show any significant variations ($p > 0.05$). This threshold value is gradually lost moving towards data sets M5, M7 and M9.

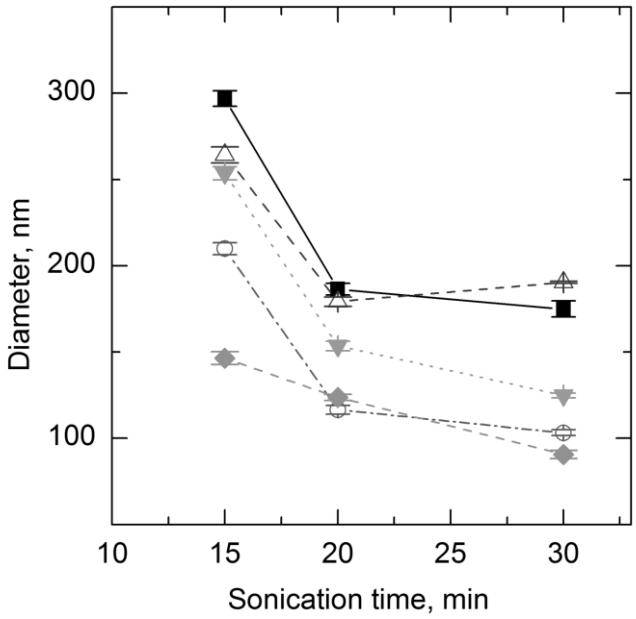

Figure 31. The average size of the NCs (as observed by DLS) as a function of the time of sonication. With respect to Table 4 experiments: (■) M1, (Δ) M3, (▼) M5, (○) M7 and (♦) M9. Samples were irradiated for 10 minutes. Markers refer to the mean values and error bars refer to the standard deviations.

3.2.3.2 Zeta-potential

Zeta-potential is a crucial physical parameter for the stability of particles suspension. Evaluation of zeta-potential was carried out on samples prepared in different manufacturing conditions. No significant differences were seen in samples prepared varying sonication time nor UV exposure time. In fact, zeta-potential is strictly correlated to the chemical nature of the particles surface. However, important differences were seen between samples prepared with and without the active ingredient. Results are provided in Table 5.

Zeta-potential was negative in every sample. This was probably due to the electric nature of the surfactant used in the synthesis, which was still present on the particles surface and helped the stabilization. No significant differences ($p > 0.05$) could be found in samples from different type of resin, thus confirming that, once polymerized, the chemical nature of the shell was similar. All initial monomers, indeed, possessed a PEG backbone.

Table 5. Zeta-potential values in case of particles obtained with different resins, using 15 min of sonication and 10 min of UV exposure.

Resin	Loading	Surface Zeta-potential, mV	Standard deviation, mV
A	-	-12.36	3.71
	curcumin	-63.35	3.77
B	-	-14.85	6.91
	curcumin	-54.27	9.61
C	-	-13.21	2.51
	curcumin	-71.37	1.45

Samples loaded with curcumin showed higher values of zeta-potential if compared with the non-loaded samples. This might be explained by interactions between SDS and curcumin, which have been suggested in literature (Wang *et al.*, 2009). These interactions might suggest the presence of curcumin in the outer part of the nanocapsules and this possibility will be taken into account during the evaluation of the release of the active ingredient. Moreover, long-term stability of the nanocapsules suspension was evaluated in order to verify that aggregation does not occur, especially in those samples characterized by low zeta-potential values. DLS analyses, carried out up to 1 month after the production, showed no significant changes in the average size, thus suggesting the absence of aggregation.

3.2.3.3 Thermal behavior

Analyses on thermal behavior were carried out to get an insight in the polymerized product. In particular, DSC scan of a sample prepared with Resin A and using 15 min sonication and 10 min UV exposure is shown in Figure 32.

DSC scan showed the presence of glass transition temperature (T_g) at ~ -44 °C in the samples prepared with Resin A. This is in agreement with literature results (Chiappone *et al.*, 2015). Thermograms did not show any residue peak at 13-14°C, thus indicating an almost complete conversion of the Resin A. Moreover, a peak at ~ 18 °C could be observed, showing the presence of hexadecane in the sample. DSC analyses were carried out also on samples loaded with curcumin. The sample was prepared using, as first attempt, 10 min UV irradiation time. The presence of T_g at ~ -44 °C and the absence of the Resin A melting peak confirmed the positive outcome of the production even if curcumin is able to absorb in the UV-spectrum.

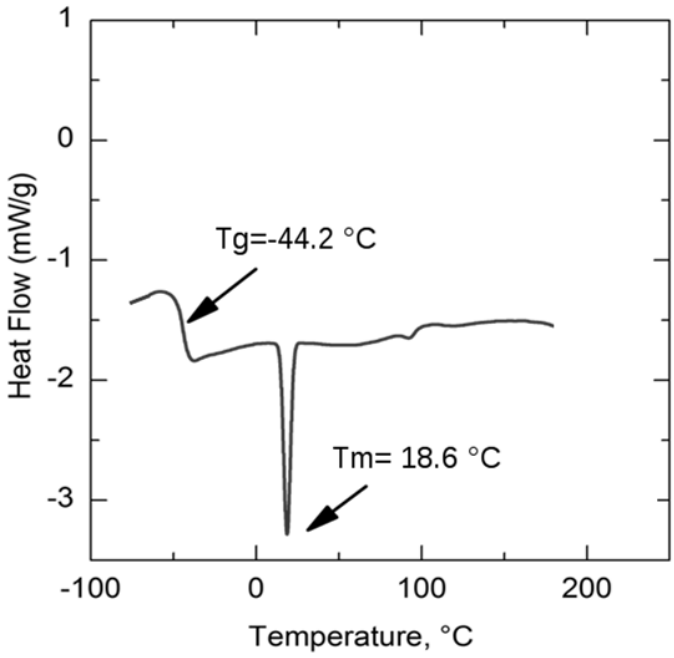

Figure 32. DSC scan of dried sample prepared with Resin A, using 15 min sonication and 10 min UV exposure.

DSC scans were performed also on samples prepared with the other two resins. Results showed the absence of non-reacted resin in case of the low molecular weight resin (Resin B, T_m ~ -7 °C), while DSC scans of samples with Resin C still showed the presence of a melting peak of the non-reacted resin at ~ 38-39 °C. However, a small glass transition temperature was observed in the Resin C sample. Since the TEM micrographs showed the presence of nanocapsules, it was possible to conclude that a partial polymerization was achieved in 10 min of UV exposure.

3.2.3.4 Active ingredient controlled release

Nanocapsules obtained in suspension were immediately used for dialysis tests. Results from UV-visible analyses were plotted against time in order to evaluate how the type of material affected the release rate. Results are shown in Figure 33.

Curcumin release tests were carried out with three different nanocapsules samples, varying the ratio between Resin A and B, in order to study how the change in crosslinking density affected the release rate. In Figure 33, it is possible to notice that there is a strong difference in the release rate between the samples prepared with 100% Resin A (M1 in Table 4) and the other two samples (M5 and M9 in Table 4).

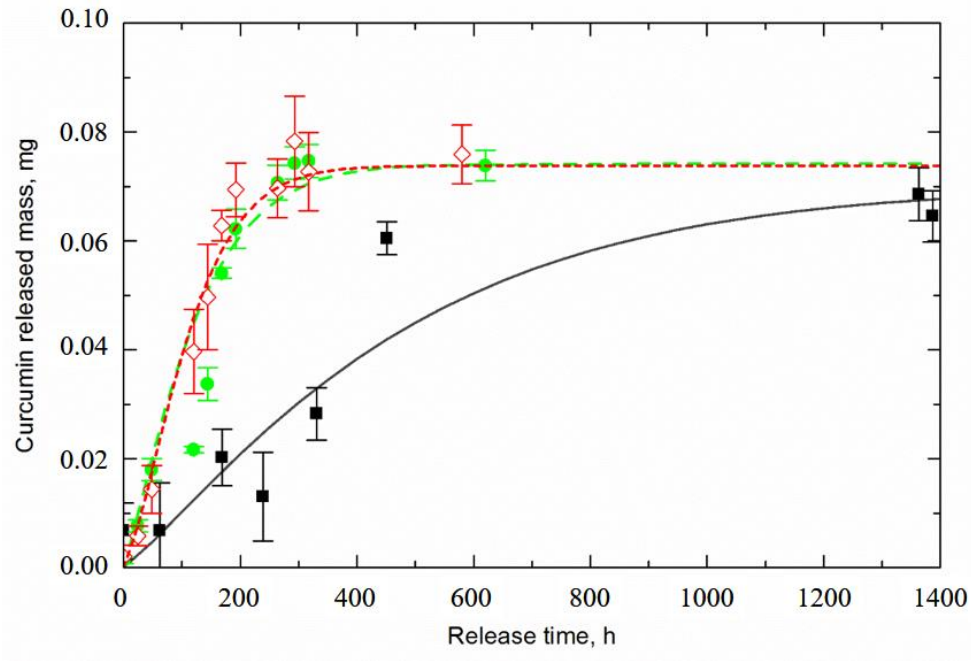

Figure 33. Release curves with nanocapsules obtained from different resins: (■) 100% Resin A, (●) 50% Resin A and 50% resin B, (◊) 100% Resin B. Samples obtained with 15 min sonication and 10 min UV exposure. Markers refer to the mean values and error bars refer to the standard deviations.

In particular, sample M1 showed a much slower release if compared to M5 and M9. This can be explained by the different structure of the polymeric material that composes the nanocapsules shell. Sample M1 has, indeed, a thermosetting polymeric shell that seems capable of strongly hindering the diffusion of curcumin outside the nanocapsules. On the other hand, samples M5 and M9 did not show significant differences in release rate. Half of the payload in samples M5 and M9 was released after ~250 h, while the same release was achieved in ~630 h in case of M1. The similar release rate of M5 and M9 might be a proof that, below a certain crosslinking density, the diffusion of the active compound through the shell is not the controlling mechanism. In fact, low crosslinked samples and non-crosslinked ones showed a similar behavior.

As to the total released amount, in the entire test the maximum released mass of curcumin was around 0.07 mg. In every sample, the expected total loaded mass was 0.096 mg. However, it seems that the release profile reached a steady state. This might be due to different causes. A fraction of curcumin might be blocked within the particles and this fraction was more or less the same in all the samples. This could be related to the higher solubility of curcumin in the hexadecane phase. On the other hand, nanocapsules might possess only that amount of curcumin. Degradation of curcumin may occured during

polymerization reaction. In fact, curcumin is able to absorb in the UV-spectrum and this could lead to degradation of the molecule. This phenomenon has been already discussed in literature, along with curcumin alkali hydrolysis and oxidation problems (Ansari *et al.*, 2005).

As a general result, release time was quite long, in the order of hundreds of hours. This can be useful in some cases, depending on the type of active ingredient or when drug administration cannot be achieved so frequently (Barzegar-Jalali *et al.*, 2008). However, it is true that, in this specific case study, the loaded amount of drug is not high enough for such applications. Therefore, other solutions will be studied in the following sections in order to overcome these issues.

3.2.4 Conclusions

Miniemulsion photo-induced polymerization of acrylate and methacrylate monomers was proven to be successful. UV irradiation showed to be a useful source for reaction triggering in the emulsion, besides the scattering and absorption phenomena involved. The initial separation of PI and monomers led to a capsule structure that was confirmed by TEM analyses. The process parameters were optimized based on the nanocapsules dimension and shape. In particular, sonication time displayed a strong effect on product dimension. This was explained by the strong effect that it has on the droplets, which were used as template during polymerization.

Different initial monomers showed peculiar effects on the reaction outcome, namely the size and shape of nanocapsules. Two monomers were selected and co-polymerized in order to study the effect of the material nature on some characteristic features of the product. Reaction was successfully achieved and the possibility to precisely design the dimension of the particles by changing the ratio between the two monomers was demonstrated. Finally, tests on the release of the active ingredient showed strong differences between samples produced with different monomers or with a mixture of them. This is particularly important in the field of controlled drug release because it enables a more accurate design of the releasing features of the product.

3.3 Photo-induced polymerization via oil-in-water miniemulsion: cationic mechanism

Cationic polymerization is a reaction mechanism in which the propagating specie is characterized by the presence of a positive charge. As we already briefly discussed, it has some advantages and some disadvantages if compared with the radical mechanism. In the following part, the study on the application of this mechanism to miniemulsion photo-induced polymerization will be described. Methods and data reported in this chapter were part of a submitted paper.

3.3.1 Materials and Methods

3.3.1.1 Materials

All reagents, if not specifically indicated, were purchased from Sigma Aldrich. They were analytical grade and used as received. Divinylether tri-ethylenglycol (DVE3) was used as monomer, see Figure 12. Photo-initiator was an antimonium salt: triarylsulfonium hexafluoroantimoniate salt (TAS-HFA), purchased from BASF, see Figure 10. Continuous phase in the emulsion consists of deionized water, obtained from a filtering system (Visio, ELGA LabWater), while the dispersed phase was hexadecane (purity > 99%). The emulsion stabilizers used were different: sodium dodecyl sulfate (SDS, purity > 99%), Pluronic PE 6100 (BAFS, Cesano Maderno, Italy) and polyvinylpyrrolidone (PVP, MW 40000).

3.3.1.2 Particles synthesis

Similarly to the case of radical mechanism, the synthesis required three main steps: preparation of the two phases, production of the miniemulsion and reaction.

The two phases were prepared separately and mixed afterwards. The continuous one was prepared adding a given amount of stabilizer into 50 g of deionized water. The solution was, then, gently stirred to promote the dissolution of the chosen stabilizer. Unlike the production of nanocapsules by radical polymerization, with the cationic mechanism, a correct interaction of water and reacting species is crucial for the propagation process and its termination. Thus, monomer was not dissolved in the continuous phase but added to the oil dispersion. The dispersed phase was prepared using hexadecane as the solvent in which TAS-HFA was added. In this case, the PI is not soluble in the solvent of the dispersed phase. Moreover, the monomer was added to this

dispersion. This choice was due to the need to promote isolation of the reacting species from the water bulk. In fact, water inhibition can hinder the reaction propagation. To obtain a good dispersion of the three non-miscible components, an intense (>4000 rpm) mechanical stirring was applied for 5 min.

To prepare the miniemulsion, the continuous phase liquid was exposed to mechanical stirring (>1400 rpm). This stirring velocity was determined by the necessity to give enough energy to the system in order to obtain the initial dispersion while avoiding the production of air bubbles in the liquid. A given mass of the monomer dispersion, PI and hexadecane was added to the solution while it was under stirring. The initial coarse emulsion was rapidly transferred in the ultrasonic bath (Sonorex, Bandelin, Berlin, Germany). Ultrasounds were applied for a certain amount of time, varying from 2.5 to 25 min.

Once the ultrasound step was finished, the procedure followed exactly the one used in case of radical mechanism, except for the absence of nitrogen gas supply. UV source was a mercury lamp (LC8 Lightingcure, Hamamatsu Photonics, Hamamatsu, Japan) equipped with optical fiber positioned at ~40 mm from the liquid surface.

3.3.2 Results

The discussion of results is provided in the following paragraphs. Differently from the study on the radical polymerization, the attention was more focused on the design of the initial miniemulsion. In fact, the water inhibition proved to be a though problem that needed to be overcome. The process parameters were studied in order to optimize the production and to study their effect on the nanocapsules characteristics.

3.3.2.1 Dimension and morphology

In the first part of the study, the effect of stabilizer type on the production of nanocapsules was analyzed. Three types of stabilizers were chosen: one anionic (SDS) and two non-ionic (PVP and Pluronic). Particles synthesis was carried out using 100 mg of stabilizer, a sonication time of 15 min and exposing the miniemulsion to UV light for 10 min. DLS analyses were carried out on the samples to investigate the particles size and PDI of the population. Results are summarized in Table 6.

DLS analyses showed that dimensions of particles obtained with SDS were significantly lower than the ones obtained with the non-ionic stabilizer. Moreover, samples obtained with PVP had a higher PDI, indicating a broader size distribution. These results might be due to a lower chemical compatibility between the non-ionic

stabilizer and the monomer. It must be also pointed out that both PVP and Pluronic possess a much higher molecular weight if compared to SDS. This could lead to some difficulty in the droplets coverage during the miniemulsion production and, thus, to a less stabilized dispersed phase. Finally, the effect of the surface charge has a strong impact on stability of suspensions. Samples prepared with SDS were characterized by a higher absolute value of surface zeta-potential, which could explain the better stabilizing effect of the ionic surfactant. For these reasons, SDS was chosen as a suitable stabilizer and used in all syntheses.

Table 6. Dimension and PDI of samples prepared with three different stabilizers. Samples were prepared using 15 min of sonication and 10 min of UV exposure.

Stabilizer	Diameter, nm	PDI, -	Surface zeta potential, mV
SDS	217.6	0.178	-71.5
PVP	292.8	0.270	-15.1
Pluronic	308.4	0.124	-26.8

Tests were carried out varying the SDS concentration, in order to evaluate which amount of surfactant was the best for the production of monodisperse population. The amount of SDS was decreased to 40 and 70 mg per 50 mL of water. Process parameters were held constant and DLS analyses were carried out on samples. Results on the dimensions and PDI of the samples did not show any dramatic changes, see Table 7.

Table 7. Dimension and PDI of nanocapsules prepared with different amounts of SDS, at different storage time. Samples were prepared using 15 min of sonication and 10 min of UV exposure.

Storage, d		SDS amount, g/50mL$_{water}$		
		0.04	0.07	0.10
0	Size, nm	214.6	222.8	217.6
	PDI	2.90	6.79	12.10
10	Size, nm	214.7	221.8	218.2
	PDI	2.86	2.54	12.13

As can be seen in Table 7, the amount of SDS did not strongly affect the nanocapsules dimensions nor their PDI. Samples prepared with lower amounts of SDS showed a phase separation visible at naked eye. Probably, at lower SDS concentration, the surfactant is not able to stabilize the whole dispersed phase, a fraction of which aggregates and separates from the miniemulsion.

The stabilized fraction has a constant droplet size and, thus, the nanocapsules have dimensions that are not affected by the SDS concentration. An amount of SDS of 100 mg/50mL$_{water}$ was chosen in order to avoid the loss of a fraction of the dispersed phase. During the definition of the best formulation, the effect of PI concentration was studied in order to obtain an efficient reaction. The PI amount was varied within 1 to 4% w/w$_{monomer}$. Results are provided in Table 8.

Table 8. Dimension and PDI of nanocapsules prepared with different amounts (w/w$_{monomer}$) of PI. Samples were prepared using 15 min of sonication and 10 min of UV exposure.

Photoinitiator	1%	2%	4%
Diameter, nm	237.3	217.6	298.7
PDI, -	0.208	0.178	0.341

For concentration of 4% of PI, nanocapsules showed higher dimensions and PDI. This could be explained by an increase in reactive species in the outer layer of the droplets which might led to a partial aggregation of the nanocapsules and, thus, to a higher average dimension as well as a more polydisperse population. For low concentration of PI, e.g. 1%, it could be seen a slight increase in both average dimension and PDI. Thus, a concentration of 2% was chosen for the following experiments.

The last formulation parameter that was studied was the amount of hexadecane. Hexadecane is the major component of the dispersed phase and, therefore, varying its amount corresponded to varying the volume of the dispersed phase. It must be noticed that, to some extent, this corresponded also to the variation of the ratio between the surfactant amount and the total surface area that it is supposed to stabilize. Hence, a decrease in hexadecane volume might lead to a better stabilization of the initial droplets. Results of this study are shown in Figure 34.

Results were in agreement with those reported in Table 7 on the variation of SDS amount. A variation on the ratio between surfactant and dispersed phase did not lead to a change in dimension. This was evaluated both in suspension, using DLS, and in absence of water, using TEM. There was an almost constant gap of ~ 40 nm between values from

the different analyses, but that could be linked with a swollen state in water suspension during DLS analyses or a partial collapse during drying in the TEM chamber.

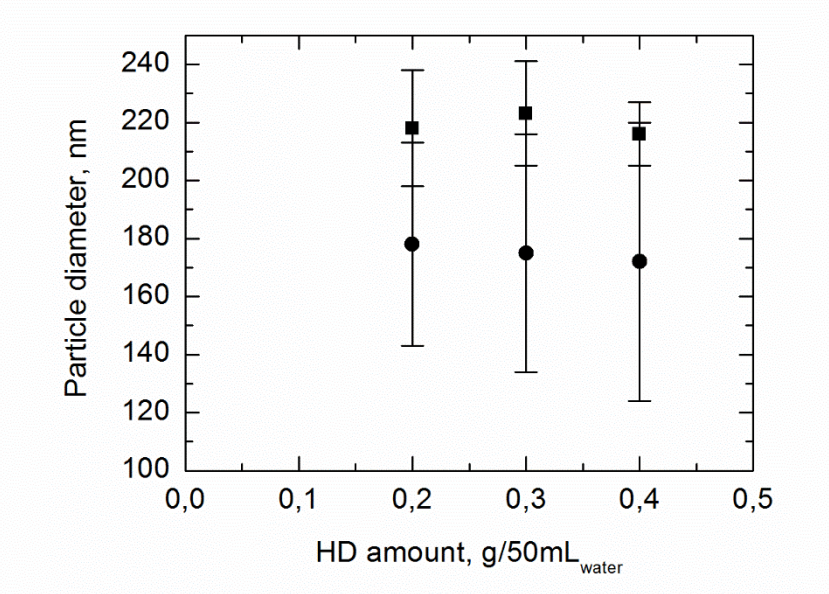

Figure 34. Diameter of nanocapsules, as evaluated with (♦) DLS and (■) TEM, vs. the hexadecane amount. Samples prepared with 15 min sonication time and 10 min UV exposure. Markers refer to the mean values and error bars refer to the standard deviations.

Presence of more SDS molecules per interfacial area did not decrease the nanocapsules dimensions. This could be the results of a steric stabilization against aggregation of droplets, in which the size was determined by the breakage mechanism which, then, was the controlling one. In the following tests, a fixed amount of 0.2 g of hexadecane was used.

TEM evaluation of the nanocapsules size was also used to confirm the structure of the sample and to access the shell thickness, see Table 9 and Figure 35.

Table 9. Shell thickness of nanocapsules vs. the hexadecane amount.

Hexadecane amount, g	0.2	0.3	0.4
Shell thickness, nm	15.3	15.6	15.6
Standard deviation, nm	3.4	3.8	3.9

Thickness of the polymeric shell did not change while changing the amount of hexadecane in the polymerizing system. This was in agreement with the results on the

nanocapsules dimension in Figure 34. Results seemed to suggest that the presence of a different quantity of hexadecane did not affect the particles production from a size and morphological point of view.

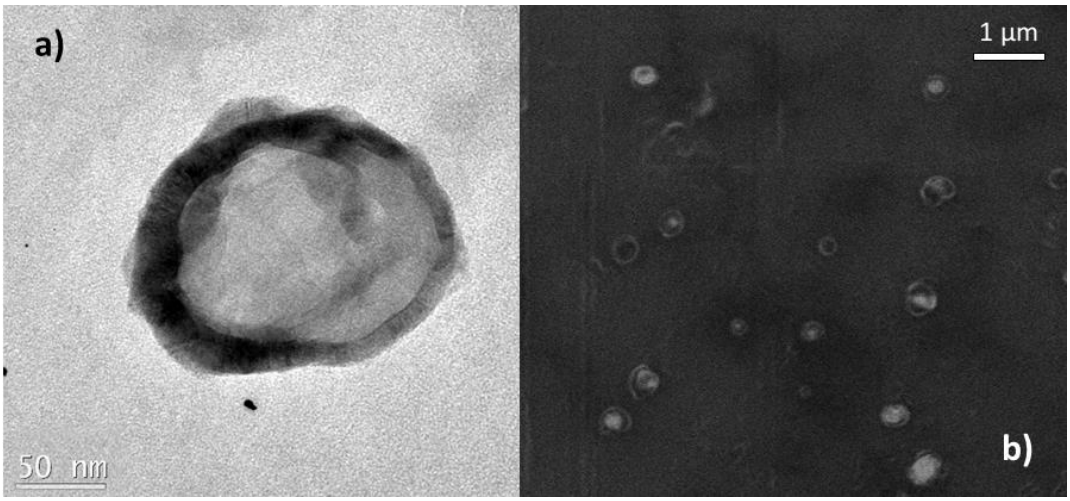

Figure 35. (a) TEM micrograph and (b) FESEM image of nanocapsule prepared with 15 min sonication and 10 min UV exposure.

Once the formulation of the miniemulsion has been optimized, the study was focused on process parameters. The first parameter studied was the time of UV irradiation. This was a crucial factor since it triggers the reaction and, thus, it might have some limitation. Results on this study are shown in Table 10.

Table 10. Diameter and PDI of nanocapsules obtained with different UV curing time. Samples were prepare with 15 min of sonication.

UV curing time, min	Diameter, nm	Std. deviation, nm	PDI, -
7.5	223.2	19.8	0.206
10	217.3	18.5	0.178
12.5	233.3	14.4	0.317
15	223.8	47.2	0.383

Varying UV exposure time did not lead to any substantial change in the dimensions of the nanocapsules that were produced. This results is similar with the one obtained during the same study on the miniemulsion with radical photo-induced polymerization. For 15 min of UV exposure, however, the population seemed more polydisperse and

standard deviation increased significantly. PDI values confirmed this trend, samples obtained with 7.5 and 10 min of exposure showed a PDI around 0.2, while for higher exposure times PDI values increased. This might be due to a further crosslinking, activated by an irradiation surplus, that promoted bonding between particles. For these reasons, a UV exposure time of 10 min was chosen and fixed for the following syntheses.

In the last part of the study on dimension and morphology of nanocapsules, the attention was focused on the effect of sonication. In fact, as already discussed in a previous section, sonication time can strongly affect the size of droplets in emulsion and, thus, the dimension of nanocapules produced using those droplets as template. Results of this study are shown in Figure 36 and Table 11.

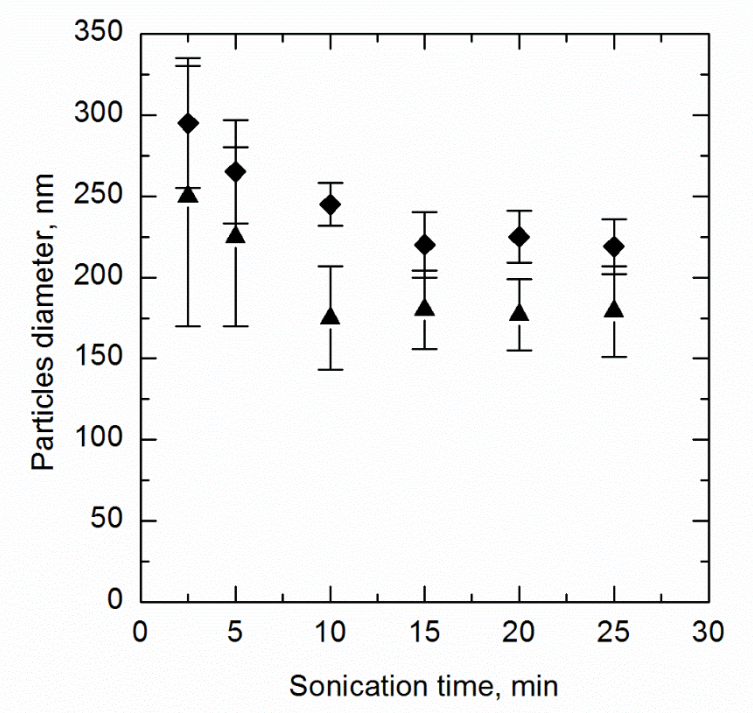

Figure 36. Diameter of nanocapsules, as evaluated with (♦) DLS and (▲) TEM vs. sonication time. Samples prepared with 10 min UV exposure. Markers refer to the mean values and error bars refer to the standard deviations.

Similarly to what was already seen in radical polymerization, an increase in sonication time led to a decrease in nanocapsules diameter. This behavior can be seen between 2.5 and 15 min of sonication. For longer sonication time, average size of the product did not change. A plateau was reached and administration of more energy did not result in smaller nanocapsules. Thus, a threshold value was present around 15 min, above which a steady state was reached and droplets breakage and coalescence were in equilibrium. This value was similar to the one obtained in the study on radical photo-

induced polymerization. In both cases, the droplets and the surfactant nature were similar: the main component of the dispersed phase was hexadecane and the stabilizing molecule was SDS. Therefore, the presence of similar effect of US time on nanocapsules dimensions seemed to suggest that the most important roles were played by these two components.

PDI of the particles population was also evaluated with DLS analyses according to the sonication time, see Table 11.

Table 11. PDI of samples at different sonication time. Samples prepared with 10 min UV exposure.

Sonication time, min	2.5	5	10	15	20	25
PDI	0.347	0.264	0.204	0.178	0.178	0.181
Std. Dev.	0.087	0.076	0.020	0.037	0.032	0.051

PDI values showed a behavior similar to the one displayed by diameter of nanocapsules while increasing sonication time. In Table 11, it can be seen an initial decrease in PDI followed by a plateau after 15 min of sonication. This means that for short sonication time the particles population is still quite polydisperse, whereas longer exposure to ultrasounds results in a more monodisperse sample. This result is in agreement with the achievement of a steady state during emulsification, in which most of the droplets are characterized by the lowest possible dimension.

3.3.2.2 Thermal behavior

Analyses on thermal behavior of the samples were carried out to confirm the presence of the crosslinked material. An example of result is shown in Figure 37.

Scans of pristine resin highlighted the presence of a melting peak at ~ -7 °C. DSC scan, in Figure 37, showed the absence of unreacted resins. Moreover, it could be seen the presence of a peak at ~17 °C which was attributed to the melting of hexadecane. The presence of a T_g at 24 °C was the proof of the production of crosslinked polymeric material. The T_g value was considerably lower than the one suggested in literature for DVE3 films. This might be due to a lower crosslinking density, which is probably the result of the interactions with water during polymerization event. It is, indeed, proven that chain transfer mechanism, and inhibition at higher concentrations, induced by water presence can result in lower T_g of the material (Sangermano, 2012).

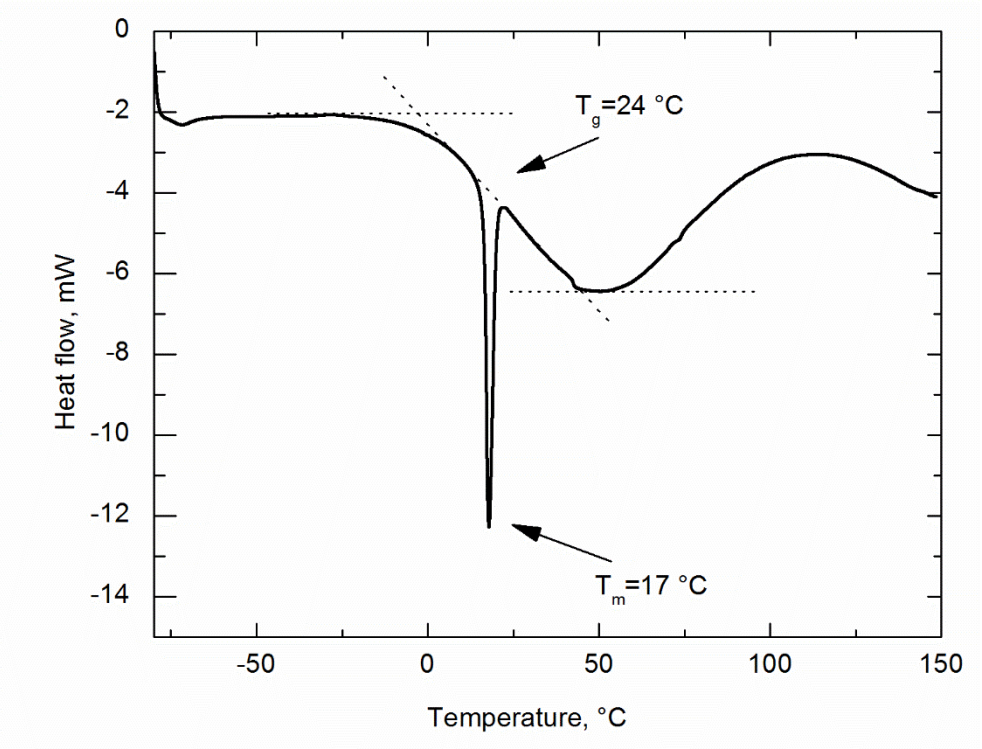

Figure 37. DSC scan of sample prepared with DVE3, using 15 min sonication time and 10 min UV exposure time. Transformations are highlighted in the graph.

3.3.3 Conclusions

In this study, the cationic photo-induced polymerization was exploited to polymerize a monomer at the interfacial area between continuous and dispersed phase in a miniemulsion. Water inhibition of the cationic mechanism was the most important issue that hindered for long time the production of polymeric particles by cationic mechanism in aqueous dispersion, and needed to be overcome. For this reason, the initial part of the study was focused on the design and optimization of the formulation. In particular, the type and concentration of surfactant were studied along with the concentration of PI and hexadecane. TEM analyses confirmed the successful production of nanocapsules with polymeric shell and liquid core. Therefore, the synthesis method developed for radical polymerization was suitable, with minor modifications, also in case of cationic mechanism.

Once the formulation had been optimized, the attention was focused on the impact of process conditions on the nanocapsules dimensions. UV exposure time was found to have a negligible impact on this parameter, at least in a given range. On the other hand,

sonication time was found to have a strong impact on particles dimensions. In particular, in the range within 2.5 to 15 min, the sonication affected the final product size, whereas for longer sonication times the effect was negligible. Moreover, this process parameter had also an impact on the polydispersity of the product, improving the size distribution and helping the production of a monodisperse nanocapsules suspension.

PART II

AEROSOL PHOTO-INDUCED POLYMERIZATION

Chapter 4

Introduction to photo-induced polymerization in aerosol

Aerosol polymerization is a rather new production technique that has been widely used in the last two decades to produce polymeric material (Esen and Schweiger, 1996; Vorderbruggen *et al.*, 1996; Gao *et al.*, 2007). The technique consists mainly of two different steps: production of an aerosol flow made of monomer droplets and polymerization during its reactor passage. Because of a small residence time into the reactor, the reaction triggering is usually achieved by exposure to UV light. This polymerization process is interesting for various reasons; first it is a continuous process that enables the quick production of polymeric particles. It does not need the presence of a liquid medium and, thus, it usually requires less cumbersome work of purification in the downstream processes, especially if compared with synthesis methods that exploit organic solvents. Moreover, it does not usually need any surfactants to stabilize the system and this is another crucial point in order to improve the product (Vorderbruggen *et al.*, 1996; Akgün *et al.*, 2013).

On the other hand, the small residence time of droplets represent an obstacle to the type of polymerization that can be applied to this process. The average residence time in an aerosol based polymerization ranges from few dozens of seconds up to 2-3 minutes. In this time range, the polymerization reaction must be almost complete, in order to ensure the production of particles that do not stick together during material collection in the

reactor outlet. Thus, a photo triggering of the reaction is the best option since it can fully cure a micron-sized volume within 10-20 seconds (Akgün *et al.*, 2013).

The aerosol formation can be achieved with different types of atomizer. Among the most used there are pneumatic, ultrasound-assisted and electrohydrodynamic sprayer. Each type of atomizer is characterized by features that make it more suitable for a certain process. The more important parameters that drive the choice of the atomizer type are: the average size of droplets, polydispersity of the droplets population and the flow rate, namely the amount of solution that can be sprayed in a given amount of time (Biskos *et al.*, 2008).

The aim of this work is to exploit aerosol photo-polymerization in order to develop a continuous technique able to produce structured polymeric particles, which can be used as drug carrier. To achieve this goal, the study was focused on the use of biocompatible monomers with a PEG-like backbone.

4.1 Overview on the aerosol photo-induced polymerization techniques

Aerosol photo-induced polymerization has been extensively used since the middle of the ’90 for different applications. Esen and Schweiger (1996) were among the first to combine the aerosol technology and polymerization; more specifically they used a vibrating orifice to produce multiacrylate monomer droplets in the range of 5-50 μm that were then polymerized by UV light. In the same period, Vorderbruggen *et al.* (1996) used polymerization in aerosol to produce microbeads for molecular recognition. The average dimension of these microbeads was 30 μm and the cationic mechanism was applied to polymerize an epoxy monomer.

In those years, various studies were carried out on the problem of particles structuring during the aerosol process. In particular, Esen’s group focused its attention on the use of ternary systems that, upon evaporation of one component and phase separation, were able to produce a core-shell structure, which was then polymerized. Microcapsules in the size range of 10-50 μm were produced, possessing a polymeric shell and a liquid core (Esen *et al.*, 1997).

The use of modified aerosol generator was studied by Gao *et al.* (2007) in order to develop an atomizer able to produce monodisperse droplets in a wide range of size, from 5 to 100 μm.

In the last 5 years, there has been a renovated interest in the field of aerosol photo-induced polymerization, using atomizers able to produce dispersion of droplets in the submicron scale. This enabled the use of aerosol technique to produce polymeric particles almost in the nanoscale. In particular, a series of studies, conducted by the Wörner’s

group, aimed at the development of this technique (Akgün *et al.*, 2013). Structured product as well as nanocomposites with ZnO were produced using a pneumatic atomizer and a quartz tube photo-reactor. Polymeric materials with spherical shapes and submicron diameter were obtained using a radical polymerization mechanism (Akgün *et al.*, 2014a; Akgün *et al.*, 2014b). The possibility of using a cationic reacting system combined with this experimental setup was also investigated, resulting in spherical particles in the 1-2 μm range (Akgün *et al.*, 2015).

Aerosol production of polymeric particles has been recently studied in order to obtain particles from co-polymerization of acrylamide and styrene. Thus, material with amphiphilic properties was obtained (Shaban *et al.*, 2016).

With this study, the use of cationic photopolymerization is further developed in order to obtain biocompatible structured particles. Phase separation during droplets conversion into particles is investigated as a way to produce various structures. Therefore, the final goal is to obtain, for the first time, porous particles and capsules using a cationic photopolymerization mechanism. This enables the use of a wide variety of monomers that are able to produce PEG-like networks, which can be interesting in drug delivery systems. Curcumin is investigated as active ingredient for the encapsulation and release from particles.

4.2 Photo-induced cationic polymerization in aerosol

Photo-induced polymerization was recognized as an alternative to the already studied miniemulsion techniques, for the production of nanostructured material. Its fascinating features, e.g. continuous process and absence of liquid medium and surfactant, make it an interesting field of study. Although the use of aerosol polymerization is able to solve many issues of liquid suspension based polymerization, it brings some problems that need to be tackled. Nanostructuring of particles is, in fact, more difficult if compared to emulsion systems in which the presence of two liquid phases enables an easier morphology design.

In the following chapter, the work on photo-induced polymerization with cationic mechanism is presented. The study has been focused on the development of an experimental setup capable of producing nanostructured material exploiting the continuous aerosol process. In particular, attention was dedicated to the design of the formulation to be sprayed and on the effect that its composition has on the final morphology and properties of the material. Methods and some of the reported results have been published (Bazzano *et al.*, 2017).

Chapter 5

On the use of Molecular Dynamics simulations for the selection of the formulation for the aerosol polymerization

Production of structured particles via aerosol photo-induced polymerization is the result of various phenomena involved in the process. Monomer reaction, diffusion of the reacting species and phase separation are in fact equally contributing to the production of different structures.

In order to try to discern between the various contributions, a separate study on phenomena involved was carried out using Molecular Dynamics (MD). Although the use of classical MD does not provide the possibility to model electron exchange, namely reaction, mass transport phenomena such as diffusion and phase separation can be studied. Therefore, this study was meant to access the impact of formulation recipes on diffusion behavior of the reacting species.

In this part of the work, the results of MD simulations were preliminary used to guide the productions of polymeric material resulting in porous structures and capsules. However, the complete procedure of particles synthesis and the description of the

experimental apparatus can be found in § 6.1, were the whole experimental campaign is reported.

5.1 Molecular dynamics: overview

Molecular Dynamics history is older than one can imagine. The idea to exploit calculation methods to access trajectory of few particles and, thus, determine their reactivity and behavior goes back to the ’30 with the work from Hirschfelder, Eyring and Topley (1936). In this study, the trajectories of simple monoatomic or biatomic molecules were calculated, without of course any computer aided system, to study their reactivity.

Nowadays, the interest is more focused on physical aspects of large boxes with thousands of molecules. The pioneers of this approach were Alder and Wainright, that in 1959 simulated liquids made of hard spheres atom models, using an “electronic computer” to solve “the simultaneous equation of motion” (Alder & Wainwright, 1959).

Along with developments in computing resources, the promising features of MD for simulations of biological systems was rapidly recognized and in the middle ’70 the first works appeared on proteins simulations (Gelin & Karplus, 1975). From that time on, the number of MD studies on biological systems increased exponentially and today lots of properties of proteins and other complex biomolecules are calculated from MD simulations (Karplus, 2003).

MD simulations found applications also outside of biological systems. Polymeric molecules are, indeed, not so different from proteins which are repetitions of units as well. Therefore, MD was applied to study polymeric systems and, in particular, to predict physical properties of polymers in solution or hydrogels (Ahlrichs & Dünweg, 1999; Paradossi *et al.*, 2011).

5.2 Aim of this work

MD has been applied to study the impact that formulation composition has on mass transport phenomena. In particular, the attention was focused on the transport of reacting oligomers within the solution. The software used in these simulation was Gromacs (version 5.0.7), an open source program well-known especially in simulation of biological systems. The molecules diffusivity (*D*) of the oligomers was evaluated using two different tools.

The first tool is related to spatial conformation of the atoms of the molecule. Radius of gyration (R_g) is defined as the root-mean-square of the distance of the molecule atoms from the molecule center of gravity. It is a measure of the effective size of the polymer

molecule. Radius of gyration is generally different from the length of the fully stretched chain, usually defined as contour length (Flory, 1953). A Gromacs tool (*gyrate*) is able to evaluate the radius of gyration from the coordinates file of the simulated system. This parameter can be used in Stokes-Einstein equation to determine diffusivity of the molecule:

$$D = \frac{k_B T}{6\pi\eta R} \quad \text{(Eq. 3)}$$

where D is diffusivity in m^2/s, k_B is Boltzmann constant in J/K, T is temperature in K, η is the fluid viscosity and R is the radius of the particle that is diffusing within the liquid. R can be substituted with R_g, which is a measure of the actual dimension of the molecule in the liquid system. Knowing the viscosity of the solvents mixture, one is capable of determining *D* from Eq. 3 (Einstein, 1956).

A second method for diffusivity evaluation uses the molecules trajectory files of the simulation in order to calculate the mean square displacement (MSD) of the molecule through time. MSD of a single particle is defined as follows:

$$MSD = \langle (x(t) - x_0)^2 \rangle \quad \text{(Eq. 4)}$$

where x(t) is the position of the atom at time t and x_0 is the position at t=0. A Gromacs tool (*msd*) evaluates the displacement of each atom of the molecule and, thus, gives a value of MSD through simulation time, which must be long enough to reach steady state. MSD can be then associated to diffusivity by the following correlation:

$$MSD = 6Dt \quad \text{(Eq. 5)}$$

which states that, in a system with only Brownian motion, MSD divided by time is constant at the steady state and is equal to six times diffusivity. This correlation is known as Einstein relation. Using these two methods, diffusivity can be calculated from simulations and associated to the morphologies given by experimental work, thus determining whether diffusion is the system controlling parameter or not, and if changes of this parameter impact on process dynamics.

5.3 Numerical methods & simulation set-up

In the first part of the study, new molecules were defined and tested in order to confirm that their behavior was similar to the one experimentally observed. Both the monomer/oligomer and solvents were defined by a coordinates and a topology file.

Coordinates files were built using Avogadro (version 1.1.1), an open source program that enables the construction of molecules and builds a relative coordinates file. Topologies were defined for each molecules using topology files of similar molecules found in literature as a reference.

OPLS (Optimized Potential for Liquid Simulation) force field was adopted for the simulation. The All Atom (OPLS-AA) version was used. This force field has been developed and optimized for simulation of organic liquids and peptides in liquid solution (Jorgensen *et al.*, 1996; Kaminski *et al.*, 2001). However, OPLS has been applied also in polymer simulation. Densities and glass transition temperatures (Metatla and Soldera, 2006) as well as elastic properties (Valavala *et al.*, 2007) have been obtained using this force field. Interactions of polymeric material with solvents, both as gel and as solute, have also been studied using OPLS (Tamai *et al.*, 1996; Godawat *et al.*, 2010).

Once all the molecules in the system were defined, simulations of cubic boxes were carried out using different conditions depending on the objective of the simulation. Different tools were used to build the simulation boxes:

1. *insert-molecules*: addition of the solute (usually the oligomer chains).
2. *solvate*: filling in the box with solvent molecules.
3. *editconf*: changing dimension of the box in order to adjust the initial density or to gain more space for addition of another solvent.

Simulation of the box could then be started. Three pre-run steps were carried out in order to equilibrate the system before the actual simulation. *grompp* tool was used to launch the runs. These were all defined by a .mdp file which contained the parameter of each run:

1. *Energy Minimization* (EM): it acts on the conformation structure of each molecule excluding every non-bonded interaction.
2. NVT: it simulates the ensemble keeping number of particles (N), volume (V) and temperature (T) constant.
3. NPT: it simulates the ensemble keeping number of particles (N), pressure (P) and temperature (T) constant.

Once the system was ready, the MD simulation took place. Despite a different name, MD is still a NPT simulation. Different parameters of the .mdp file had to be chosen in order to optimize the calculation outcome:

- *integrator*: md (leap-frog integrator).
- *nsteps*: varied in the range within 100,000 up to 30,000,000.
- *dt*: timestep, it varied depending upon the type of system.
- *nst* (*xout*, *vout*, *energy*, *log*, *xout-compressed*): it defines the frequency of data saving and was not fixed.
- *continuation*: yes (continuity with the previous NPT run)
- *constraint_algoritm*: lincs (holonomic constraints)
- *constraints*: all-bonds (all bonds are contraints)
- *cutoff-scheme*: Verlet
- *rcoulomb*: 1.0 (electrostatic cutoff, nm)
- *rvdw*: 1.0 (van der Waals cutoff, nm)
- *coulombtype*: PME (Particle Mesh Ewald for long-range electrostatics)
- *pme_order*: 4 (cubic interpolation)
- *fourierspacing*: 0.16 (grid spacing for FFT)
- *tcoupl*: V-rescale (modified Berendsen thermostat)
- *tc-grps*: names of the compounds in the system
- *tau_t*: 0.1 (for every compound, time constant for the energy transport)
- *ref_t*: 300 (reference temperature, K)
- *pcoupl*: Parrinello-Rahman
- *pcoupltype*: isotropic
- *tau_p*: 2.0 (time constant for the pressure coupling)
- *ref_p*: 1.0 (reference pressure, bar)
- *pbc*: xyv (periodic boundary conditions, 3D)
- *gen_vel*: no (velocity generation is off)

Post-processing of data was different depending on which property was evaluated. In the following paragraphs, the most important evaluations will be explained.

5.3.1 Mass density

Mass density evaluation was useful as a proof that the defined molecules behave in a similar way as they do in nature. In order to access this property, the *energy* tool was employed. It is able to analyze energies as well as other properties like density, total pressure and pressure tensor. Boxes with dimension of 7x7x7 nm were filled in with a large number of molecules of the same type, ranging from 3000 up to 5000. Initial density was significantly below the experimental one. This was due to the impossibility to get an efficient molecule packing during insertion in the box and, therefore, a simulation is needed to induce it. It must be noticed that all materials were in liquid form at the simulated conditions.

5.3.2 Viscosity

In order to study how molecules behave from a transport phenomena point of view, viscosity was evaluated using *tcaf* tool. Simulation boxes were built with the same method used for density evaluation. After a preliminary simulation of 20-30 ns, carried out in order to reach equilibrium within the box, a further short simulation with a narrow timestep and more frequent data saving was implemented. Output files from this second run were used in *tcaf* tool to calculate pressure tensor and, thus, solvent viscosity.

The *tcaf* tool is able to estimate the shear viscosity, η, from autocorrelation functions of the transverse currents in the cubic box. η values are obtained as fitting parameters. A function dependent on the calculation vectors (k-vectors) is used for the fitting and its limit for k → 0 gives the final η value (Palmer, 1994).

5.3.3 Diffusivity

Diffusivity of compounds was evaluated using two different approaches. In the next paragraphs, we will briefly discuss about these two ways of calculating the same property.

In every simulation on oligomer behavior, however, five different molecular weight molecules will be used. These are possible outcomes of polymerization reaction and were built with Avogadro following a constant scheme, see Figure 38.

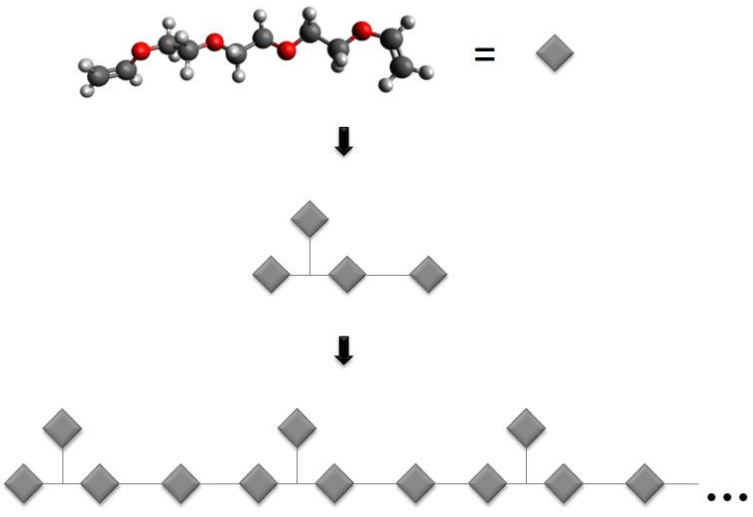

Figure 38. Schematics of molecules building.

5.3.3.1 Radius of gyration and Stokes-Einstein equation

Conformation of the molecule within the solvent can be used to access its mobility in the systems, namely its diffusivity. The parameter that was used as measurement of particles dimension was the radius of gyration, defined as a mean of the atoms distances from the molecule center of gravity.

$$R_g = \sqrt{\frac{1}{N_a}\sum_{i=1}^{N_a}(x_i - x_{mean})^2} \quad \text{(Eq. 6)}$$

where N_a is the total number of atoms in the molecule, x_i is the *i*-th atom coordinate and x_{mean} is the coordinate of the center of gravity (Flory, 1953). This parameter varies during the simulation. It starts from a random conformation, which was the ones used during its manual built up, and changes towards the equilibrium one that is dependent on the interactions with the solvent. Once the equilibrium conformation is achieved, only minor fluctuations are present. R_g can be used, then, in Stokes-Einstein equation (Eq. 3), together with temperature and viscosity, to obtain diffusivity, in case of Brownian motion, of a particle with equivalent radius. In this case, viscosity was calculated using an empirical correlation (Kendall and Monroe, 1917):

$$\mu_{mix} = \left[\sum_{i=1}^{n} y_i * (\mu_i)^{1/3}\right]^3 \quad \text{(Eq. 7)}$$

where y_i is mass fraction of the *i*-esim component, μ_i is the dynamic viscosity of the *i*-esim component in Pa*s, *n* is the number of components and μ_{mix} is the mixture dynamic viscosity expressed in Pa*s. Dynamic viscosity of the single component was obtained both by literature and by simulation (see § 5.3.2). However, the literature values were used in this calculation.

Another important correlation, in which R_g is present, is the Flory equation defined as follows:

$$R_g = MW^{\alpha} \quad \text{(Eq. 8)}$$

where MW is molecular weight of the molecule and α is a correlation coefficient. This is an empirical equation that was developed by Flory using high MW linear polymers (Flory, 1953). Nonetheless, an attempt was made to use this equation to study the high or low solvation effect of the solvents mixture on the oligomer. In particular, α values were taken into account. Following Flory's results, α varies from 1/3, in case of bad solvent, up to 2/3 in case of good solvent. It can be seen as a measure of the tendency of the polymer to unfold and expose its atoms to solvent interactions.

5.3.3.2 Mean square displacement

MSD can be used to determine diffusivity simply by applying Einstein's relation, see Equation 5. Gromacs has a dedicated tool for the calculation of MSD from trajectory files of the simulation: *msd*. It averages MSD over the whole set of atoms of the molecules. The major advantage of this way to calculate MSD is that it is implicitly taking into account viscosity of the solution. Thus, it does not need a separate specific simulation to calculate this other parameter. Results of this post-processing calculation were plotted on a MSD/6*t* vs. 1/*t* cartesian graph, where *t* is simulated time. An example of outcome of this study is given in Figure 39.

Two situations were observed: a ballistic section in which MDS/6*t* decreases while time increases, and a steady state section in which MSD is directly proportional to time. In the second section, MSD/6*t* is constant and, following Eq. 5, is equal to diffusivity.

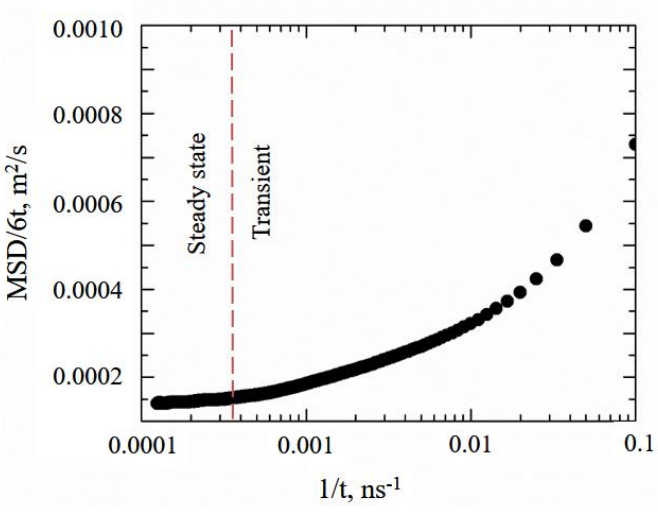

Figure 39. Example of result from Gromacs' *msd* calculation.

5.4 Results

In this section, the main results of this MD study will be presented and discussed. At first, the topology file is validated, i.e. the molecular structure of the reacting species, upon some basic properties such as mass density and dynamic viscosity. Then, an environment similar to the one of droplets during reaction will be simulated and results on transport phenomena will be presented.

5.4.1 Mass density

Three steps of pre-run were simulated and in the last one (NPT) a significant reduction of the box dimensions is already observed, thus shifting towards higher bulk density. MD simulation results were post-processed and results are reported in Table 12 along with literature values and relative errors (Lide, 2007).

In Table 12, it can be seen that the simulated densities of boxes filled with pure compound were fairly in agreement with literature values. This is particularly important because the initial box was really diluted and the NPT-like simulation caused a shrinking of the system that equilibrated to the final reported value. Thus, the first proof of agreement with reality was achieved.

Table 12. Mass densities of liquids as observed by MD simulation and from literature. Values at 20 °C.

Compound	Simulated mass density, kg/m^3	Experimental mass density (Lide, 2007), kg/m^3	Error, %
DVE3	1002.57	990	1.27
Hexadecane	791.45	773	2.39
2-octanone	840.91	819	2.68
2-ethylhexanol	833.14	831	0.03

5.4.2 Viscosity

The viscosity of pure components was evaluated in order to confirm that the new defined molecules possessed transport behavior similar to the one observable in nature. Results are reported in Table 13.

Results showed that simulated viscosities of pure compounds were similar to experimentally ones. Relative errors were a bit higher than the ones obtained in density calculation but the evaluation of viscosity from MD simulation is usually trickier. Indeed, *tcaf* tool can be used for simulation of pure compounds at low pressure.

Table 13. Dynamic viscosities of liquids as observed by MD simulation and from literature (Lide, 2007). Values at 20 °C.

Compound	Simulated viscosity, cP	Experimental viscosity, cP	Error, %
DVE3	2.956	2.64	11.97
Hexadecane	3.271	3.025	8.13
2-octanone	0.878	0.840*	4.52
2-ethylhexanol	5.931	6.20	4.34

** value extrapolated from literature values at different temperature*

5.4.3 Diffusivity

In this section both radius of gyration and mean square displacement results will be briefly discussed.

5.4.3.1 Radius of gyration

Radius of gyration of the monomer and different molecular weight oligomers was calculated using *gyrate* tool. In this study, various types of formulations were tested and the behavior of the propagating oligomer was evaluated. Simulations were divided into two groups based on the type of formulation that was simulated: formulations for porous particles or for capsules.

In all simulations, R_g varied through time until a steady state value was reached. The molecule, which was built in a random conformation, rotates its σ bonds in order to minimize its total energy by increasing or decreasing interactions with the solvent. The macroscopic effect of this phenomenon is the folding and unfolding of molecules. R_g was evaluated as mean of all values fluctuating in the steady state. An example of result is provided in Figure 40.

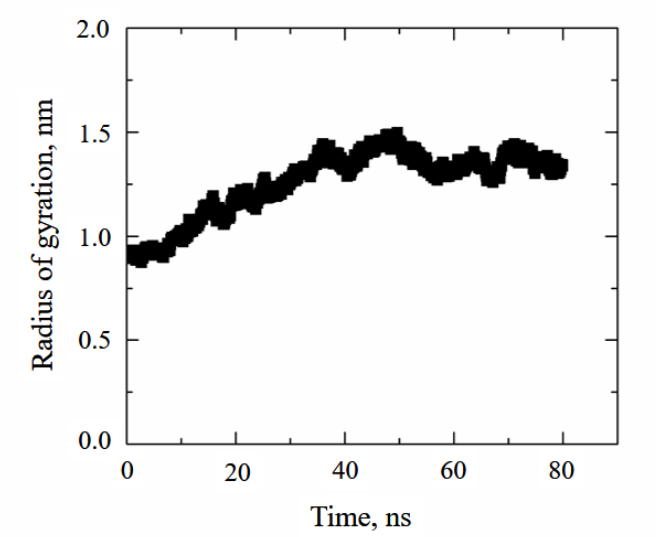

Figure 40. Example of R_g dynamic during simulation time.

As to the formulations for porous particles, different recipes identical to the experimental ones were simulated, changing the ratio between solvents and the monomer amount. A complete list of simulated systems for porous particles is provided in Table 14. The attention was focused on the use of a solvents mixture containing a polar and a non-polar solvent. Thus, the idea was to vary the ratio between these two solvents in order to promote or hinder phase separation.

Table 14. List and recipes of simulated systems (concentrations reported as mass%).

Sample	Exp. Name	DVE3	hexadecane	2-octanone	Solvents ratio
S1	P6	70	5	25	5
S2	P5	70	10	20	2
S3	P4	70	15	15	1
S4	P3	70	17.5	12.5	0.71
S5	-	67	17	16	0.94
S6	-	60	26	14	0.54
S7	-	60	20	20	1

In the first part of the study, using 70% oligomer, solvent ratio was varied within 0.71 to 5. As it will be further discussed in Chapter 6, values lower than 0.71 experimentally led to phase separation during formulation preparation and, thus, were not simulated. In each of these systems, different length oligomers were simulated ranging from 1 up to 32 repeating units. Results on the impact that solvents ratio had on R_g are reported in Figure 41.

In Figure 41, it can easily be seen that the solvent ratio has a strong impact on the behavior of the molecule while it grows. Data were fitted using a power law, which corresponds basically to Flory's Law (Eq. 8). Values of the exponent ranged from 0.48 up to 0.64, within the same suggested range of the Flory exponent. A trend was observed in the values of α and it was reported in Figure 42. An asymptotic trend could be observed in α values while increasing solvent ratio. This was reasonable since 2-octanone was a good solvent of the monomer, while hexadecane was used as phase separator. The highest value of α was 0.649, in agreement with Flory's Law which sets 0.667 as the upper limit. On the other hand, the lowest value was 0.480, which was rather high for a system in incipient phase separation. It must be taken into account, however, that Flory's Law is valid for linear polymers with higher MW. Thus, in our system, with a relatively short chain, which was also slightly branched, it was reasonable that molecules ability to fold might be hindered or simply less evident. The values of α in each recipe were compared with morphologies obtained by spraying the same formulation in the aerosol photo-reactor. Results of this comparison are shown in Figure 43.

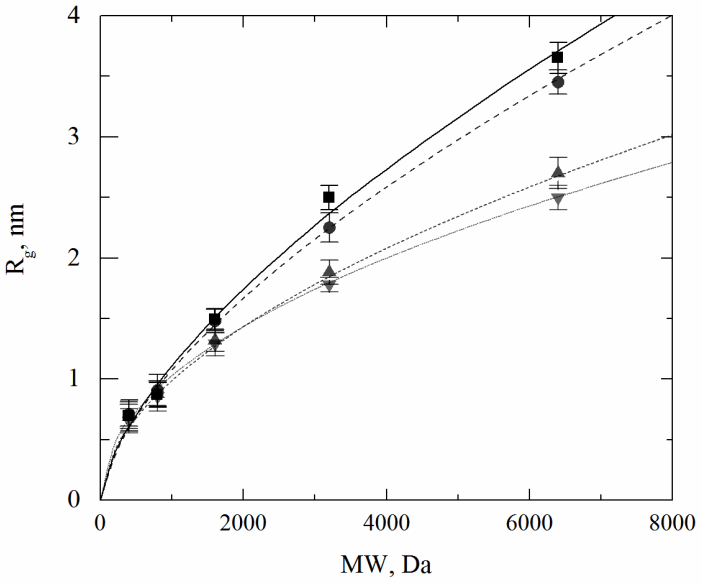

Figure 41. Radius of gyration vs. oligomer MW and the formulation type: (▼) S4, (▲) S3, (●) S2 and (■) S1. Markers refer to mean values and error bars to standard deviations.

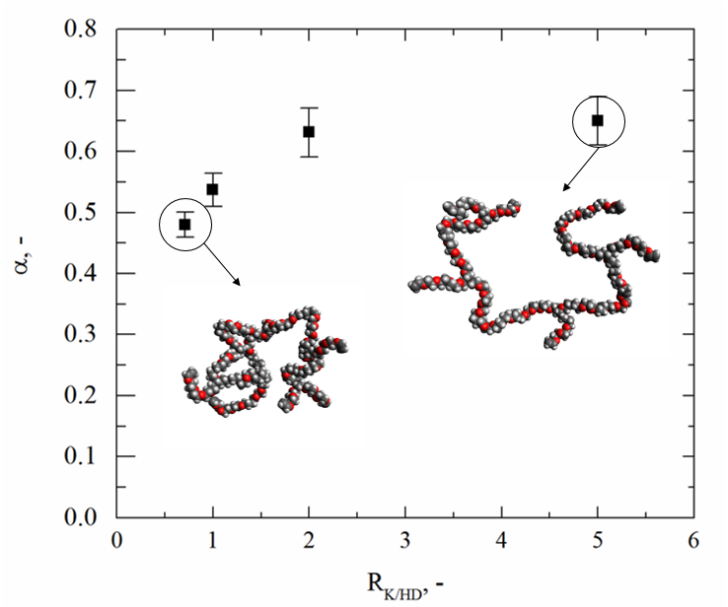

Figure 42. Values of α vs. the solvent ratio $R_{K/HD}$. Markers refer to mean values and error bars to standard deviations. Within the graph area are also reported two examples of oligomer conformation at the equilibrium in the case of $R_{K/HD}$= 0.71 and $R_{K/HD}$= 5.

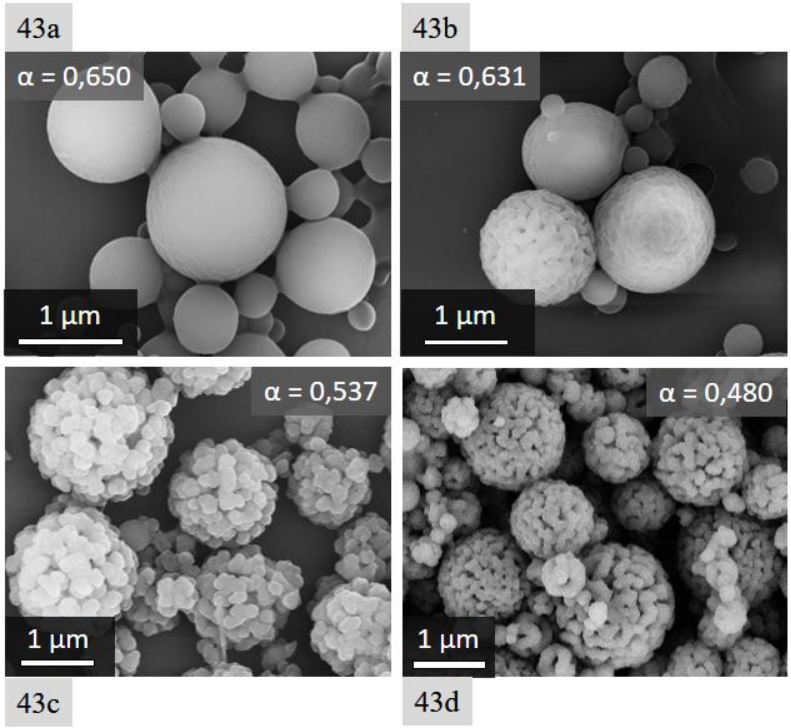

Figure 43. Comparison between α and the particles morphologies as observed experimentally: (a) S1, (b) S2, (c) S3 and (d) S4.

Interestingly, different values of the α exponent corresponded to different types of morphology. This suggested that phenomena related to molecules conformation, for example diffusivity, and solvent interaction are crucial in the structuring of particles. In particular, at high α values, particles morphology did not appear porous, whereas for values lower than 0.6 it could be observed a porous structure. Finally, porous structures were different for α values of 0.537 and 0.480. These results confirmed, to some extent, the initial thesis of the importance of phase separation control. In this system, as already discussed, there were no solvents able to interact with the reaction process. Thus, interaction between polymer and solvents from a solvation point of view was crucial in the structuring event and this study on calculation of this impact will be confirmed by the experimental work shown in Chapter 6.

Using Stokes-Einstein equation diffusivity of different molecular weight oligomer in different environment was calculated. This calculation was necessary in order to obtain a key parameter for the study on structuring of particles. While α values could be linked with solvation of molecules, this correlation is hindered by non-matched hypotheses between simulation and Flory's theory. Therefore, to support the weak evidence given by evaluation of α, diffusion was evaluated. Calculation of dynamic viscosity was carried out using Eq. 7. Results are reported in Figure 44.

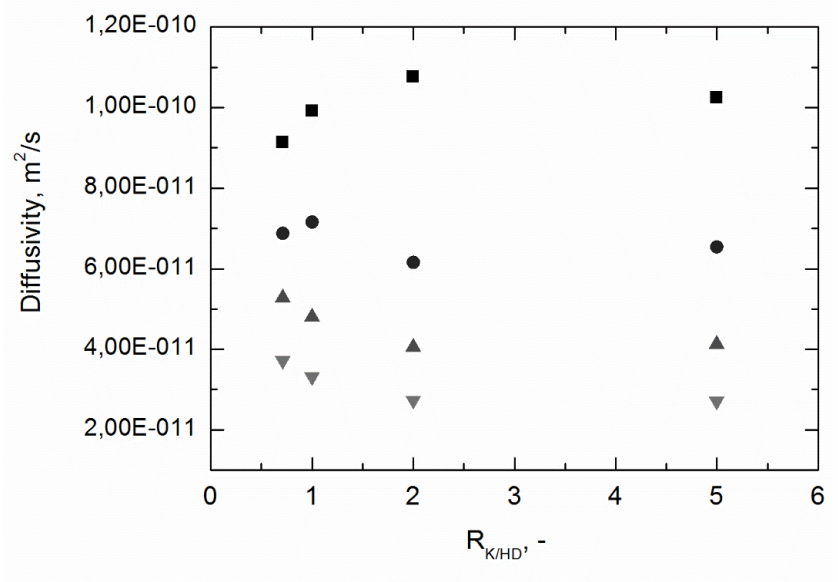

Figure 44. Diffusivity of oligomers vs. solvent ratio and their MW: (■) 800, (●) 1600, (▲) 3200 and (▼) 6400 Daltons. Markers refer to mean values and error bars to standard deviations.

Results highlighted how, while increasing molecular weight of the oligomer, formulation composition becomes crucial for a high diffusivity of the reacting specie. At the beginning, for a MW lower than 1000 daltons, diffusivity was almost independent of $R_{K/HD}$. Once MW increased up to 3000 and above, a trend in diffusivity could be observed. In particular, at low $R_{K/HD}$, diffusivity was enhanced by the folded conformation of the molecule, which was more likely to phase separate. This difference in diffusivity between the formulations might be the reason for the different morphologies that could be obtained. Results on diffusivity confirmed, then, the outcomes of the study on R_g behavior and α evaluations.

The impact of monomer concentration on oligomer behavior was studied by simulating systems with decreasing monomer amount. Results are summarized in Figure 45. These rather surprising results showed that decreasing monomer amount, the oligomer molecule tends to stretch more. This could be due to a lower viscosity of the formulation or the increased amount of 2-octanone, which seemed to be a better solvent, for the oligomer, than the monomer itself. To investigate this aspect, viscosity was calculated and diffusivity in such a system was evaluated, see Figure 46. Viscosity resulted dependent on monomer concentration in the formulation and decreased while decreasing DVE3 amount. This trend, however, did not hinder the increase in diffusivity, see Figure 46b, while increasing monomer amount. It seemed, then, that the solvent mixture was able to cause the oligomer to stretch and thus resulted in a lower diffusivity even if the viscosity was lower.

As confirmation of this behavior, in Figure 47 FESEM images of particles are shown as obtained with 70% and 60% of monomer, using a $R_{K/HD}$ ~1 in both cases. The morphology of particles confirmed, to some extent, the behavior observed in MD calculations. Particles obtained with lower monomer amount appeared as big clusters of weakly interconnected polymer domains. This situation was similar to the one of particles obtained with 70% of monomer, but in this case the interconnections were even weaker than before and most of the material appeared as separate non-spherical polymeric domains. Clusters were indeed so big that were probably the result of agglomeration during solvent evaporation for samples preparation in the FESEM chamber. As suggested in literature, this type of morphology was the result of delayed phase separation (Sherrington, 1998) and that was in agreement with MD calculations, which suggested a better solvated system.

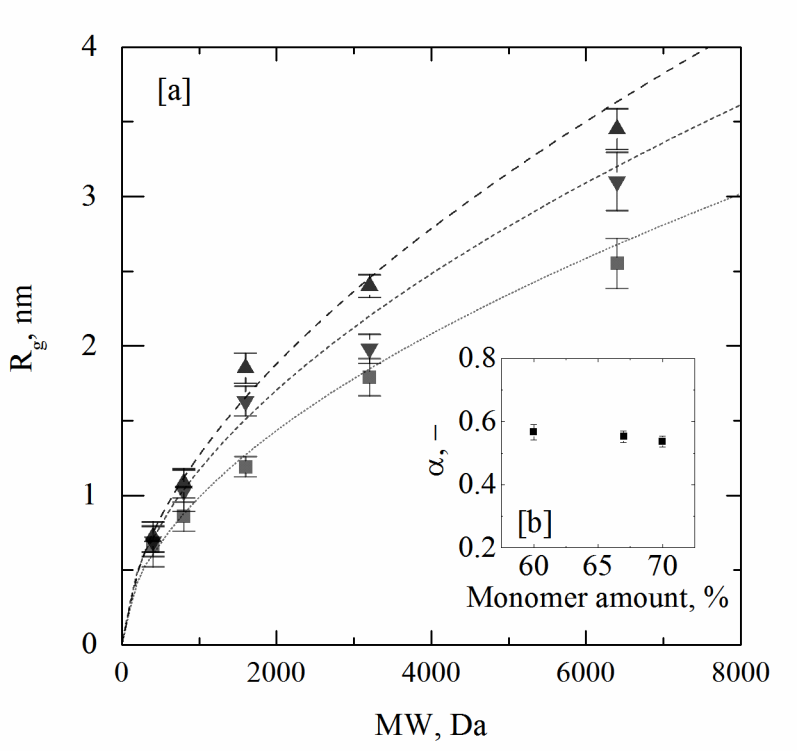

Figure 45. (a) Radius of gyration vs. oligomer MW and formulation type: (■) S3, (▼) S5 and (▲) S7. (b) A values vs. the monomer concentration. Markers refer to mean values and error bars to standard deviations.

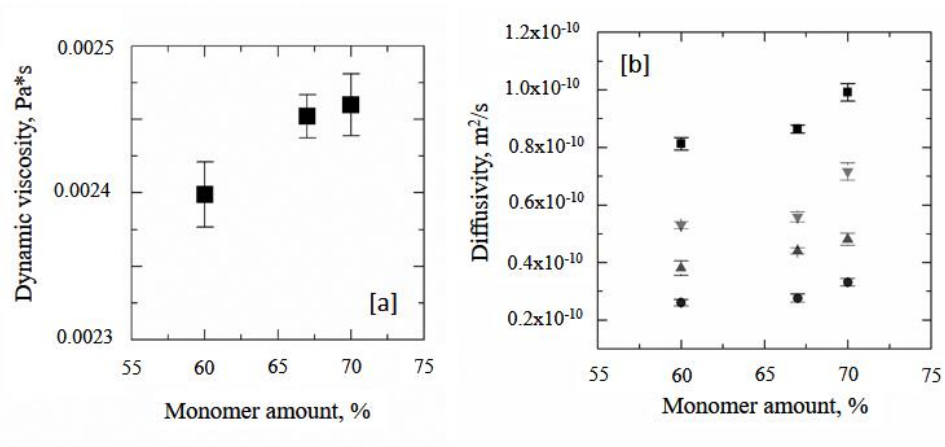

Figure 46. (a) Viscosity vs. the monomer concentration. (b) Diffusivity of oligomers vs. the monomer concentration and MW: (■) 800, (▼) 1600, (▲) 3200 and (●) 6400 Daltons. Markers refer to mean values and error bars to standard deviations.

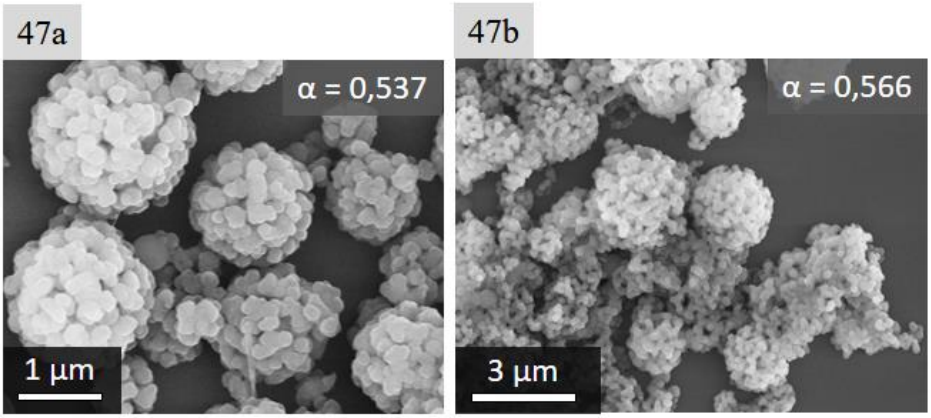

Figure 47. FESEM images of particles obtained using $R_{K/HD}$=1, with (a) 70% and (b) 60% monomer.

As to the formulations for production of capsules, the same type of study was carried out. In this case, however, another effect was present and could not be taken into account using MD tools: chain transfer mechanism of alcohol. Thus, the simulation aimed at describing how transport properties changed in presence of the alcohol, but not how the polymeric structure did.

The first set of simulations were carried out in order to study the effect of 2-ethylhexanol to 2-octanone ratio ($R_{A/K}$) on oligomer diffusivity. In the second part of this study, focus was shifted towards the ratio between 2-octanone and hexadecane. List of the simulations is provided in Table 15.

Table 15. List and recipes of simulated systems (concentrations reported as mass%).

Sample	Exp. Name	DVE3	2-octanone	hexadecane	2-ethylhexanol
S8	C14	60	5	25	10
S9	C15	60	7	25	8
S10	C17	60	10	25	5
S11	C16	60	9	26	5
S12	C18	60	7.5	27.5	5

Formulations S8, S9 and S10 were simulated varying $R_{A/K}$, thus studying the solvation effect of two good solvents for the oligomer. Results on the folding/stretching of the molecules are shown in Figure 48.

Similarly to what observed in the formulations for the porous particles, the solvents ratio played an important role in the molecule conformation. Decreasing the $R_{A/K}$ resulted in a lower coefficient of the power law fitting α. Thus, referring to Flory's Law, 2-ethylhexanol proved to be a better solvent when compared to 2-octanone. This, it must be stressed, has nothing to do with its ability to be a chain transfer reagent, but only on its non-reacting interactions with the oligomer. In Figure 48b, values of α are reported at different $R_{A/K}$. An asymptotic trend seemed present, but the studied range was limited by several factors. The $R_{A/K}$ values did not exceed 2 because alcohol amount could not be further increased, due to its high activity in chain transfer mechanism (CTM), which lead to the production of sticky particles. On the other hand, an alcohol amount of 5% was experimentally found to be the minimum to induce a sufficient CTM and thus creating capsules. Therefore, $R_{A/K}$ values lower than 0.5 were not studied.

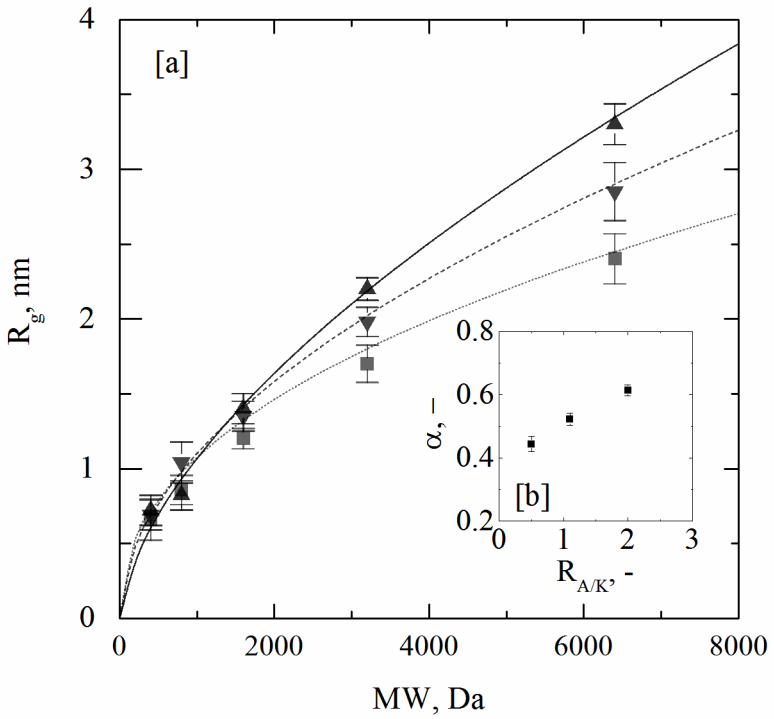

Figure 48. (a) Radius of gyration vs. the oligomer MW and formulation type: (▲) S8, (▼) S9 and (■) S10. (b) α vs. the solvent ratio. Markers refer to mean values and error bars to standard deviations.

The three values of α were, then, compared with their relative particles morphologies. Results are shown in Figure 49. In such a system, as it was already mentioned, other phenomena were as crucial as diffusivity and phase separation, for example CTM. In Figure 49a, the presence of sticky particles can be seen. This is not

related to the calculated high α value but with a high amount of 2-ethylhexanol that caused a strong CTM. For lower $R_{A/K}$ values CTM effect seemed not so strong, see Figure 49b and Figure 49c. Thus, two different morphologies might be the result of different behavior of the oligomer in solution, highlighted by a different α value.

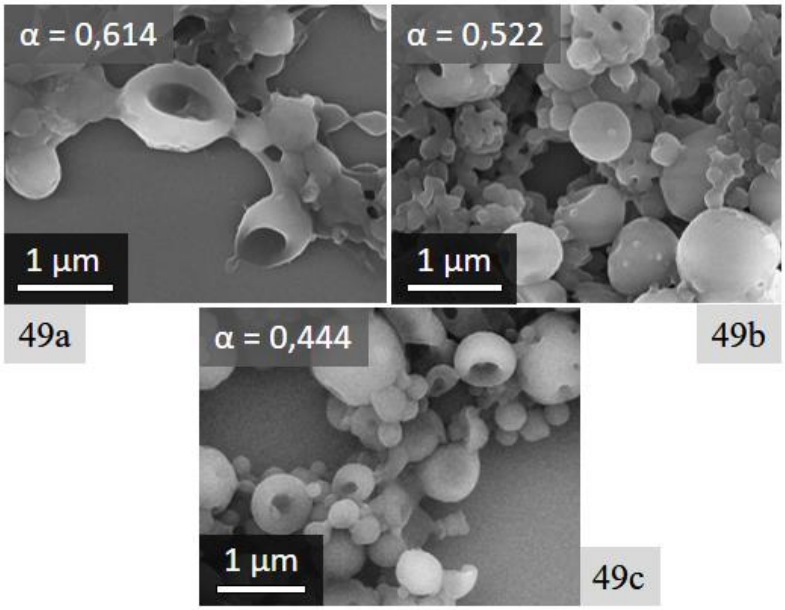

Figure 49. Comparison between α and particles morphologies. Samples prepared using formulation (a) S8, (b) S9 and (c) S10.

Diffusivity of oligomer molecules was evaluated in formulations with different $R_{A/K}$. Viscosities were calculated using Eq. 7 and results are shown in Figure 50. Similarly to what has been observed evaluating α, diffusivity results highlighted a greater mobility of oligomer solvated in 2-octanone rich environment, where the oligomer presented a folded conformation. For low MW oligomers, there was no significant difference between the various values of $R_{A/K}$, but when MW is increased a trend could be observed.

Once the solvation effect of 2-ethylhexanol has been studied, the focus shifted towards a second parameter: 2-octanone to hexadecane ratio ($R_{K/HD}$). A set of simulations similar to the one of porous particles was carried out and results are shown in Figure 51. Post-processing of simulation data showed that $R_{K/HD}$ seemed to have a limited impact on α values. There was an initial slight increase in α while increasing the $R_{K/HD}$, but it was not significant. Moreover, a further increase in the ratio led to a small decrease in α. It must be taken into account, however, that the studied range was limited by all the previous optimization steps.

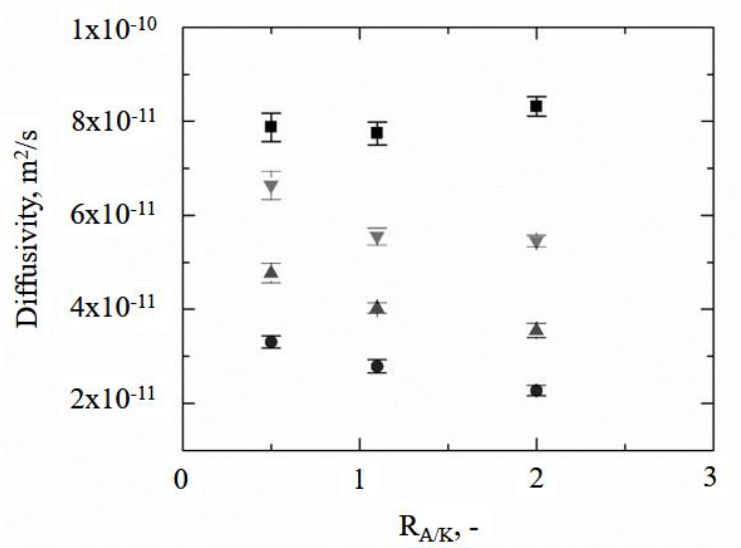

Figure 50. Diffusivity of oligomers vs. $R_{A/K}$ in the formulation and MW: (■) 800, (▼) 1600, (▲) 3200 and (●) 6400 Daltons. Markers refer to mean values and error bars to standard deviations.

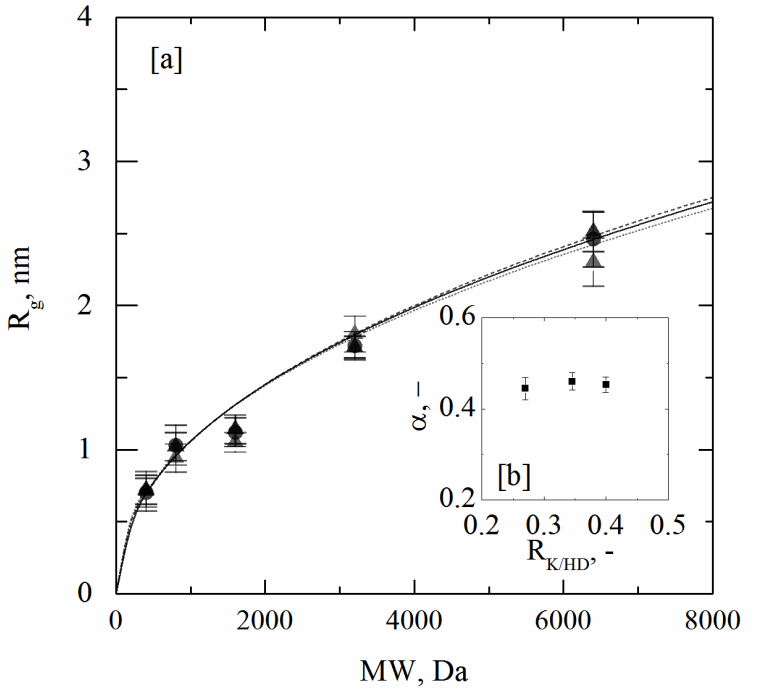

Figure 51. (a) Radius of gyration vs. the oligomer MW and formulation type: (■) S10, (▲) 11 and (●) S12. (b) α vs. the solvents ratio. Markers refer to mean values and error bars to standard deviations.

In Figure 52, the morphologies of samples prepared using formulation S10 and S12, namely the extreme of the studied range, are shown. As can be seen, the two samples showed a rather similar morphology with particles possessing few holes on the surface. This might be a proof of the low importance of $R_{K/HD}$ in the studied range. However, collapsed structures were present only in the S12 sample, see Figure 52b, which indeed possessed a lower α value. Wether this is due to an actual difference in transport behavior of the molecules or to some other unknown reasons, such as non-simulated interactions between the various solvents, it could not be said by this type of evaluation.

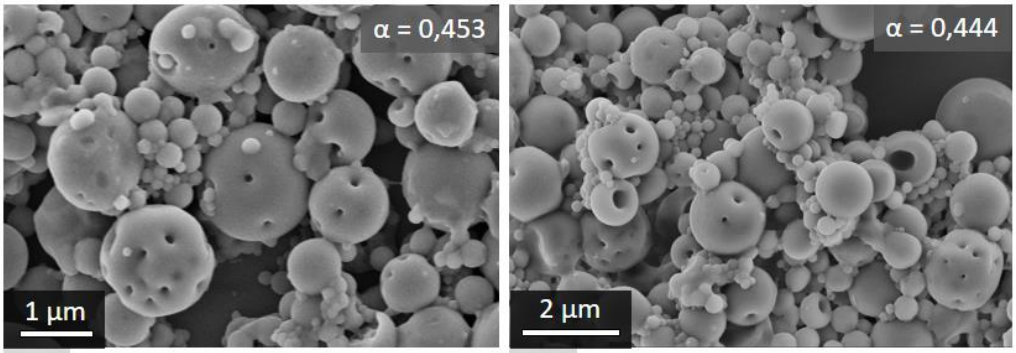

Figure 52. Comparison between α and particles morphologies. Samples prepared using formulation (a) S10 and (b) S12.

To access this property, the same type of evaluation was carried out calculating the diffusivity of oligomers in formulations with different $R_{K/HD}$. Results, shown in Figure 53, pointed out a similar outcome. In the small range of investigation, the value of $R_{K/HD}$ did not have a strong impact on the transport behavior of oligomers.

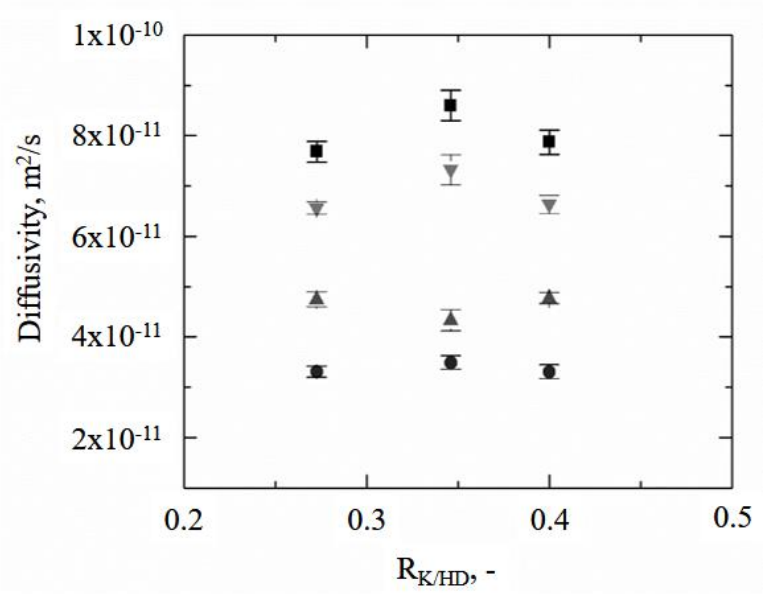

Figure 53. Diffusivity of oligomers vs. $R_{K/HD}$ in the formulation and MW: (■) 800, (▼) 1600, (▲) 3200 and (●) 6400 Daltons. Markers refer to mean values and error bars to standard deviations.

Varying the ratio $R_{K/HD}$, no trend was visible, not even increasing the MW of the oligomer. This was probably due to the narrow studies range, in which no significant change in *D* can be seen. Results of the diffusivity study were, then, in agreement with the preliminary study carried out on the Flory's exponent, which did not show any difference in solvents interaction between the three formulations. Thus, the slight differences between samples obtained with formulation S10 and S12 cannot be ascribed to a significant difference in diffusivity.

5.4.3.2 Mean Square Displacement

Direct evaluation of diffusivity by molecules MSD was carried out in order to confirm the previous results on the various solvents ratio effects. As aforementioned, this evaluation technique was able to calculate diffusivity without a separate calculation of solution viscosity and for this reason could be more accurate. On the other hand, the previous study was able to access also another crucial aspect of the process: solvation effect on the oligomer. Thus, MSD was applied only as a proof of the observed trends and more emphasis was given to the results on radius of gyration. In Figure 54, results of the MSD method and comparison with previous results are provided.

Diffusivities of the oligomer in formulations for porous particles were calculated with both methods and compared. Two important outcomes were easily observable: a trend in diffusivity was visible also in MSD calculation and the MSD results were, on average, five times lower than the ones obtained by Stokes-Einstein equation. The first feature was important to confirm the trend discussed in the previous paragraph and to avoid calculation biases induced by separated viscosity evaluation.

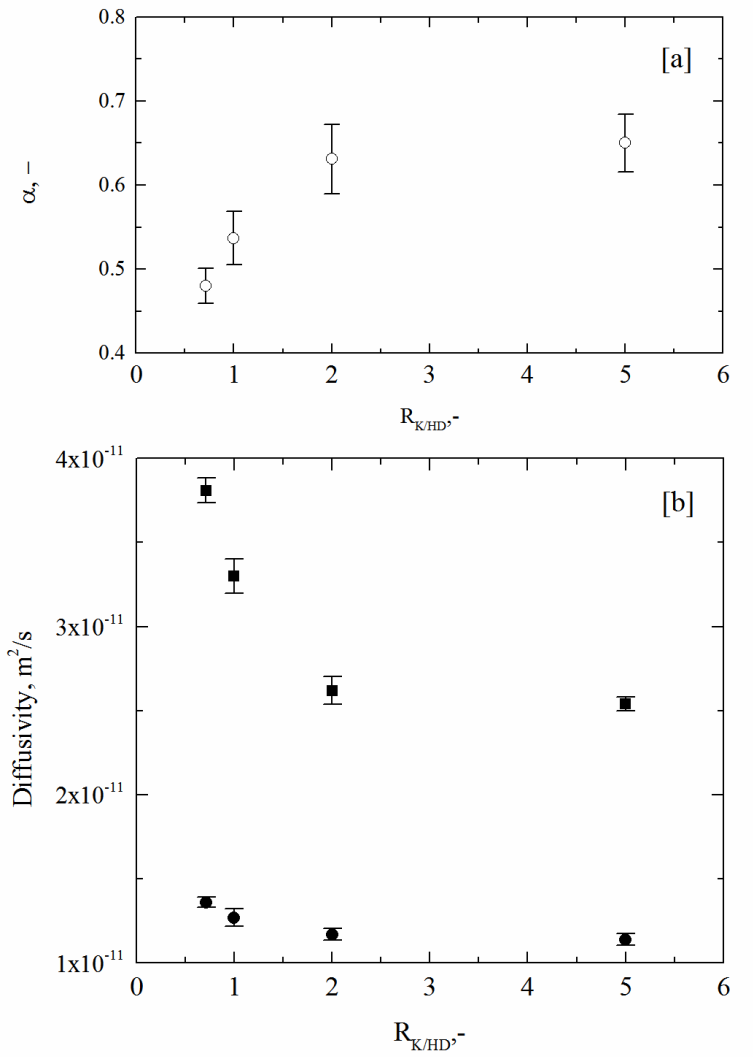

Figure 54. (a) α vs. $R_{K/HD}$. (b) Comparison between diffusivity values obtained by (■) R_g and (●) MSD methods. Diffusivities of the 6400 Dalton MW oligomer are reported vs. $R_{K/HD}$ in the case of porous particles. Markers refer to mean values and error bars to standard deviations.

Big differences between the outcomes of the two methods were systematic and not related to the type of formulation. Thus, it was possible to conclude that probably Stokes-Einstein equation overestimated diffusivity in such system. In fact, it did not take into

account the shape of the object that was diffusing and this might have been a great source of error especially when the actual shapes is a slightly folded chain.

A similar comparison is presented in Figure 55. Diffusivity of the oligomer in the various formulations for capsules was evaluated by both R_g and MSD methods. Similarly to the previous outcomes, diffusivity calculated by MSD methods resulted four or five times lower than the ones given by Stokes-Einstein equation. Moreover, the trend in diffusivity seen with R_g method was maintained in MSD calculation.

As a general result, diffusivity calculated by both methods showed rather similar and consistent results. Possible errors on viscosity evaluation were not significant and did not alter the variation of diffusivity induced by changes in the formulation.

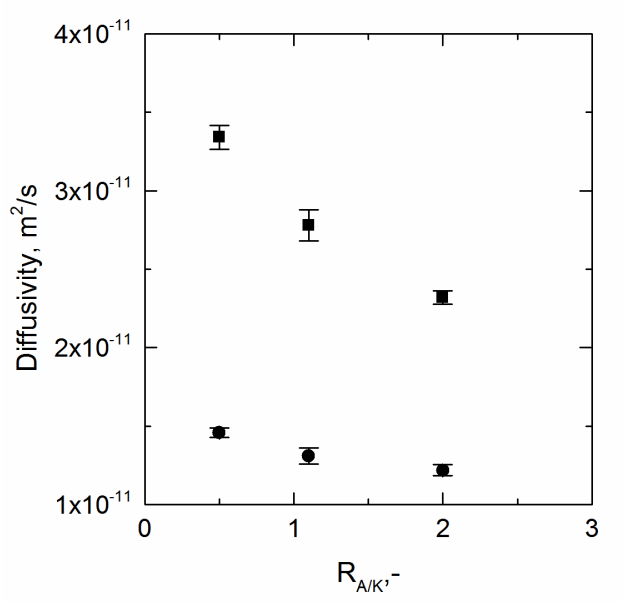

Figure 55. Comparison between diffusivity values obtained by (■) R_g and (●) MSD methods. Diffusivities of the 6400 Dalton MW oligomer are reported vs. $R_{A/K}$ in case of capsules. Markers refer to mean values and error bars to standard deviations.

5.5 Conclusions

In this study, the attention was focused on the evaluation of transport phenomena within the droplets during reaction event. In particular, mobility of oligomer molecules was estimated by diffusivity calculations and the impact of different formulations on this parameter was evaluated.

The exponent of Flory's law, α, was also calculated for each formulation. This was used to preliminarily evaluate how the solvent mixture was able to solvate the oligomer, thus giving an estimation of its behavior with respect to phase separation, which was

crucial for the structuring process. Results highlighted how this parameter varied between different formulations. Morphologies examples were linked to the α value, showing that, specifically in porous particles, it played an important role for the final morphology.

In the study on capsules, a similar work was carried out pointing out how some combinations of solvents could be used to design a fast phase separating system. In this case, however, MD simulations could not take into account the effect of CTR presence, which was crucial for the network structure and, thus, for its mobility during reaction and capsules production. This last aspect will be further investigated for an experimental point of view in Chapter 6.

Chapter 6

Experimental investigation of the photo-induced aerosol cationic polymerization

6.1 Materials & Methods

In this section, data on the reagents used are reported, as well as the procedure used to synthetize polymeric particles.

6.1.2 Materials

All reagents, if not specifically indicated, were purchased from Sigma Aldrich. They were analytical grade and used as received. DVE3 was used as main monomer. Di(ethylene glycol) vinyl ether (VE2) and 2-ethylhexyl vinyl ether (EHVE) were chosen as co-polymers in some tests. All these monomers possess a PEG-like backbone and were selected in order to avoid immunogenic response. The selected photo-initiator was triarylsulfonium hexafluoroantimoniate salt (TAS-HFA), purchased from BASF. It is the

critical compound of the formulation, possessing many risk phrases. Therefore, in case of drug delivery, its concentration must be carefully designed. Solvents added to the initial monomer solution are reported in Table 16. Regarding hexadecane, previous toxicological tests on nanoparticles filled with this solvent proved the absence of significant toxicity properties (Bazzano *et al.*,2016). The other solvents can be easily evaporated, as will be discussed in the following section. However, most of them are safe to handle, for example 2-octanone is used as flavoring ingredient for food.

Table 16. List of the solvents used in the initial formulation.

Name	IUPAC name	Purity
hexadecane	hexadecane	>99%
acetone	propan-2-one	>99.9%
2-butanone	butan-2-one	>99.5%
2-octanone	octan-2-one	>98%
hexanol	hexan-1-ol	>99%
isooctanol	2-ethylhexan-1-ol	>99.6%

Nitrogen gas was withdrawn from a cylinder (Air Liquide, Paris, France) and its purity was higher than 99.999%. Curcumin was chosen as example of active ingredient. It was purchased in powder form, with a purity of ~65%. Absolute ethanol (purity>99.8%) was used to extract curcumin from the powder.

6.1.3 Particles synthesis and equipment

Particles synthesis was carried out using an experimental setup that consists of a pneumatic atomizer (ATM 220, Topas GmbH, Dresden, Germany) and a quartz tube photo-reactor, see Figure 56. The monomeric formulation was prepared by dissolving a given amount of monomer into different solvents, varying the ratio between the various compounds present. The PI was added as last compound, to avoid pre-polymerization before spraying.

The initial formulation was strongly dependent on the expected outcome of the polymerization process. The morphology of the final particles, in fact, was given by the interplay of various phenomena such as phase separation, diffusion of the reacting

material, reaction rate and gelation rate. To obtain porous material, two solvents were added: hexadecane and 2-octanone. The first one was a non-polar solvent and therefore was used as "bad solvent" for the growing PEG-like material. On the other hand, 2-octanone was a rather polar solvent, which was considered as "good solvent" for the reacting system. By varying the ratio between these two solvents, it was possible to create an environment in which phase separation could be promoted or slowed down.

Since the objective is the production of capsules, it must be remarked that the high reactivity of the bi-functional monomer hinders the production of the polymeric shell. At the same time, a crosslinked material is necessary to obtain mechanically stable and well defined particles that do not stick together. To solve this problem, a further solvent was added in order to delay gelation of the product and give more time to the reacting oligomers to migrate towards the border of the droplets during phase separation. In addition to hexadecane and 2-octanone, an alcohol was added since the –OH group is able to subtract carbocations from the propagating species. The alcohol acts as chain transfer reagent (CTR) delaying the gelation of the polymeric system and lowering the final amount of gel (Sangermano, 2012). Two different alcohols were tested as CTRs.

The overall amount of solution that was prepared for each tests was between 18 and 25 mL. This value was given by the clearance between the bottom of the flask, in which the solution was held, and the Venturi system tube that drove the solution to the nozzle. Schematic of the system is provided in Figure 56b.

Within the nozzle, once the solution is atomized, there is a system to recirculate the bigger droplets that are generated. An elbow forces a direction change in the aerosol flow and the droplets, that are strongly subject to inertia and, thus, are not able to follow the direction change, impact on a plate. The aerosol is carried, by the nitrogen flow, through a tubing system and to the reactor inlet, see Figure 56a. Reactor (R1) consist of a cylindrical quartz tube (length 440 mm, inner diameter 52 mm) surrounded by 6 UV fluorescent lamps (length 420 mm) positioned at 50 mm from the reactor wall. The excimers emit light with a peak at wavelength of 308 nm and the measured irradiance is approximately 5 mW/cm^2.

The mean residence time of droplets inside the photo-reactor depends upon the nitrogen gas pressure applied in the nozzle. Using a nitrogen overpressure of 1 bar, from supplier data it is known that the mean residence time varies within 50 to 60 s. Applying a higher pressure results in shorter residence time, whereas overpressures below 1 bar can extend this parameter. Uncertainty on the mean residence time are given by the type of atomized solution, in particular by its viscosity and, thus, by the mean diameter of the droplets. A different droplets size results, in fact, in different cross sectional area and therefore in different drag acting on the droplets.

At the reactor outlet, the solid aerosol was collected with different devices. Polytetrafluoroethylene (PTFE) membrane filters were used to collect the total sample during the study on particles size distribution. Two different types of membranes were

used: one with 200 nm pore diameter and the other with 50 nm pore diameter. These devices added a further pressure drop to the system slowing down the aerosol flow. Furthermore, they proved to be critical in some experiments because of clogging problems.

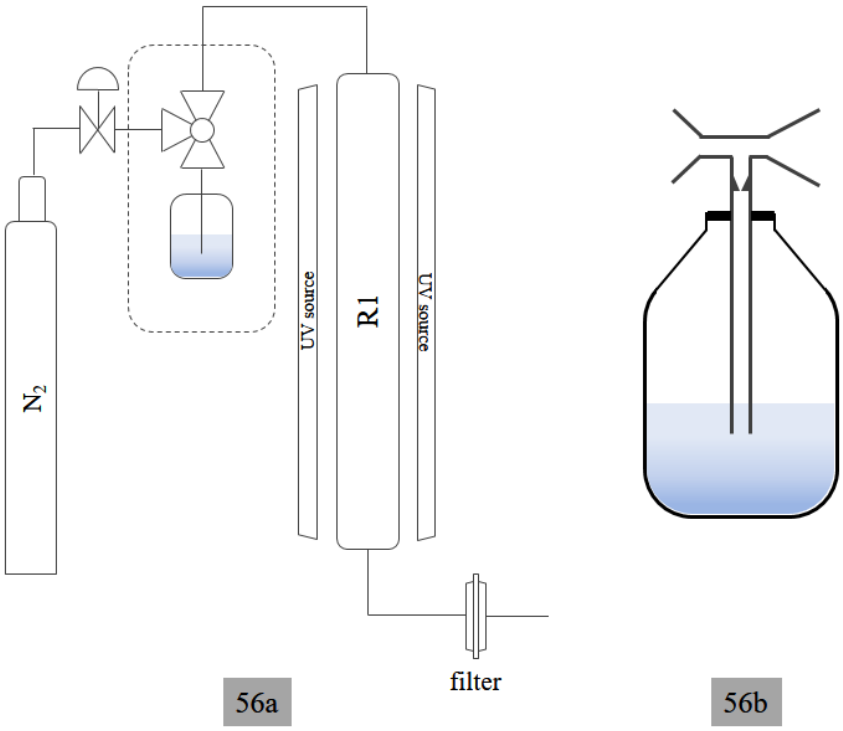

Figure 56. Schematics of (a) the production system and (b) the solution withdrawing system. In the upper part of the tube, a schematized nozzle and Venturi system are shown.

In other cases, aluminum plate was used as binder in order to avoid clogging and the slowing of nitrogen flow. The plate was positioned in contact with the outlet reactor tube and inertial collision was exploited for the separation of the product from the nitrogen flow. It was used in those tests were the morphology was the only important parameter, since it was not able to block the smaller particles that followed the nitrogen stream.

6.2 Results

In the following section are summarized and discussed the results of the study on structured particles obtained by aerosol photo-induced polymerization.

6.2.1 Dimension and morphology

Effect of nitrogen gas pressure

As first experiment, spherical non-structured particles were produced in order to use them as a blank and determine the population size distribution at specific injecting conditions. Formulation was prepared with 98% DVE3 and 2% TAS-HFA, nitrogen pressure was held at 1 bar and the formulation was sprayed for 1 h. PTFE membrane with 50 nm pore size was used to collect the material. The FESEM images and the particle size distribution of this production are shown in Figure 57.

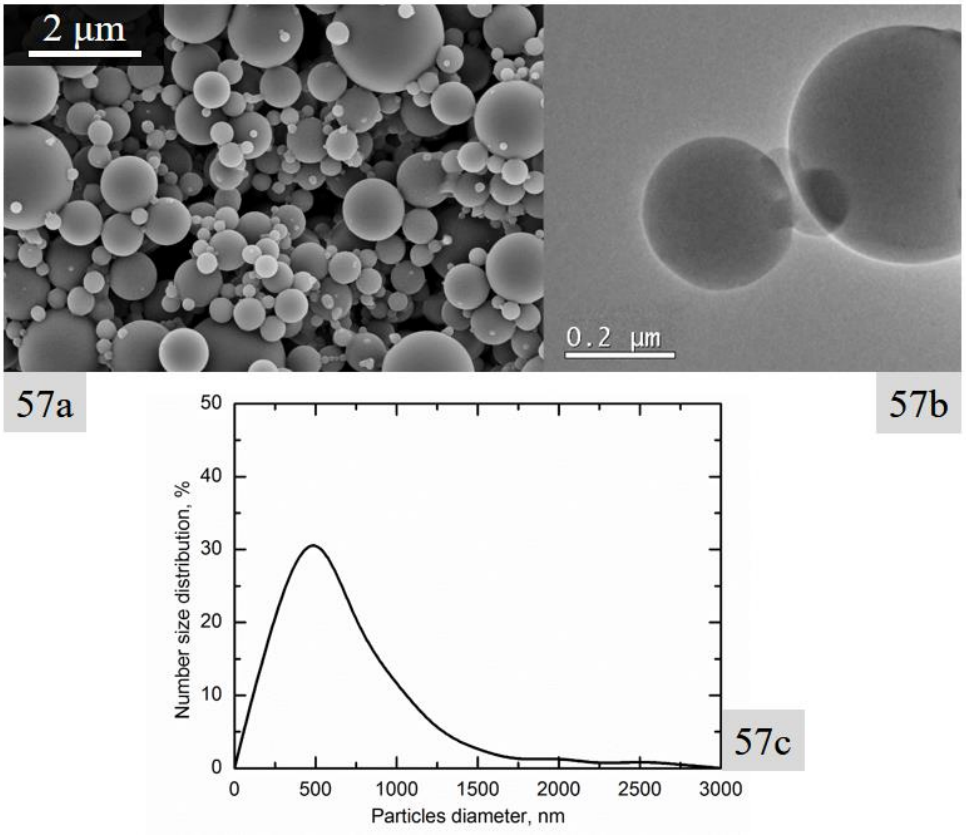

Figure 57. (a) FESEM image, (b) TEM micrograph and (c) size distribution of sample prepared with 1 bar nitrogen pressure. The starting formulation is made of 98% DVE3 and 2% TAS-HFA.

The FESEM images showed that the particles range from few hundreds of nanometers up to 4-5 µm. The TEM analysis was carried out in order to have an insight of the inner part of the particles. Micrographs confirmed that the product consisted of full solid particles, without any visible internal structure. The size distribution analyses were carried out on more than 200 particles and the results highlighted the presence of a quite polydisperse sample, with a peak in frequency at ~ 500 nm.

To access the impact that nitrogen pressure has on the nozzle performances and, thus, on the particle size distribution, tests at different overpressures were carried out on the same formulation. Pressure was varied from 0.5 up to 2.5 bar, in Figure 58 some examples of results are shown.

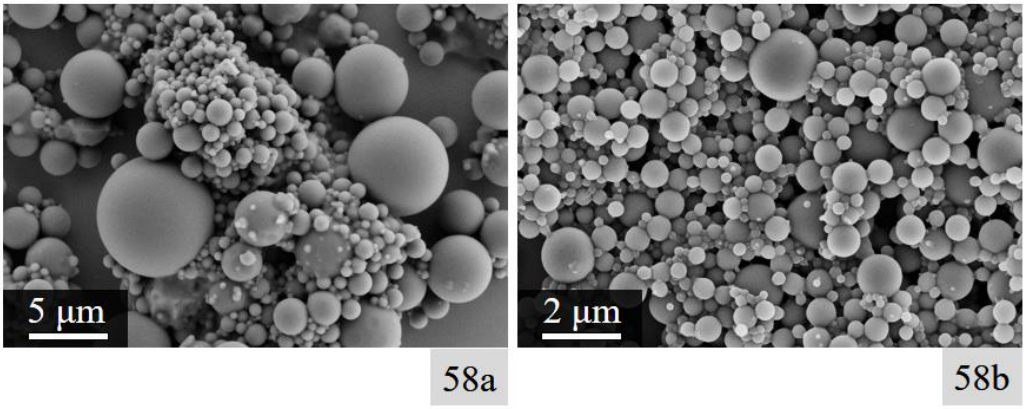

Figure 58. The FESEM images of samples prepared with nitrogen overpressure of (a) 0.5 bar and (b) 2 bar. The starting formulation is made of 98% DVE3 and 2% TAS-HFA.

In Figure 58, it is possible to see a certain improvement in the monodispersity of those samples produced at higher nitrogen overpressure. Particles population produced at 0.5 bar, see Figure 58a, showed dimensions ranging from hundreds of nm up to almost 10 µm, whereas the largest particles in Figure 40b have diameter in the range of 1 to 2 µm. Analyses on the mean diameter of particles and the size distribution of the samples were carried out to confirm this preliminary discussion and the results are reported in Figure 59.

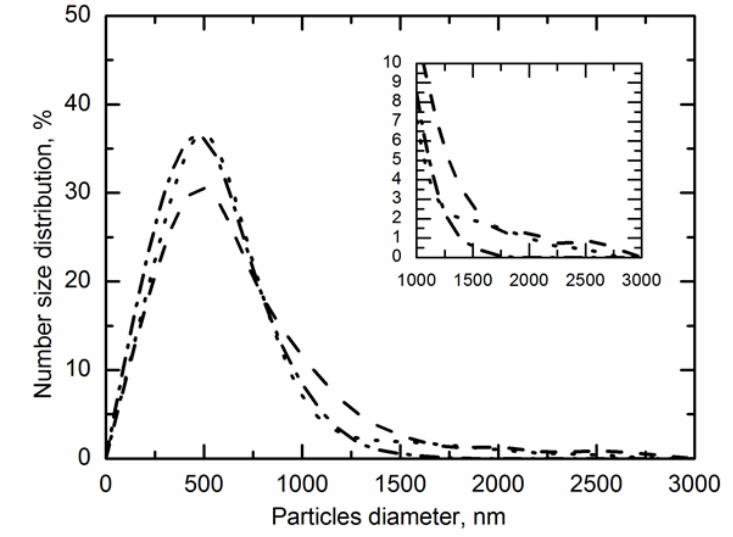

Figure 59. Numeric frequency distributions of samples produced at (·····) 0.5 bar, (-----) 1 bar and (·-·-·) 2 bar. The enlargement of the distributions for larger dimensions is also provided.

In Figure 59, results suggest that overpressure has no impact on the most likely dimension of particles. Nonetheless, it has an impact on the presence of particles with large dimension. In the enlargement of Figure 59, in fact, it is possible to see the absence, in samples prepared with a gas overpressure of 2 bar, of particles with dimension larger than 1.7 μm. On the other hand, particles that are produced at lower nitrogen overpressure had larger diameters. It must be underlined that the distributions are numerical, thus, even if the percentage of larger particles is low, the overall volume of large particles is not negligible. For this reason, the possibility to act on the nozzle pressure to obtain samples without larger particles can be crucial in the development of the technique.

Production of porous particles

During morphology studies, the first part of the work was committed to the production of porous polymeric material. As already explained, this goal was pursued using a mixture of two solvents to induce phase separation during the reactor passage.

First experiments were carried out using different types of solvents in order to find the best ones. Hexadecane was chosen as non-solvent since it has been thoroughly studied as phase separation reagent in many polymeric systems (Vadalia *et al.*, 1994; Müller and Smith, 2005). Different good solvents for DVE3 were tested in order to access their solvating effect in the system. Ketones were chosen since there are generally good solvents for rather polar substances. Three low molecular weight ketones were tested:

acetone, 2-butanone and 2-octanone. In Figure 60 examples of particles produced with DVE3, hexadecane and ketone are shown.

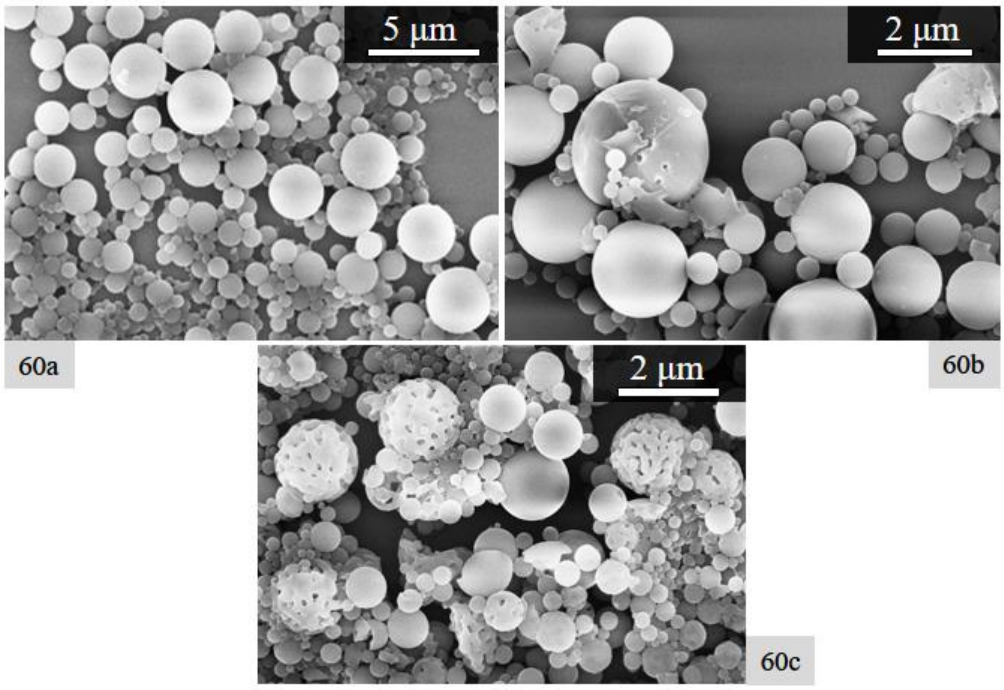

Figure 60. FESEM images of particles obtained using ~70% DVE3 and a mixture of hexadecane and (a) acetone, (b) 2-butanone and (c) 2-octanone.

As can be seen in Figure 60, not all the ketones could induce a proper phase separation. Particles prepared with acetone were spherical, without neither signs of pores nor structuring, see Figure 60a. This could be explained by a dramatic evaporation of the solvent during the solution atomization, with a consequent phase separation before the reaction that led to the production of spherical particles without pores on the surface. On the other hand, it might be that some hexadecane droplets were stuck in the particles core, were evaporation is less likely to take place.

Increasing the ketone molecular weight, namely using 2-butanone, led to a product with many particles with visible defects on the surface and, in case of broken particles, also in the inner part, see Figure 60b. The explanation of this phenomenon was found in a slower evaporation of the good solvent, which is less volatile than acetone, and in a higher compatibility of the 2-butanone with the monomer compound. In fact, solubility tests pointed out that a lower 2-butanone quantity was needed to solubilize DVE3 and hexadecane, if compared with acetone.

As last test, 2-octanone was used as good solvent, see Figure 60c. In the FESEM image, some particles with surface pores can be seen, while other particles appear to have

a smooth continuous surface. The presence of both porous and solid particles was ascribed to the incipient non-uniformity of the solution that, after few minutes of spraying, separated into two phases within the flask.

Among the ketones applied for the structuring, 2-octanone was the one that gave the most interesting results. It was the most compatible solvent. For 2-octanone, in fact, the amount of solvent required to homogenize a DVE3-hexadecane mixture was almost half of that used for 2-butanone case. Moreover, 2-octanone proved to be capable of inducing a phase separation and the production of porous particles. Finally, it must be highlighted that the best results in terms of structuring were achieved with the less volatile of the ketones, suggesting that pores formation is not cause by expansion upon evaporation but rather by a phase separation in liquid state. For these reasons, 2-octanone was chosen as good solvent for the following experiments.

Once the two solvents for the production of porous particles were chosen, a series of tests was designed. Experiments were carried out with an almost constant mass percentage of DVE3 as monomer and different amounts of hexadecane and 2-octanone. It must be taken into account that in this section all the tests were carried out on constant PI-to-monomer mass ratio, which was held constant at 0.01. Therefore, even if it is not specified, the PI amount was already considered in the DVE3 mass percentage. List of the performed experiments is given in Table 17. Solvents ratio was defined as the ratio between the mass of the ketone (2-octanone) and that of the paraffin (hexadecane).

Table 17. Formulations prepared varying the ratio between hexadecane and 2-octanone. DVE3 mass percentage was held constant at 70%.

Formulation	Hexadecane (mass%)	2-octanone (mass%)	Solvents ratio
P1	30	0	0.00
P2	20	10	0.50
P3	17.5	12.5	0.71
P4	15	15	1
P5	10	20	2
P6	5	25	5
P7	0	30	-

Being hexadecane a bad solvent for the monomer, experiment P1 did not result in a homogeneous solution and, therefore, the solution was not sprayed. Nonetheless, it was

important to study the whole range of possibilities with those two solvents. In order to reach homogeneity, 2-octanone mass percentage was increased.

Solution P2 was still non-homogeneous. In order to study the effect of a 0.5 solvents ratio, the formulation was slightly changed, using 73% DVE3, 18% hexadecane and 9% (w/w) 2-octanone. With this recipe, the solution seemed enough homogeneous and it was sprayed. An example of result is given in Figure 61. Particles reported in Figure 61 were characterized by a certain degree of porosity, even though the whole sample did not appear homogeneous. Both solid spherical particles and particles with surface indentation were recognized among the porous ones.

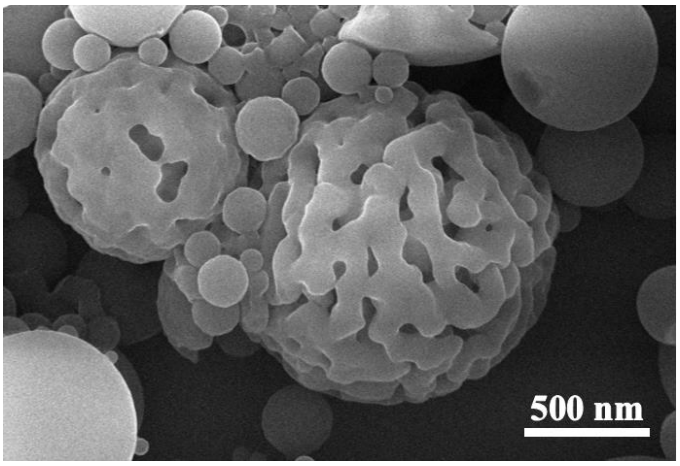

Figure 61. FESEM image of particles prepared with 73% DVE3, 18% hexadecane and 9% 2-octanone.

Starting from experiment P3, the solutions were homogeneous and were used for particles production. In Figure 62, results obtained with formulation P3 are shown.

Sample prepared with formulation P3 and nitrogen pressure of 1.5 bar showed a porous structure. Particles were still spherical, but FESEM images revealed the presence of pores on their surface, see Figure 62a. Interconnected polymer domains were visible in the images and formed the particles porous structure. Nucleation of solid domains in the droplet was caused by phase separation during the reaction and, thus, a precise control over this phenomenon was crucial for the design of particles structure. In particular, some literature study highlighted the importance of the phase separation time with respect to the polymerization time. If the first phenomenon happens fast during reaction, the remaining liquid is still rich in monomer, while if the phase separation is delayed the liquid phase is dilute in monomer. This plays an important role on the interconnections between the polymer domain that separated from the liquid, after the reaction is completed (Sherrington, 1998).

TEM analyses performed on this sample, see Figure 62b, showed that the porous structure was present on the surface of the particles as well as in the inner part. Moreover, this happened also in those particles with dimension below 500 nm.

Size distribution evaluation, reported in Figure 62c, showed an increase in the most probable dimension of particles when compared to the one characteristic of particles prepared without solvents. In particular, the peak is shifted from ~480-500 nm towards ~700 nm. Moreover, particles with diameter within 1.5 to 2 µm are present with higher percentage than the samples prepared with only DVE3. This could be due to a worse atomization process or to a coalescence of droplets prior to droplet-to-particle conversion. Presence of solvents should lower the overall viscosity, therefore making easier the atomization step. Thus, the increase in average particles size might be due to droplets coalescence.

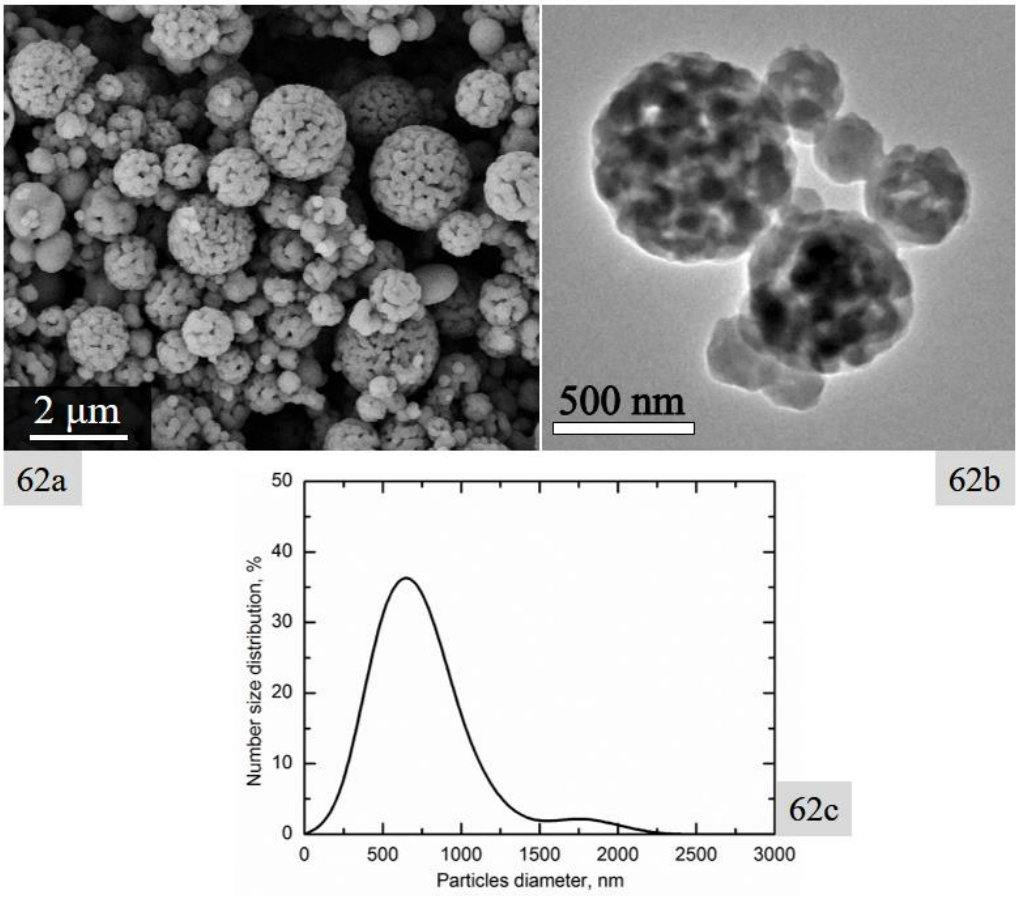

Figure 62. (a) FESEM image, (b) TEM micrograph and (c) relative size distribution curve of sample prepared with formulation P3.

The ratio between the two solvents was varied, formulation P4 was prepared with equal mass fraction of hexadecane and 2-octanone, using 1.5 bar nitrogen pressure. Results of the FESEM analyses are reported in Figure 63. Particles morphology was significantly different from the previous sample. Particles were still rather spherical, but were made of dozens of weakly connected polymer domains. This was in agreement with the observation of Sherrington (Sherrington, 1998). In this formulation, richer in 2-octanone, the solubility of the growing polymer in the solvent mixture was higher and thus phase separation was supposed to take place later than in the previous formulation. Thus, the separating solid was bigger and the liquid was less concentrated in monomer. Therefore, in the last part of the reaction, weak polymeric connections were obtained between the domains.

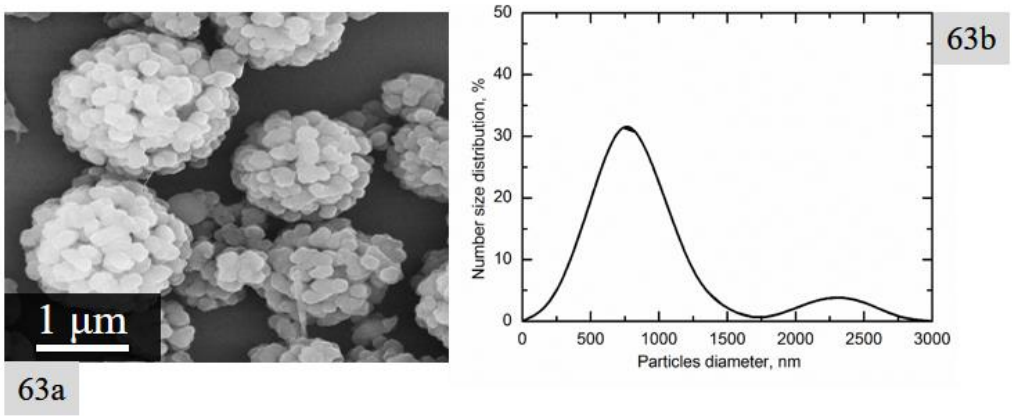

Figure 63. (a) FESEM image and (b) relative size distribution curve of sample prepared with formulation P4.

Particles size distribution was similar to the one obtained with formulation P3, with the most likely dimension around 700 nm and the presence of a further peak at around 2.3 µm. This high dimension peak might be due to a coalescence of droplets within the reactor. In fact, if the phase separation is delayed, homogeneous droplets are more likely to merge, upon contact, than already well defined particles.

Solvents ratio was further increased in formulation P5, where 2-octanone mass fraction was double than the one of hexadecane. Results obtained using 1.5 bar nitrogen pressure are shown in Figure 64. Morphology of the sample differed from the one of particles obtained with equal amounts of the two solvents. Particles surface seemed more continuous, without well-defined domains. Superficial roughness was present and in few particles it was possible to see an actual porosity, which however seemed only superficial. Adding a higher amount of 2-octanone, the phase separation was delayed to a later stage in the reaction. This probably led to the production of a solvent swollen crosslinked polymer, with little volume in which phase separation actually took place. Upon drying in the FESEM sample preparation and analyses, a fraction of the solvent

was removed and roughness was produced by partial collapse of the material. Some particles showed a superficial porosity, which might have been the result of a surface evaporation that led to phase separation in this limited outer volume.

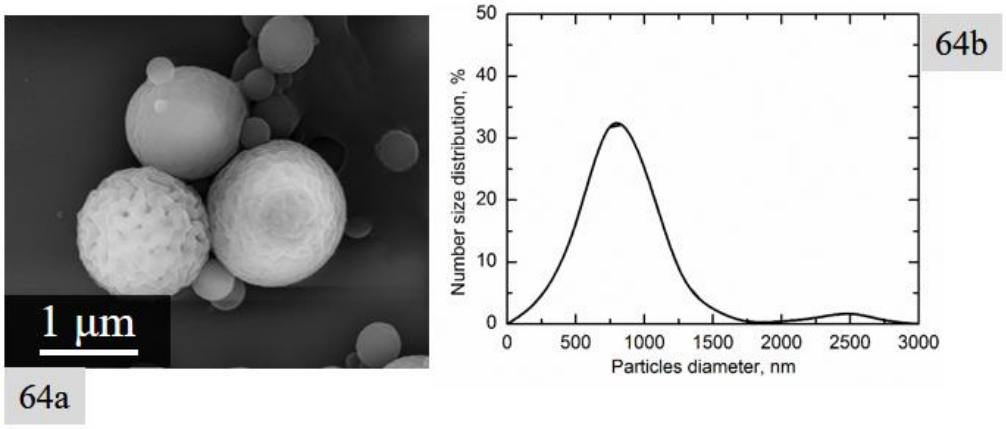

Figure 64. (a) FESEM image and (b) relative size distribution curve of sample prepared with formulation P5.

The size distribution evaluation showed a further increase in mean particles size, see Figure 64b. The most common size shifted towards more than 800 nm, while a second peak was present at 2.5 µm. Since 2-octanone was the less viscous solvent in the mixture, the viscosity of the whole solution decreased by increasing its mass fraction. Thus, the shift towards higher particles dimension cannot be explained by a bigger size of sprayed droplets. Therefore, coalescence of aerosol droplets must have occurred during reactor passage and this might have been facilitated by the delayed phase separation and the consequent absence of rigid structures within each droplet.

With respect to the samples obtained with formulation P6 and P7, no sign of visible structuring were present on particles surface. Probably, in sample P6 the ratio between 2-octanone and hexadecane was so high that phase separation did not take place. Similarly, formulation P7 lacked of any phase separator and, therefore, polymerization was achieved without any visible structuring. So, both the two samples appeared identical to the samples obtained with only DVE3 and PI.

A study about the effect of nitrogen pressure on the morphology was carried out on one of the most promising formulation, namely formulation P3, see Figure 65.

Nitrogen pressure was varied within 1 to 2.5 bar. FESEM analyses were carried out in order to study samples morphology and size distribution. In Figure 65, it was possible to see that different nitrogen pressures did not change significantly the particle morphology. This result was expected, since nitrogen pressure acts mainly on the nozzle performance and, thus, on the droplets size. On the other hand, this parameter had an

impact on the mean residence time of particles inside the photo-reactor. Results showed that a decrease in residence time did not negatively affect the process. Reaction was not hindered by higher nitrogen pressure up to 2.5 bar, even if it led to a residence time shorter than 30 s. This proved that it was possible to obtain a structured material in less than 30 s exposure time to UV light. This feature was crucial for increasing production rate of the process.

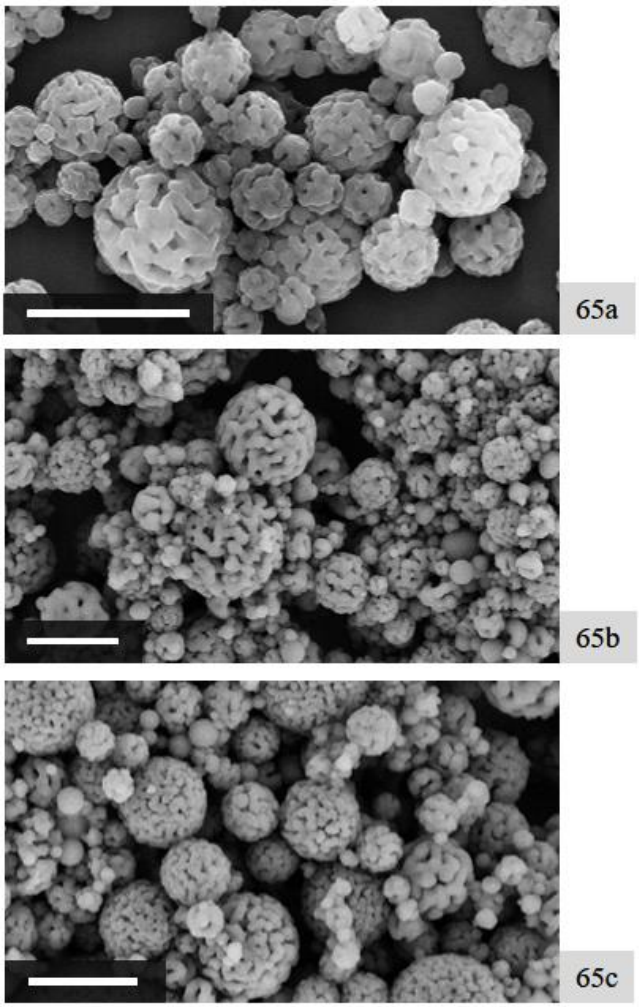

Figure 65. FESEM images of samples prepared with formulation P3 using different nitrogen pressure: (a) 1 bar, (b) 1.5 bar and (c) 2.5 bar. All scale bars refer to 2 μm.

Evaluation of the particle size distribution was carried out to access the effect of nitrogen pressure on the mean particles dimension, see Figure 66. Results showed some differences in size distribution of samples produced with different nitrogen pressure, thus confirming the results obtained in the previous similar study conducted in absence of solvents.

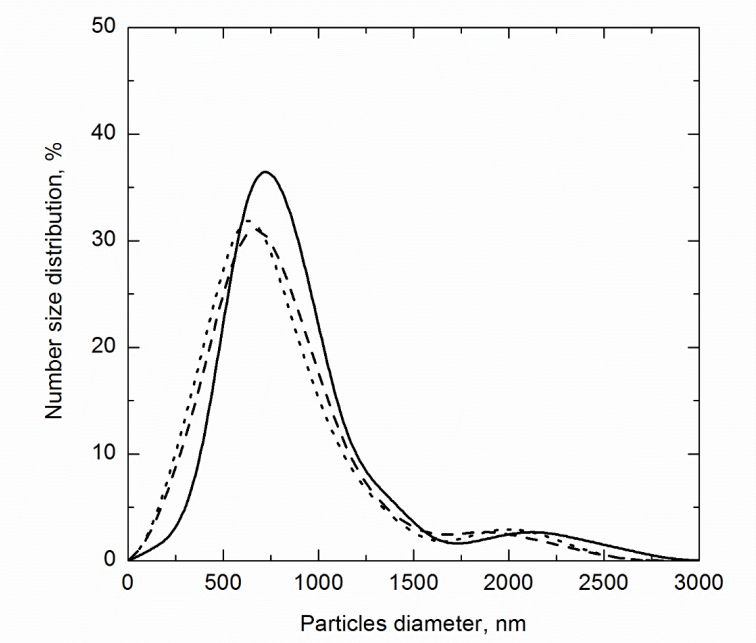

Figure 66. Size distribution of samples prepared with formulation P3 at (—) 1 bar, (---) 1.5 bar and (•••) 2.5 bar as nitrogen overpressure.

An increase in nitrogen pressure led to the production of samples with size distribution slightly shifted towards lower dimensions. In particular, the peak for the sample produced at 1 bar was at ~750 nm, whereas samples obtained with higher pressure showed peaks at 600-650 nm. The evaluation of the larger particles also highlighted an improvement in those samples produced with at least 1.5 bar, namely a slightly reduction in the mean size of the second peak.

Production of capsules-like particles

Production of capsules with dimension below 2 μm was studied, starting from the previous work on production of porous particles and modifying the formulation. Aerosol photo-induced polymerization has already been used for microcapsules production. However, dimension of microcapsules, in that previous study, was nearly ten times higher than the ones investigated using this experimental setup (Esen *et al.*, 1997).

During production of porous particles, phase separation of crosslinked material was promoted and its kinetics was crucial in the structuring process. However, in order to obtain a polymeric shell, it is essential to promote migration of oligomeric or polymeric material to the outer layer of the droplet prior to the gelation of the structure. Otherwise, it is impossible to cause migration and merging of already highly crosslinked material. For this reason, delay of gelation was induced in the reacting droplets. The aim was to

suppress crosslinking, during the early stage of reaction, in order to leave more time to migration of separating oligomers towards the outer layer of the droplet.

This goal was pursued using two different approaches: inducing a chain transfer mechanism or lessening the overall crosslinking sites. Chain transfer mechanism (CTM) was promoted by addition of a compound able to subtract protons to the reacting species. In the case of cationic reaction mechanism, there are many polar compounds that can act as CTR: water, alcohols, etc. These compounds are able to subtract H^+ to the reacting chains and transferring them to other reactive groups. The overall effect of this CTM is an increased reaction rate as well as a reduced total gel content and a reduced crosslinking density at the end of the reaction (Sangermano, 2012). With this technique it is possible to act on the propagation reaction, delaying the gelation of the thermosetting polymeric structure. Another technique that can be used is to act on the amount of PI and, thus, of propagating species. This technique can be combined with CTM in order to compensate the high sequestration of carbocation from the CTR.

On the other hand, the addition of a further monomer can be used to design the structure of the final copolymer. In particular, adding a small fraction of mono-functional monomer can significantly decrease the number of functionalities and, thus, the crosslinking density of the material. This technique acts in a similar way as CTM on the crosslinking but has one major difference. Since, usually, mono-functional monomer are less reactive when compared to the bi-functional ones, addition of a mono-functional monomer can significantly decrease the reaction rate. This effect can cause some issues for less residence time in the reactor, similar to the one that is used in the experimental setup. CTM, instead, increases the reaction rate and this crucial difference must be taken into account when dealing with fast propagating monomers and the evolution of the molecular weight has a strong impact on the structuring process.

In this study, both CTM and copolymerization with a mono-functional monomer were tested in order to obtain the particle structuring in which the polymer constitutes the shell of a capsule.

As first attempt, CTM was adopted and two different alcohols were tested for their ability to delay gelation of the structure: 1-hexanol and 2-ethylhexanol. The effect of alcohol presence on the production of solid particles was tested. A strong CTM, indeed, might cause the production of sticky material with too low crosslinking density. In Table 18, the list of the experiments is reported.

Formulations with different ratios between alcohol and monomer were tested. The aim of these experiments was to access the ability of the two alcohols to cause a CTM and thus preventing crosslinking. Results of this study are shown in Figure 67. It was possible to notice that both compounds caused, after a certain concentration, the production of collapsed structures. 1-hexanol did not show any problem when used at 2% and 5% in mass, while for higher amounts the particles were sticky (C3) or completely blurred. On the other hand, samples prepared with 2-ethylhexanol showed the presence of

clearly distinct non-sticky particles until the concentration of 10%. Samples prepared with 15% in mass of 2-ethylhexanol were sticky, whereas in presence of 20% of the alcohol the sample appeared as sticky indistinct material without a shape. This is supposed to happen because of the dramatic decrease in crosslinking density caused by the CTM (Sangermano, 2012).

Table 18. List and recipes of experiments performed on the alcohol effect.

Sample	DVE3 (mass%)	1-hexanol (mass%)	2-ethylhexanol (mass%)
C1	98	2	0
C2	95	5	0
C3	90	10	0
C4	95	0	5
C5	90	0	10
C6	85	0	15
C7	80	0	20

A further evaluation and comparison between the two types of alcohol was carried out in presence of the phase-separator, namely hexadecane. This test aimed at studying the interaction of the alcohol when phase separation is induced. Moreover, it was also important to know how the two alcohols could be used as good solvents in order to get an homogeneous solution. List of the performed experiments is provided in Table 19. Differences in the formulation using the two alcohols were caused by a different solvating power between the CTRs. In particular, 2-ethylhexanol proved to be a better solvent than 1-hexanol in this system.

Samples morphologies were characterized using FESEM and results are reported in Figure 68. It could be seen that at low solvents concentration some superficial defects appeared. This was mostly evident in samples prepared using 1-hexanol and might be caused by a complete phase separation of hexadecane in a well-defined volume of the droplet. Thus, the polymeric fraction was composed by the result of polymerization in presence of only 1-hexanol.

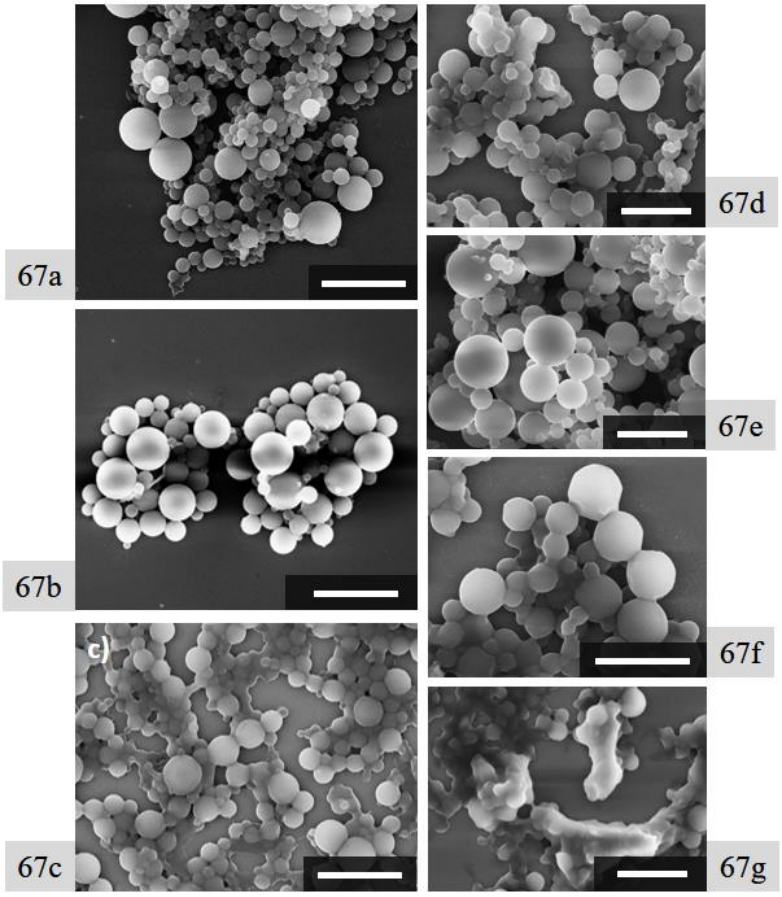

Figure 67. FESEM images of samples prepared with different formulations: (a) C1, (b) C2, (c) C3, (d) C4, (e) C5, (f) C6 and (g) C7. All scale bars refer to 2 µm.

Table 19. List and recipes of experiments performed on the alcohol effect in presence of hexadecane.

Sample	DVE3 (mass%)	Hexadecane (mass%)	1-hexanol (mass%)	2-ethylhexanol (mass%)
C8	80	10	10	0
C9	70	20	10	0
C10	65	20	15	0
C11	80	12.5	0	7.5
C12	70.5	17.5	0	12
C13	60	25	0	15

For higher amounts of alcohol, particles showed the presence of pores on their surface, see Figure 68b and 68e. This porosity, nonetheless, was different from the one observed in samples produced with hexadecane and 2-octanone. The pores were smaller and more rounded. The particles surface was more continuous, if compared to the one of previous porous particles. Since the monomer amount was similar in the two tests, one could conclude that there must have been a higher void in the inner part of the particles. Thus, this represented a step towards the production of capsules.

When the concentration of alcohol reached 15% (w/w) in mass, productions significantly changed their morphology. Particles were sticky and, especially in case of 1-hexanol, the material was gelatinous. Few particles prepared with 15% (w/w) of 2-ethylhexanol, however, showed a partial collapse of the structure, similar to the one that has been shown in literature and linked with a capsule structure (Akgün *et al.*, 2014b). This promising feature, in addition to a higher solvating activity, was crucial for the choice of 2-ethylhexanol as CTR for the second part of the study on capsules production.

As can be seen in Figure 68f, such amounts of alcohol, that are required for the solution homogeneity, led to the production of sticky particles. In order to maintain a relatively high amount of solvents and reach homogeneity without overdosing alcohol, 2-octanone was added as good solvent that does not act as CTR.

Once 2-ethylhexanol has been chosen as CTR, the study was focused on its activity on the polymerization and, especially, on the optimum ratio between monomer and CTR. For this purpose, a series of tests varying the ratio between 2-ethylhexanol and monomer were carried out. A list is provided in Table 20. Starting from a 1:6 ratio, the alcohol amount was decreased up to 1:12. Samples were characterized using FESEM and results are reported in Figure 69.

Particles prepared with 1:6 ratio, as well as the ones obtained with 1:7.5, were sticky. Nonetheless, a structure could be seen in the FESEM images. Few particles, in sample C14, possessed a structure similar to the one that is characteristic of collapsed hollow particles. Particles morphology slightly changed in sample C15, while some particles showed partial collapses similar to sample C14, particles with porous-like morphology were present. This happened especially in the bigger particles, which needed longer times for the complete migration of the polymer and, thus, were more likely to be porous.

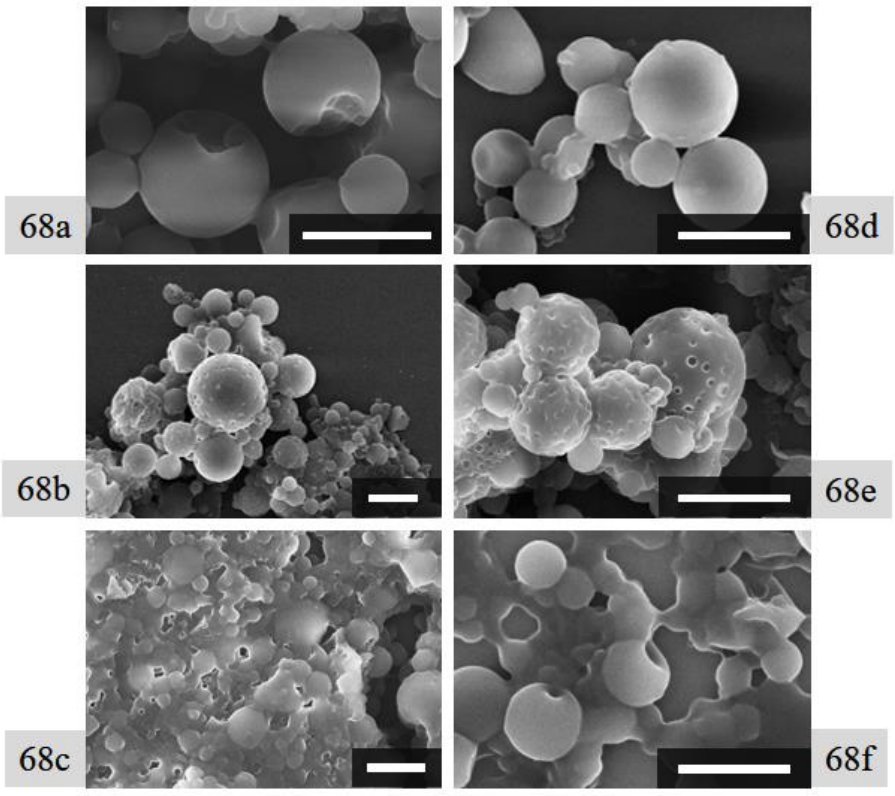

Figure 68. FESEM images of samples prepared with different formulations: (a) C8, (b) C9, (c) C10, (d) C11, (e) C12 and (f) C13. All scale bars refer to 1 μm.

A further decrease in the ratio, see sample C16, led to the production of particles with more spherical shape and continuous surface, with few collapsed particles. Few broken particles, with initial diameter larger than 2 μm, showed the presence of internal non-connected spherical voids. This confirmed the difficulty of getting a proper core-shell separation within the bigger droplets.

The last formulation, C17, showed the best results in terms of morphology. Particles were fairly spherical with some collapsed structures indicating the presence of one main void volume in the inner part of particles (Blomberg *et al.*, 2002). Particles collapse could be due to analyses conditions. In particular, high vacuum in the FESEM chamber can cause a strong evaporation of the solvent entrapped within the particle core, thus causing the structure to collapse. For this reason, the 1:12 ratio was chosen as the most promising one for the next part of the study.

After the study on the alcohol-to-monomer ratio, the formulation C17 was optimized, in order to improve morphology, acting on phase separation and diffusion phenomena. Solvents amounts were varied and the FESEM characterization was performed. Hexadecane amount was increased, while 2-octanone was decreased in order to induce phase separation in the first stage of the reaction. Solubility tests were carried out in order

to design the formulation for the incipient phase separation. Formulation with 60% DVE3, 5% 2-ethylhexanol, 7.5% 2-octanone and 27.5% (w/w) hexadecane (C18) gave the best results, see Figure 70.

Table 20. List and recipes of experiments performed on the alcohol-to-monomer ratio.

Sample	DVE3 (mass%)	Hexadecane (mass%)	2-octanone (mass%)	2-ethylhexanol (mass%)	Alcohol-monomer ratio
C14	60	25	5	10	1:6
C15	60	25	7	8	1:7.5
C16	60	25	9	6	1:10
C17	60	25	10	5	1:12
C18	60	27.5	7.5	5	1:12

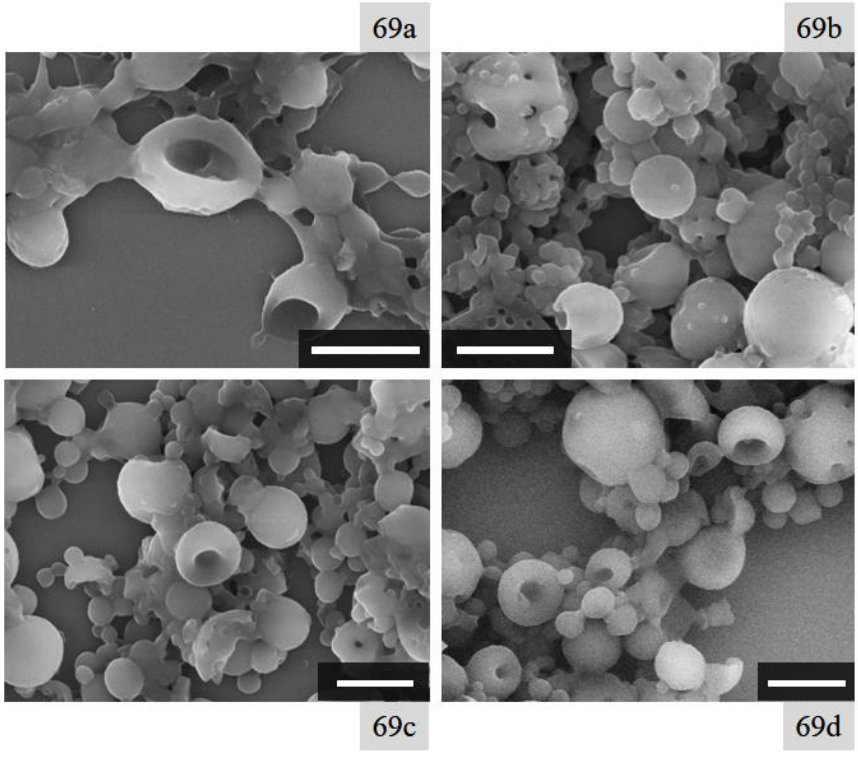

Figure 69. FESEM images of samples prepared with different formulations: (a) C14, (b) C15, (c) C16, and (d) C17. All scale bars refer to 1 µm.

C18 formulation was tested at two different nitrogen pressures in order to have an insight into the effect that pressure conditions might have on production. The morphology of the two samples was similar. Both spherical particles with holes on the surface and collapsed particles were present in the samples. Particles size distribution, see Figure 70d, confirmed the improvement in polydispersity of samples prepared with higher nitrogen pressure. An increase from 1 to 1.5 bar led to the production of more monodisperse population and a decrease of almost 200 nm in average diameter.

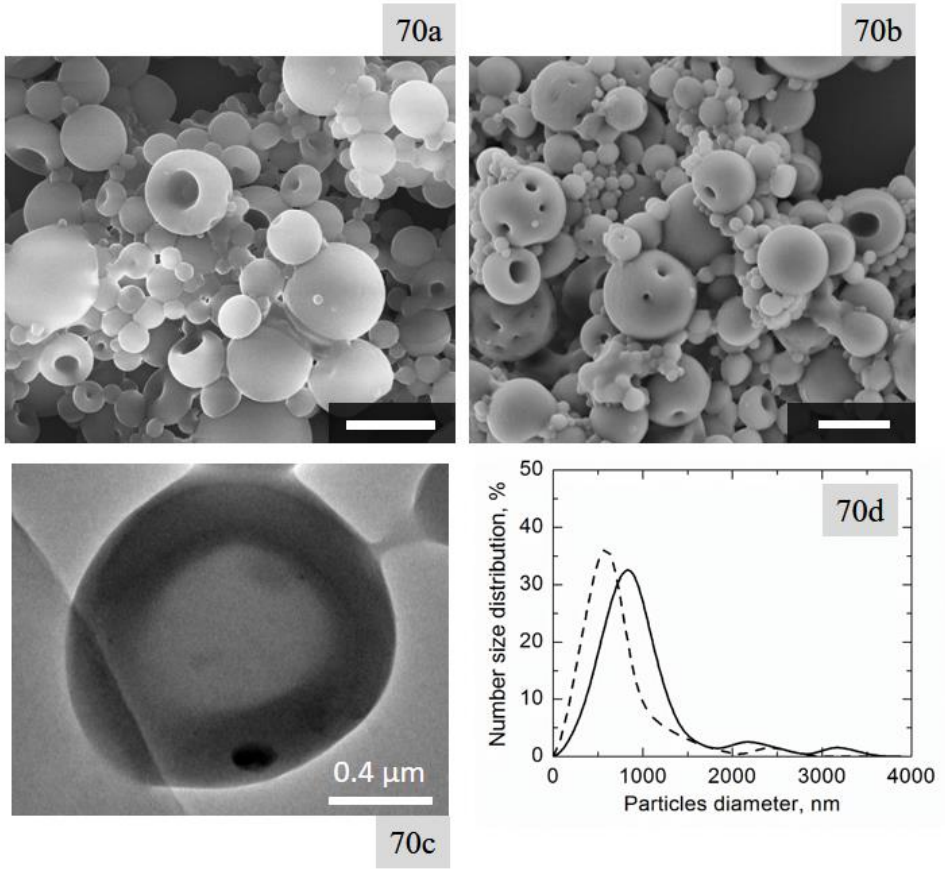

Figure 70. FESEM images of samples prepared with formulation C18 using different nitrogen pressure: (a) 1 bar and (b) 1.5 bar. Scale bars refer to 1 µm. TEM micrograph (c) of particle obtained with C18 formulation and 1 bar nitrogen pressure. Size distribution curves (d) of the two samples.

In the last part of this study on CTM as a way to obtain capsules, the amount of monomer was decreased in order to produce thinner polymeric shells. In such study, the ratio alcohol to monomer was held constant and the amounts of the other two solvents was changed according to the solubility tests. In Table 21, the experiments list is provided.

Results of this study are reported in Figure 71. Both particles obtained with 56% and 51% (w/w) of monomer showed a rather spherical shape and dimensions similar to those previously obtained. Pores were present on the surface, indicating a non-continuous polymeric shell.

Table 21. List and recipes of experiments performed to decrease the monomer amount.

Sample	DVE3 (mass%)	Hexadecane (mass%)	2-octanone (mass%)	2-ethylhexanol (mass%)
C19	56	30.9	8.4	4.7
C20	51	31	12.7	4.3

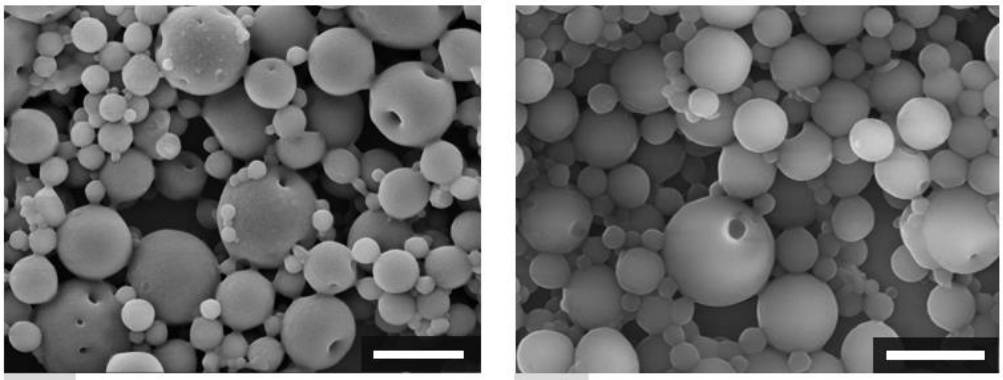

71a 71b

Figure 71. FESEM images of samples prepared with formulation (a) C19 and (b) C20. All scale bars refer to 1 μm.

All the experiments until the one with formulation C20 were carried out using 1% of PI with respect to the total monomer amount. Starting from the promising formulation C20, a study on the effect of PI concentration was carried out. PI mass percentage, referred to the monomer amount, was varied in the range within 0.2% to 2% (w/w). List of the experiments is provided in Table 22.

Solvents concentrations were changed in order to maintain a homogeneous solution in presence of higher amount of PI. Concentration of hexadecane and 2-octanone was designed in the worst scenario, presence of 2% PI, and kept constant in all the experiments. Although all the experiments listed in Table 22 did produce polymeric material and, as we will discuss further in the FT-IR section, the conversion was almost complete, particles morphology was not the expected one, see Figure 72. Particles

possessed non-spherical shapes and were often grouped in clusters. This happenned mainly in the samples prepared with low amount of PI such as C21 and C22 and might be due to the high solvating effect of 2-octanone which delayed the phase separation and hindered the structuring. On the other hand, 2-octanone amount could be lowered because it was crucial for the homogeneity of the initial formulation. Thus, the study on the PI concentration proved only the possibility to obtain material with different PI amount but not the possibility of nanostructuring.

Table 22. List and recipes of experiments performed to study the effect of PI.

Sample	DVE3 (mass%)	Hexadecane (mass%)	2-octanone (mass%)	2-ethylhexanol (mass%)	PI (%mass*)
C21	51	29	15.7	4.3	0.2
C22	51	29	15.7	4.3	0.5
C23	51	29	15.7	4.3	1
C24	51	29	15.7	4.3	2

**referred to the monomer amount*

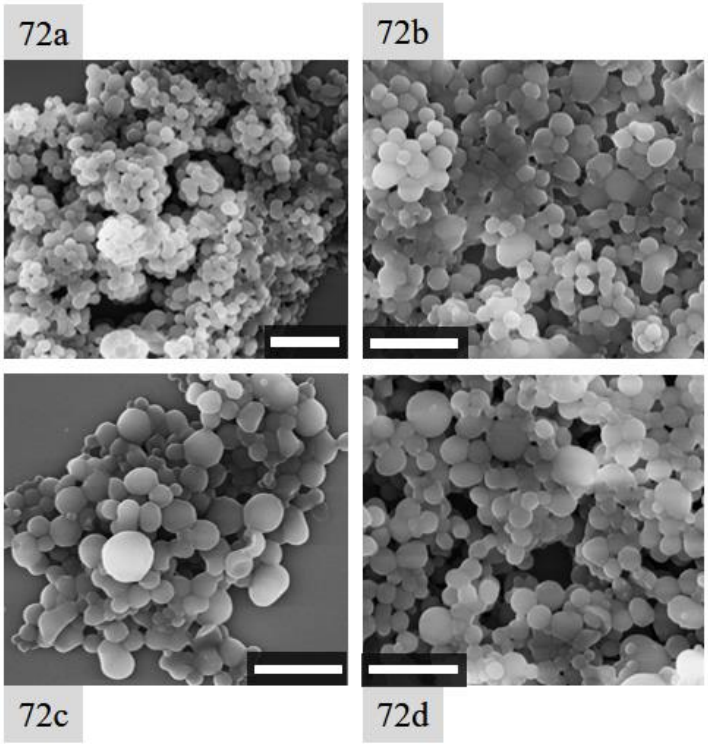

Figure 72. FESEM images of samples prepared with formulation (a) C21, (b) C22, (c) C23 and (d) C24. All scale bars refer to 2 μm.

Once the use of CTM to produce capsules was optimized, a new method to obtain capsules was investigated: copolymerization of DVE3 with different amounts of mono-functional monomers. The addition of a less reactive co-monomer should, as a matter of fact, not only slow down the reaction rate, but also produce a less crosslinked material which might be able to segregate and form the polymeric shell.

As first attampt, formulations with a ratio between mono-functional and bi-functional of 1:4 were tested in absence of solvents. Nitrogen pressure was kept constant at 1 bar and 1% (w/w) of PI was used to trigger the reaction. FESEM images of the samples so obtained are provided in Figure 73.

Two different monomers, both vinyl ethers, were chosen for the copolymerization: di(ethylene glycol) vinyl ether (VE2) and 2-ethylhexyl vinyl ether (EHVE). The first one is very similar to DVE3 except for the lack of one carbon-carbon double bond and an ethylene glycol segment. The second one is a more viscous branched molecule that is supposed to create more spacing between the crosslinking sites.

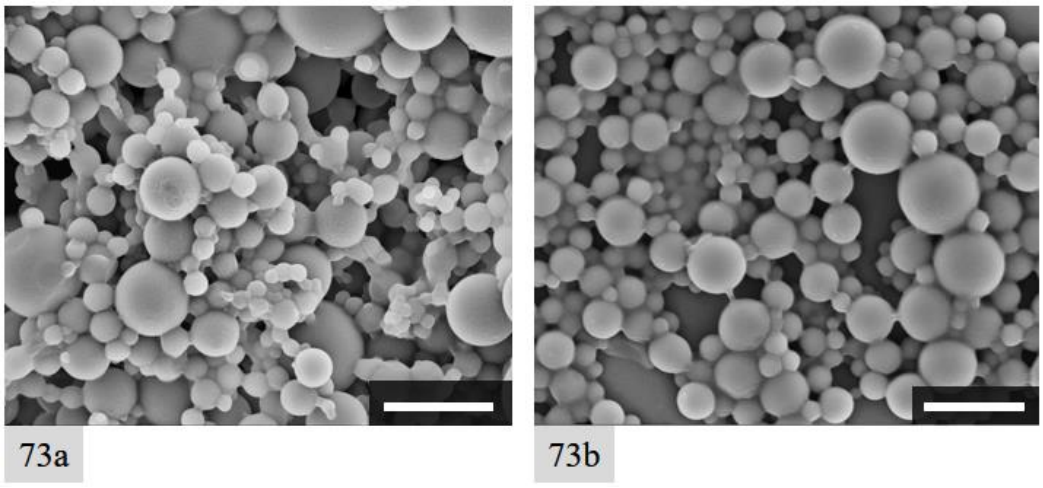

Figure 73. FESEM images of particles obtained using 80% of DVE3 and 20% of (a) VE2 and (b) EHVE. All scale bar refer to 2 μm.

Solid particles produced with two mono-functional co-monomers and DVE3 showed some differences. In Figure 74, it can be seen that the sample is slightly sticky and some defects were present on particles surface. On the other hand, particles prepared with EHVE as co-monomer did not show any major defects, besides being rather sticky. Size distribution was evaluated for both the two systems and results are provided in Figure 74.

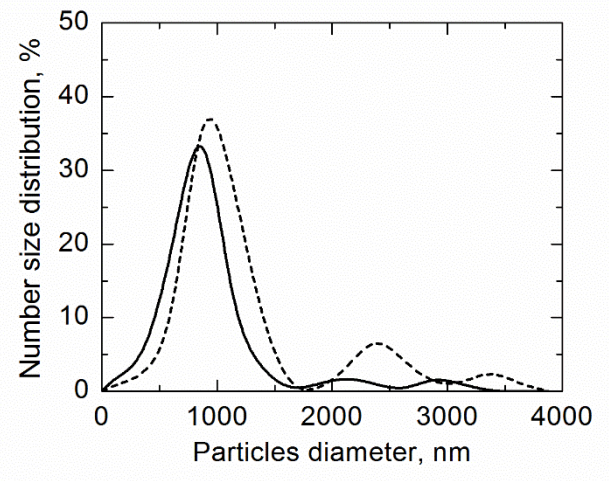

Figure 74. Size distribution of samples obtained using 80% of DVE3 and 20% of (---) VE2 and (—) EHVE.

Co-polymerization was proved feasible in both cases. Nonetheless, EHVE was chosen for further studies because VE2 showed significant defects in particles, which should have been perfectly spherical. Moreover, the production with EHVE showed a lower polydispersity compared to the one with VE2, see Figure 74.

Experiments were carried out using the 1:4 mixture of EHVE and DVE3 and adding the solvents that were used to produce porous particles. In this case, the slowing of gelation is supposed to help in the structuring of particles, thus obtaining a polymeric material that is confined at the border of the initial droplet. The list of the experiments is provided in Table 23.

Table 23. List and recipes of experiments performed to study the nanostructuring in presence of co-polymerization.

Sample	DVE3 (mass%)	EHVE (mass%)	2-octanone (mass%)	hexadecane (mass%)
CP3	55.7	14.3	12.5	17.5
CP4	40	10	20.8	29.2

Two different formulations were tested, one with 70% (w/w) and the second with 50% (w/w) amount of monomers. Ratio between 2-octanone and hexadecane was chosen in order to be in proximity of the phase separation. PI amount was kept constant at 1% of

the total monomer content. The solutions were sprayed using 1 bar nitrogen pressure and results are shown in Figure 75.

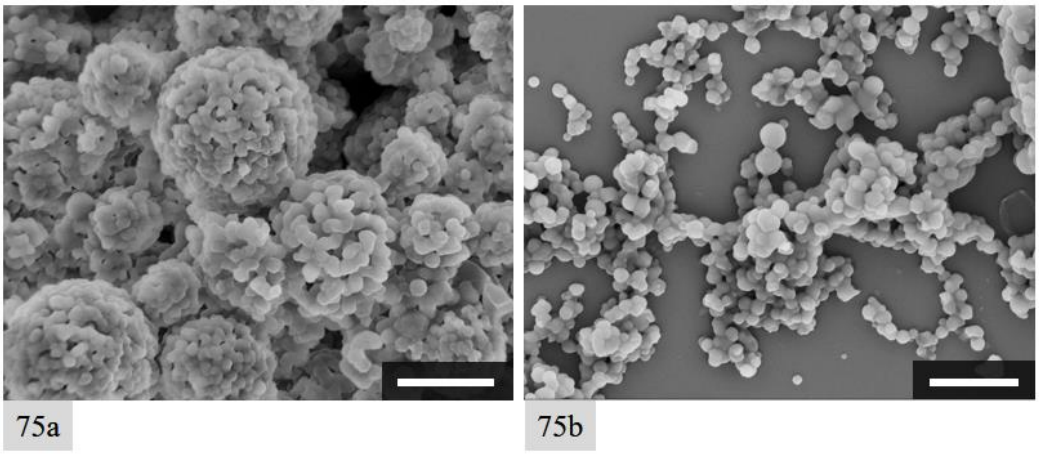

Figure 75. FESEM images of samples prepared with formulation (a) CP3 and (b) CP4. Scale bars represent 2 μm.

Results highlighted the presence of rather porous structures in samples CP3. Particles were bigger than those previously obtained, even if compared with samples prepared only with the monomers mixture. This might be caused by merging of droplets during the aerosol passage. Solvents could indeed delay the production of distinct and non-sticky particles, thus giving more time for droplets merging. The particles consisted of polymeric domain weakly connected one another. When decreasing the total monomer amount, however, these agglomerates did not possess mechanical stability anymore and resulted collapsed into non-spherical separated polymer particles.

This situation was similar to the one encountered in porous particles study when, in highly solvated systems, phase separation was delayed and, from a single "mother" droplet, agglomerates or dispersions of polymeric domains were generated. A possible explanation of this result was the double effect of mono-functional monomers presence. Not only the crosslinking density was diminished but also the reaction rate was decreased by the presence of lower amount of functionalities. Thus, growing polymers experienced phase separation later on during the reaction stage and the migration towards the outer layer of the droplet was hindered.

For this reason, it was not possible to obtain capsules just by adding mono-functional monomer. This part of the study, however, highlighted an important feature of structuring during polymerization: reaction should not be slowed down; otherwise, a slow phase separation is able to hinder the structuring.

6.2.2 Thermal behavior

Differential scanning calorimetry was applied in order to access the thermal behavior of the samples. Glass transition temperature (T_g) was evaluated for samples obtained in presence of different solvents and, thus, it was possible to study the effect of manufacturing on the particles crosslinking density.

In Figure 76, a series of transformations can be seen. At ~18 °C, an endothermic peak is present, indicating hexadecane melting and thus the presence of some residue of solvent. Similarly, the two endothermic peaks at ~ -20 and ~140 °C indicate the presence of some residual 2-octanone. A T_g was observed at 51 °C, a typical value for DVE3 based material. A complete list of the results on the evaluation of T_g is provided in Table 24. T_g values showed the important effect of alcohol presence on the polymeric molecular structure, while presence of hexadecane and 2-octanone did not induce significant changes on this parameter.

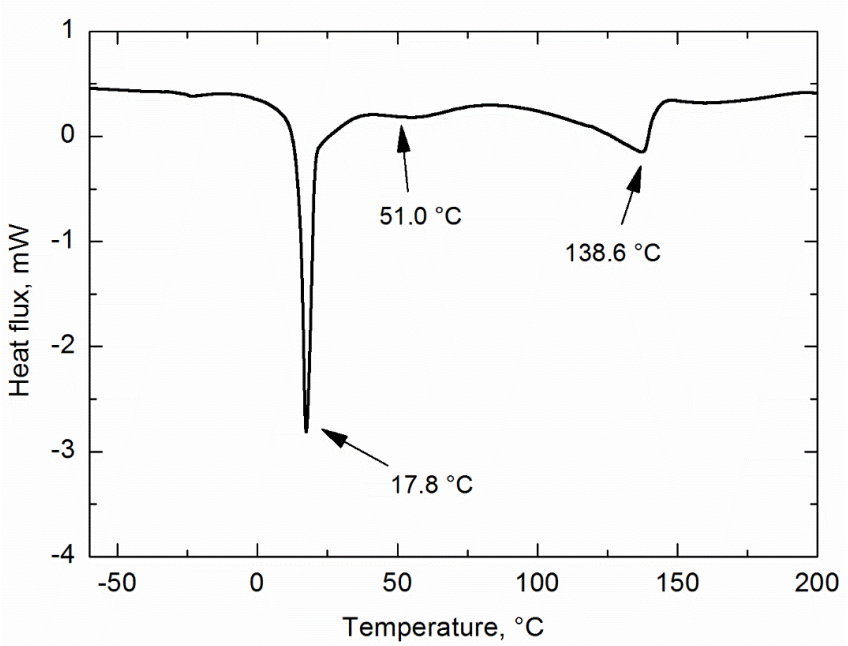

Figure 76. DSC scan of samples prepared with formulation P3.

Results reported in Table 24 showed that, within the studied range, the presence of hexadecane and 2-octanone does not cause a significant change in T_g. Therefore, these two solvents should not interact with the reaction. On the other hand, samples prepared with 2-ethylhexanol showed a dramatic decrease in T_g value. This was in agreement with literature studies that suggested how presence of CTM might results in lower crosslinking density of the material (Sangermano, 2012).

Table 24. T_g values of samples prepared with different types and amounts of solvents.

Sample	DVE3	hexadecane	2-octanone	2-ethylhexanol	T_g, °C
S1	100	-	-	-	52.4
P3	70	17.5	12.5	-	51.0
P4	70	15	15	-	51.7
P5	70	20	10	-	50.2
C16	60	25	9	6	9.1
C17	60	25	10	5	7.2
C18	60	27.5	7.5	5	7.6

6.2.3 Evaluation of monomer conversion during polymerization

Monomer conversion in the reactor passage was monitored using FT-IR analysis. Tests were carried out on the initial formulation and on the final product. In order to be able to distinguish between the different compounds in the system, spectra of the pure compounds were acquired. Results are shown in Figure 77 and Figure 78.

IR spectrum of pristine DVE3 showed the presence of different peaks. The C=C stretching characteristic of vinyl compounds is evident at ~1640 cm^{-1}, while the peaks at ~ 1100 cm^{-1} are characteristic of the stretching of the ether groups (Brown & Poon, 2014). These peaks were taken into account for the evaluation of monomer conversion.

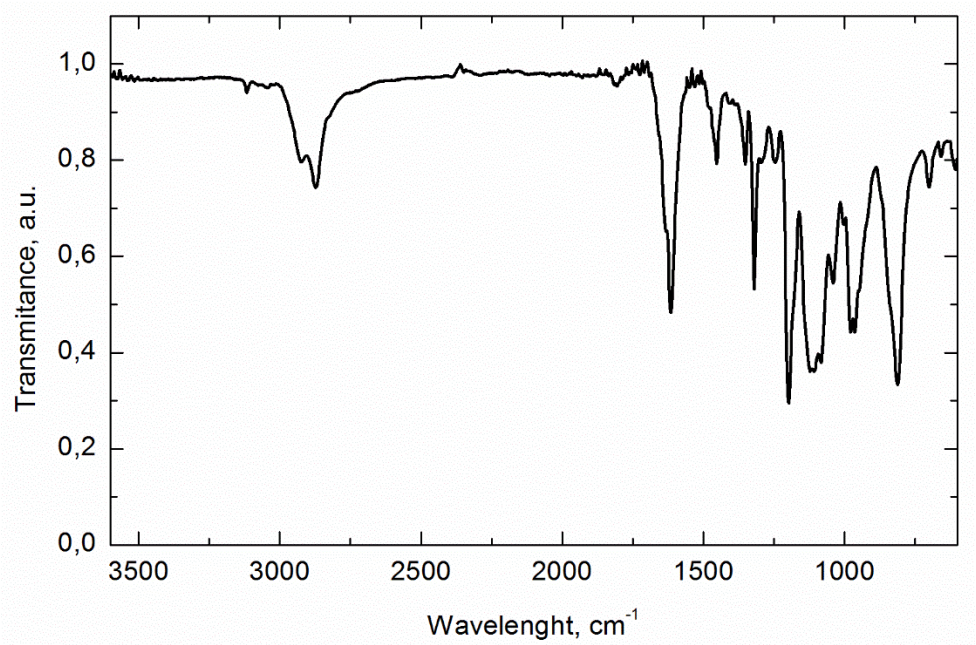

Figure 77. FT-IR spectrum of pure DVE3.

Hexadecane has the simplest spectrum, which shows the characteristic peaks of alkane, namely the C-H stretching at 2800-3000 cm^{-1} and the two bending of CH_2 and CH_3 respectively at 1450 and 1400 cm^{-1}. These peaks were present also in the other two solvents, which were characterized by additional peaks. Spectrum of 2-octanone was characterized by the presence of a sharp peak at ~1740 cm^{-1}, representative of the C=O stretching. Finally, 2-ethylhexanol spectrum showed a broad peak at ~3340 cm^{-1} relative to the O-H stretching (Brown & Poon, 2014).

FT-IR analyses were performed before and after polymerization to study the conversion and to have an insight into the residue of solvents in the polymerized material. As first experiment, FT-IR analysis was carried out on formulation with only DVE3 and 1% (w/w) of PI. The same evaluation was performed on the polymerized material at the reactor outlet. Results are shown in Figure 79, where it can be seen the change from the initial solution to the polymerized one.

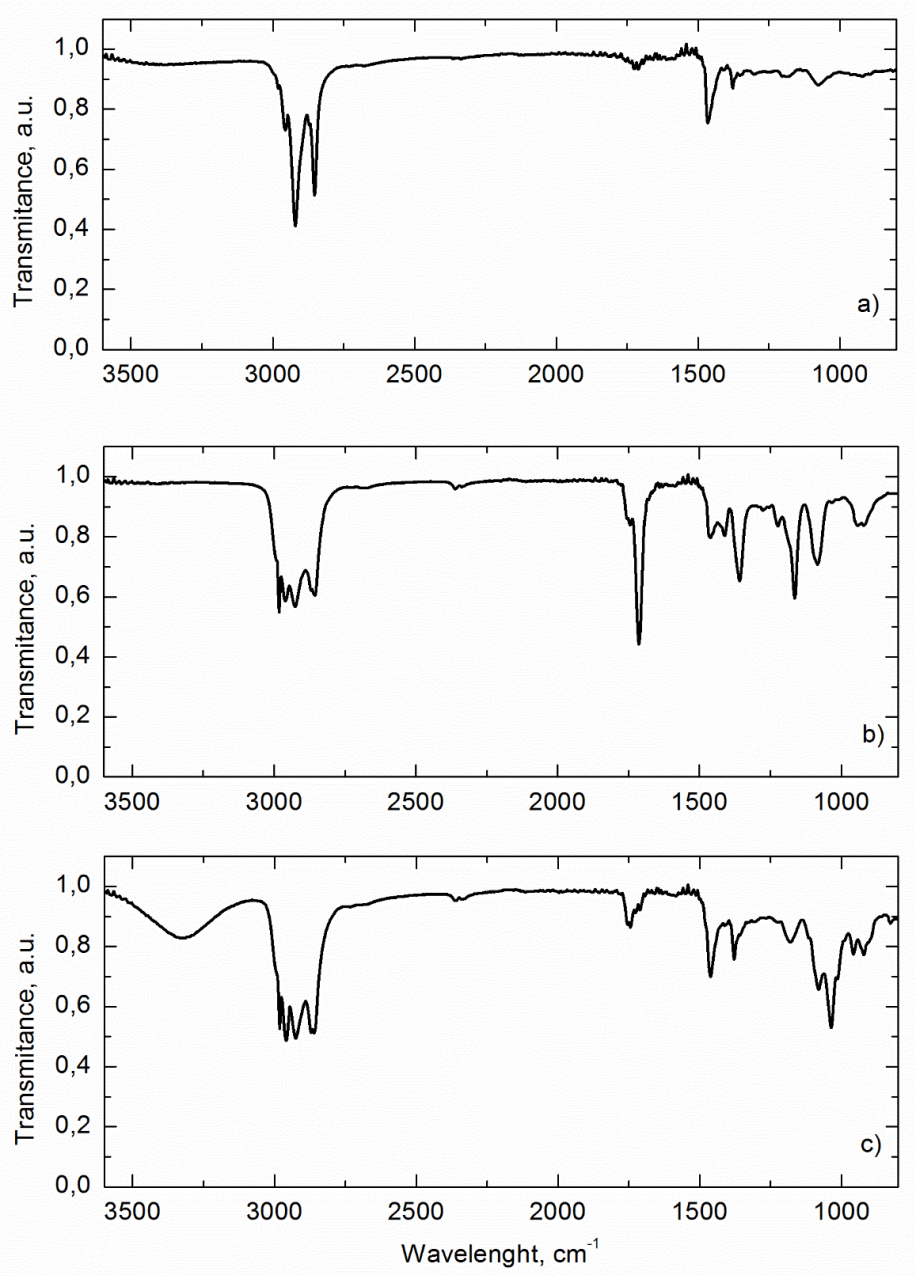

Figure 78. FT-IR spectra pure solvents: (a) hexadecane, (b) 2-octanone and (c) 2-ethylhexanol.

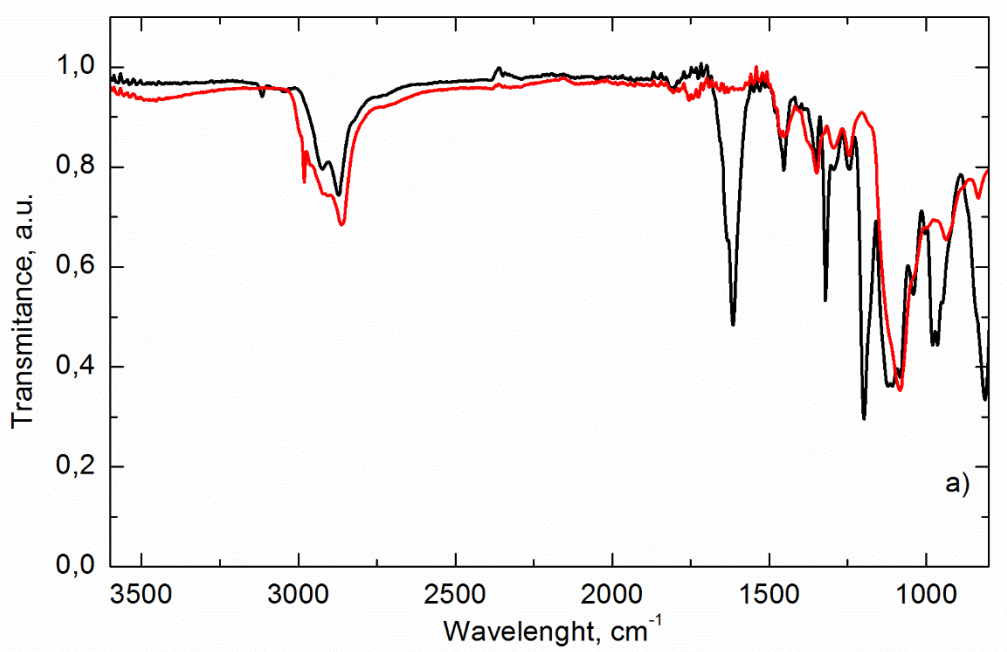

Figure 79. FT-IR spectra of DVE3 plus 1% PI (—) before and (—) after reactor passage.

The peak of C=C stretching bond (~1640 cm^{-1}) completely disappeared after reactor passage, while the reference peak at ~1100 cm^{-1} did not significantly change. Conversion was calculated using the following equation:

$$X_m = 1 - \frac{A_{CC,1} * A_{CO,0}}{A_{CC,0} * A_{CO,1}} \qquad \text{(Eq. 9)}$$

where:

X_m = monomer conversion

$A_{CC,0}$ = area of the C=C peak before irradiation (~1640 cm^{-1})

$A_{CO,0}$ = area of the C-O peak before irradiation (~1100 cm^{-1})

$A_{CC,1}$ = area of the C=C peak after irradiation (~1640 cm^{-1})

$A_{CO,1}$ = area of the C-O peak after irradiation (~1100 cm^{-1})

Using data reported in Figure 79, conversion in the reactor was almost complete, with the disappearing of 98% (w/w) of C=C. Given the "living" character of this type of reaction, the actual conversion during the reactor passage might have been lower. Presence of distinct particles, however, gave a hint about the fact that an almost complete conversion was present during material collection in the outlet tube. Moreover, the

absence of non-reacted monomer is crucial in many applications and needed to be checked in every production.

The same evaluation was carried out on samples produced at different nitrogen pressures, thus studying the effect of mean residence time on monomer conversion. Results are reported in Table 25. Results did not show any significant impact of nitrogen pressure on the total monomer conversion. Besides, well-defined spherical particles were obtained with all the tested pressures. Thus, a short mean residence time should not hinder the production of material with good features.

Table 25. Monomer conversion vs. nitrogen pressure.

Nitrogen pressure, bar	1	2	2.5
Monomer conversion, %	98	96	97

Tests were performed also varying the PI amount in order to study its effect on monomer conversion. Formulations consisted of DVE3 and PI. PI concentration was varied within 0.5% to 2% and results of the FT-IR evaluation are shown in Table 26.

Table 26. Monomer conversion vs. PI concentration.

PI concentration (%mass)	0.5	1	2
Monomer conversion, %	98	98	97

As can be seen in Table 26, PI concentration did not affect the total monomer conversion in the studied range. Thus, for the following experiments, a concentration of 1% w/w was chosen according to the literature data (Decker, 2002).

As to the study on porous particles, similar analyses were carried out in order to study the effect of solvents. Presence of solvents in the product was monitored following the disappearance of certain peaks. Hexadecane does not have peculiar peaks so it was not possible to control its presence, whereas 2-octanone was evaluated referring to the characteristic peak at 1740 cm^{-1}. Formulations with different initial amount of 2-octanone were analyzed in order to verify if it was possible to get a somehow precise evaluation of the 2-octanone concentration. Results are shown in Figure 80.

A calibration curve was achieved in the studied range within 12.5% to 30% of 2-octanone. Height of peaks was measured and correlated to the known concentration. The result of this study is shown in Figure 81.

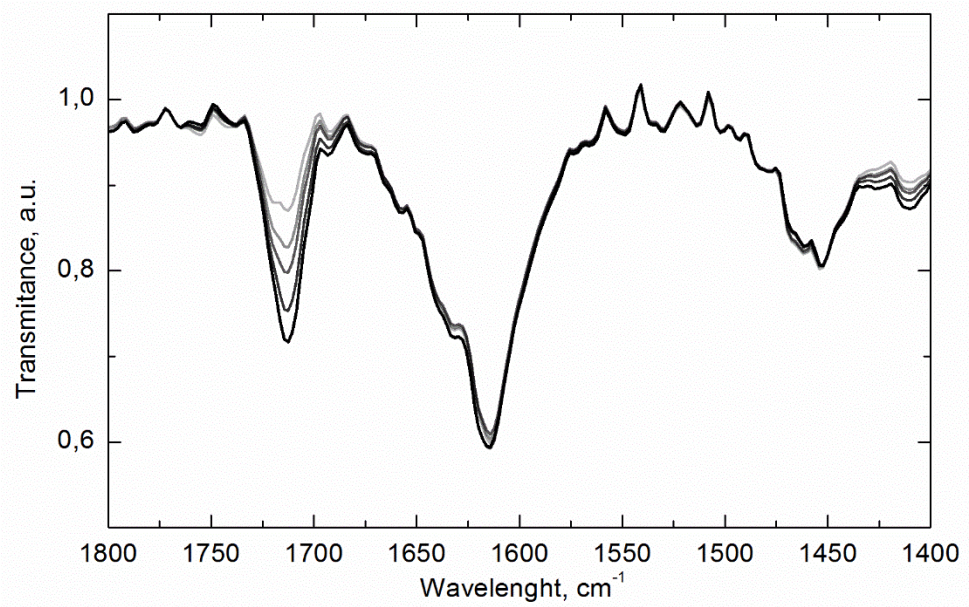

Figure 80. FT-IR spectra of formulations with 70% (w/w) DVE3 and different amounts of 2-octanone: (—) 12.5%, (—) 15%, (—) 20%, (—) 25% and (—) 30%.

There, it can be seen that a good correlation was present between the two parameters and, in the evaluated range, it was possible to access the concentration of 2-octanone using FT-IR analysis.

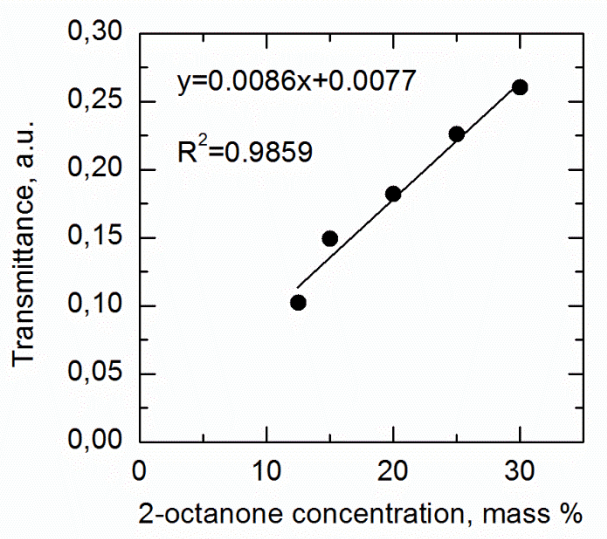

Figure 81. Calibration curve for detection of 2-octanone.

FT-IR analyses were carried out on all the formulations and polymerized samples that were tested for porous structure. In Figure 82, an example of result is presented.

There, it could be seen that both peaks, at ~1740 cm^{-1} and at ~1640 cm^{-1}, disappeared after irradiation in the aerosol photo-reactor. Disappearing of the C=C stretching peak was a proof of the complete monomer conversion.

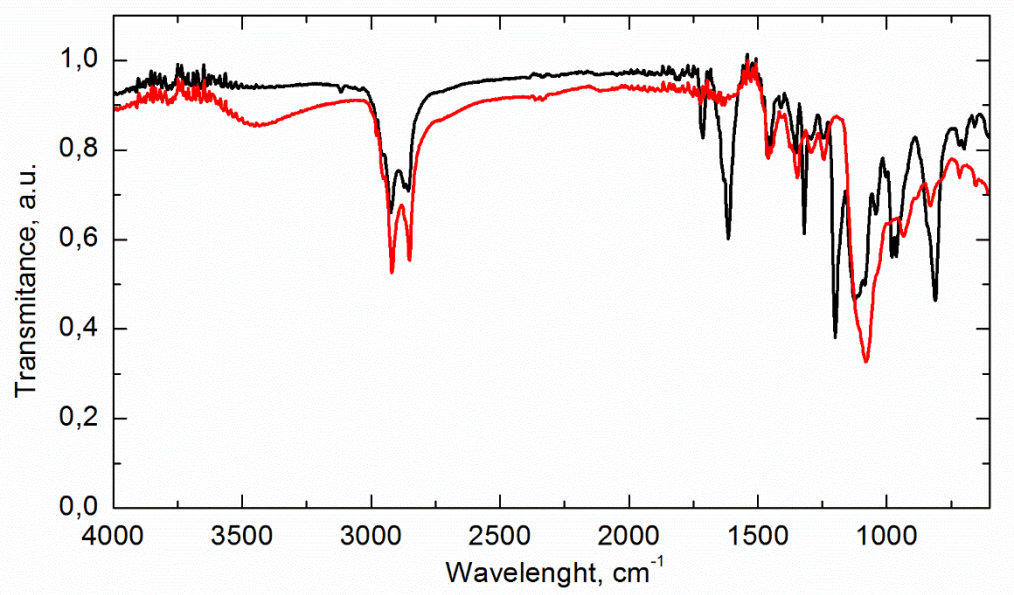

Figure 82. FT-IR spectra of (—) formulation P4 and (—) polymeric material obtained in the reactor outlet.

Equation 3 was used to evaluate the conversion taking into account also the C-O stretching at ~1100 cm^{-1} which was used as reference peak. Moreover, the lack of the C=O peak at ~1740 cm^{-1} showed the absence of 2-octanone in the final product. This was probably related to the evaporation of the solvent or some chemical modifications of the double bond.

To tackle this uncertainty, some specific tests were performed. Formulations were dropped on a glass and spread in order to obtain a liquid film. Irradiation, using a similar source and intensity, was performed for different time-lengths and the material was immediately analyzed with FT-IR spectroscopy. This type of experiment was carried out for every formulation from P3 up to P7. An example of result is provided in Figure 83.

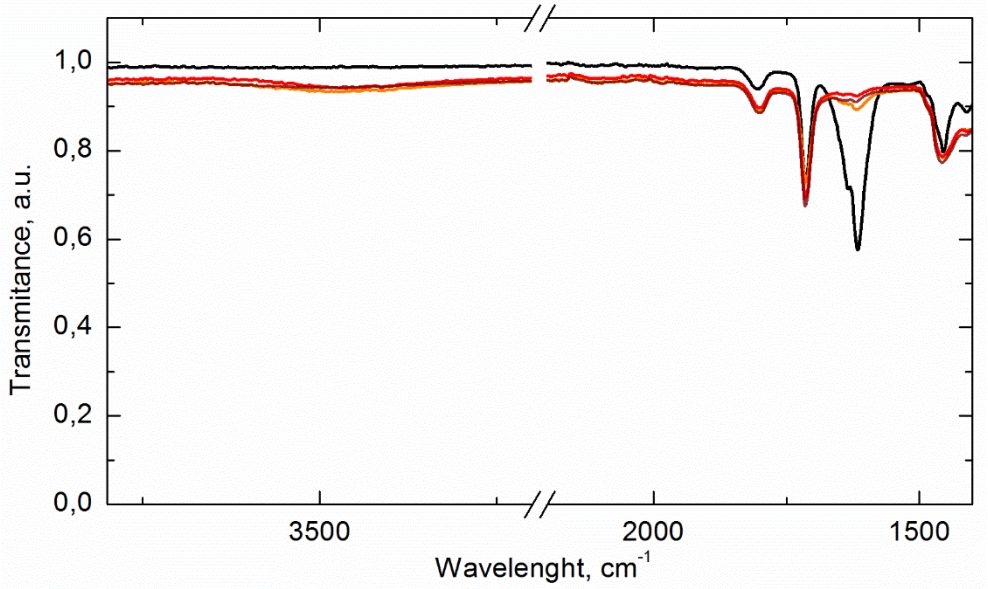

Figure 83. FT-IR spectra of (—) formulation P7 film and of film after (—) 15 s, (—) 30 s and (—) 60 s of UV irradiation.

As it can be seen in Figure 83, 15 s of UV irradiation are able to provoke, or at least trigger, the complete monomer conversion, which was monitored by the disappearance of 1640 cm^{-1} peak. On the other hand, the C=O stretching peak did not decrease in intensity for UV irradiation lasting up to 60 s. This confirmed that 2-octanone did not react upon UV exposure or at least in the same time interval in which polymerization takes place. Irradiated samples, however, showed the presence of a broad peak at ~3400 cm^{-1}, which is characteristic of O-H bond. This was present also in the samples obtained by aerosol photo-polymerization and this was believed to be caused by water adsorption on the sample.

In order to confirm the thesis of water adsorption after polymerization a specific test was carried out. Samples were collected during particles production in the first minutes. FT-IR analyses were performed on these samples at different times after polymerization and the spectra are shown in Figure 84.

Results showed in Figure 84 highlighted the changes that a particles production faced in the first 30 min after irradiation. Right after polymerization, C=O stretching peak was still visible at ~1740 cm^{-1}, while for longer storage time the peak intensity decreased indicating the presence of evaporation of 2-octanone. Another peak change that was worth mentioning was the one characteristic of O-H group at ~3400 cm^{-1}. This peak was already present in the initial formulation because of the 2-ethylhexanol, but after reaction its intensity increased, probably due to water adsorption. Moreover, there was a further

increase in intensity of the O-H peak in the 30 min after production, indicating an additional water adsorption.

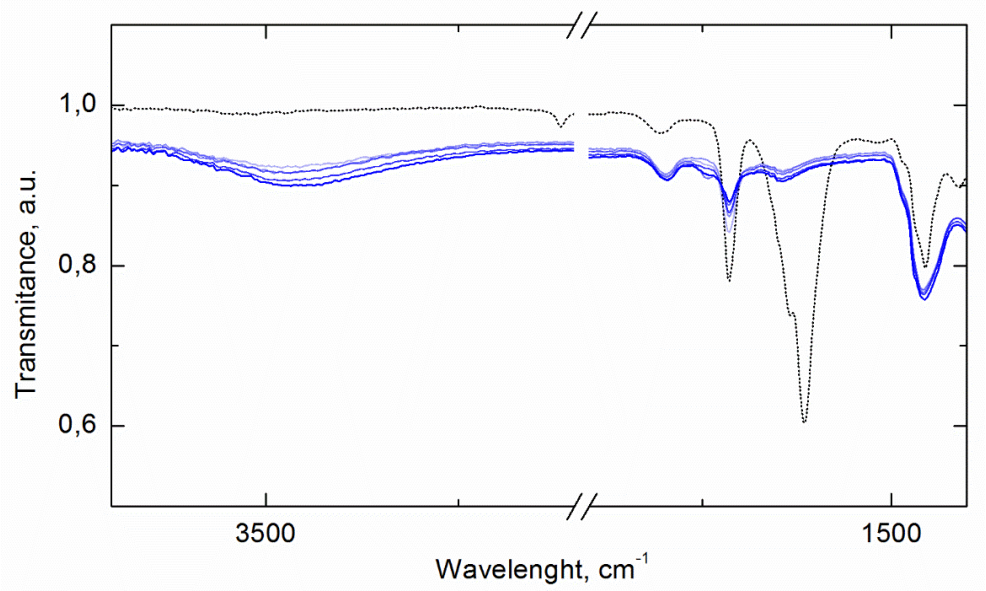

Figure 84. FT-IR spectrum of (---) formulation with 70% DVE3, 20% 2-octanone, 3% 2-ethylhexanol and 7% hexadecane. FT-IR spectra of reacted material at (—) 0 min, (—) 5 min, (—) 10 min, (—) 15 min and (—) 30 min after production.

Data on samples made of porous particles are shown in Table 27. Equation 3 was applied to evaluate monomer conversion, whereas for 2-octanone very small peaks were present and calibration curve was not applied. FT-IR analyses proved that the presence of solvents did not hinder monomer conversion, which was almost complete with every formulation used. In fact, the two solvents were inert in the system, as partially already proven by tests carried out on films, see Figure 83.

Table 27. Monomer conversion vs. formulation concentrations.

Formulation	Solvents ratio, -	Monomer conversion, %
P3	0.71	99
P4	1	98
P5	2	98
P6	5	99
P7	-	98

Regarding the study on capsules production, FT-IR analyses were crucial to prove that CTM did not alter the conversion in the process. Thus, similarly as before, every production was tested before and after irradiation. At the beginning, a test similar to the one present in Figure 84 was carried out in order to study the effect of alcohol and 2-octanone together. A formulation consisting of 75% w/w DVE3, 15% w/w 2-octanone and 10% w/w 2-ethylhexanol was spread on a glass surface to get a thin film and irradiated for different amounts of time. Results are shown in Figure 85.

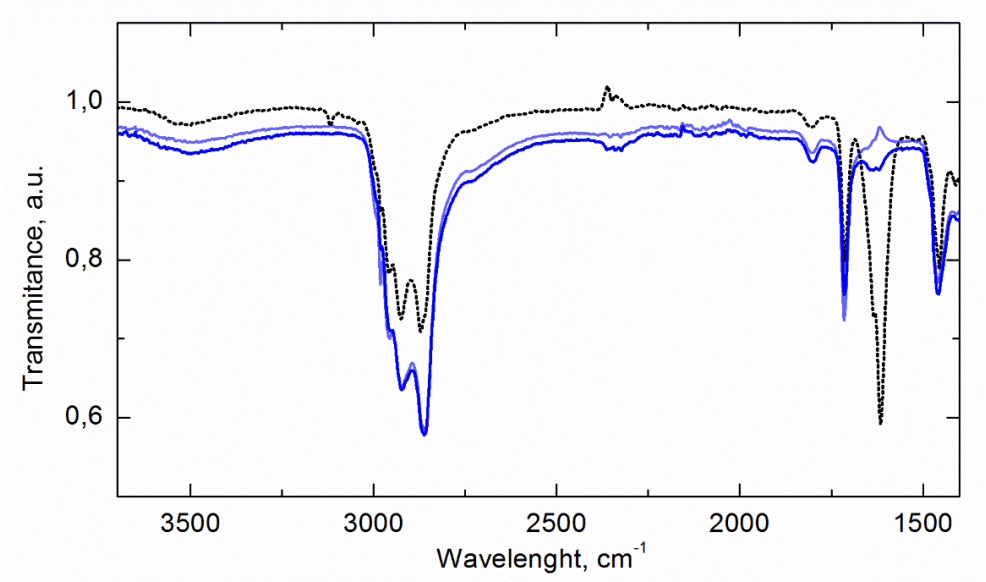

Figure 85. FT-IR spectra of (---) formulation (75% DVE3 – 15% 2-octanone – 10% 2-ethylhexanol) film and of film after (—) 15 s and (—) 30 s of UV irradiation.

Results on the film polymerization highlighted a high conversion even with 15 s of irradiation, while the peak at ~1740 cm^{-1} did not show any significant decrease, similarly to the results obtained in Figure 83. Thus, even in presence of the alcohol, a good conversion was obtained easily and 2-octanone did not take part into the reaction. Moreover, in all the spectra it could be seen a broad peak at ~3400 cm^{-1} which was linked to the presence of alcohol.

Once this system conversion in film polymerization was studied, the focus shifted towards the main goal, namely aerosol photo-polymerization of this quaternary system. An example of result is provided in Figure 86.

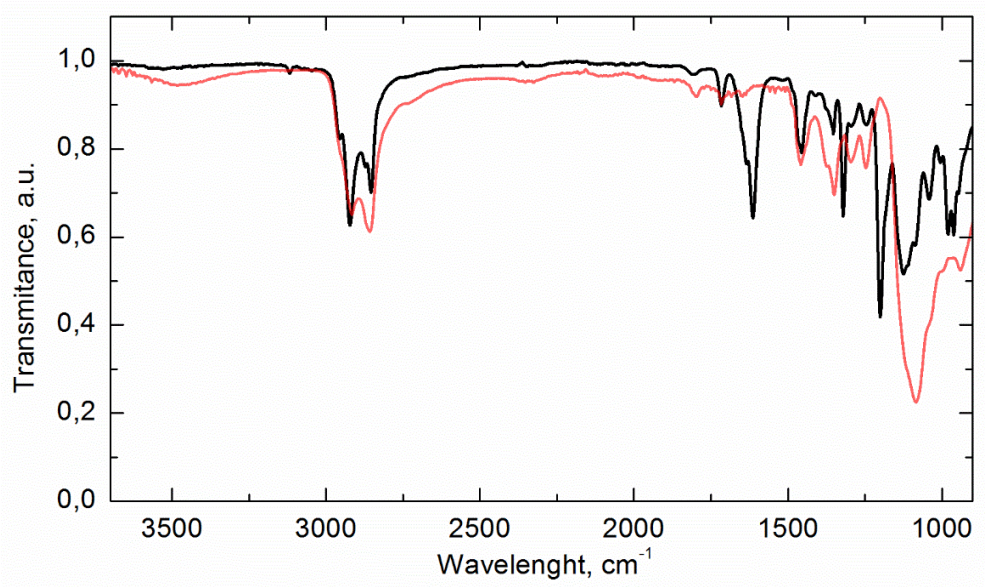

Figure 86. FT-IR spectra of (---) formulation C18 and (—) the relative material obtained after reactor passage.

In Figure 86, it could be seen that C=C peak disappeared during reactor passage, thus confirming a full monomer conversion. Similarly to what happened in the production of porous particles, the C=O peak disappeared probably because of evaporation of 2-octanone. In addition, the already present broad peak of the O-H group increased in intensity probably because of the adsorption of water during storage.

Monomer conversion was evaluated using Equation 3 in the capsules main productions and results are shown in Table 28. Results suggest that, in the studied range, there was no significant effect of the alcohol amount on the monomer conversion. Literature suggested that some impact of alcohol on monomer conversion is present, in particular an increased conversion might be the result of the CTM that is induced by the alcohol. In this system, however, monomer conversion in absence of solvents was already complete, thus not visible effects could be observed.

Finally, monomer conversion in samples C21-C22-C23 and C24 was almost constant and no trend was observed. Therefore, PI concentration did not show any impact on the total monomer conversion.

Table 28. Monomer conversion vs. formulation concentrations.

Formulation	Alcohol to monomer ratio, -	Monomer conversion, %
C14	1:6	99
C15	1:7.5	99
C16	1:10	100
C17	1:12	99
C18	1:12	99
C19	1:12	98
C20	1:12	98
C21	1:12	99
C22	1:12	98
C23	1:12	99
C24	1:12	98

6.2.4 Controlled release of an active ingredient

The particles obtained by aerosol photo-polymerization were tested upon their capability to control the release of a model drug. An active ingredient was encapsulated during particles production and release was monitored by UV-vis spectroscopy.

Curcumin was selected as an example of active ingredient. It is an anti-oxidant and anti-inflammatory compound that has been widely studied as example of drug characterized by interesting features, but that presents low bioavailability. Curcumin solubility is low in water-based fluids, such as the ones present in the human body (Bazzano *et al.*, 2016). Moreover, curcumin stability is low in many fluids, especially at pH close to neutrality (Tønnesen, 1992). Thus, many studies tried to enhance its bioavailability by encapsulation.

In Chapther 3, it has been observed that the presence of a UV absorbing compound such as curcumin did not result in the hindering of photo-polymerization (Bazzano *et al.*, 2016). The main problem with curcumin is the possibility of UV-driven degradation. Stability of curcumin to UV light has been debated and some works on the enhancement of photo-stability are present (Tønnesen *et al.*, 2002). Curcumin decomposes through multiples steps into feruloyl methane, ferulic acid and vanillin. The final product of the degradation gives to the material a brownish color which can easily be detected, whereas

the first degradation product is still yellowish (Tønnesen, 1992) and can be disguised as curcumin upon UV-vis analyses. Although those aspects are important, in this study the attention was focused on the ability of the product to release the drug.

Purified curcumin was dissolved in the initial formulation and sprayed to obtain particles encapsulating the active ingredient. Different structures were tested, ranging from solid particles to porous and capsules structures. A list of the tests is provided in Table 29.

Table 29. List and recipes of experiments performed to study the nanostructuring in presence of curcumin. Numbers represent mass percentage in the formulation.

Sample	DVE3	hexadecane	2-octanone	2-ethylhexanol	curcumin*
L1	100				0.75
L2	70	18	12		0.75
L3	60	27.5	7.5	5	0.75

**curcumin amount is referred to the percentage of monomer in the formulation*

The visual inspection of the samples revealed a product similar to that obtained in absence of curcumin, but with a bright yellow color. This was given by curcumin and could be used to state that no advanced degradation of the active ingredient was achieved during reaction. As already discussed, in fact, curcumin possess a bright yellow color, which does not change in the first stage of degradation, while it turns to brownish for the advanced stages (Tønnesen, 1992).

FESEM analyses were carried out on samples prepared with curcumin to study particles structure. Results are provided in Figure 87. FESEM images pointed out the possibility to obtain a structured product in presence of curcumin. Formulation that were used, in fact, were almost the same that gave, in the previous experiments, the best morphologies in both porous particles and capsules. Particles dimensions were evaluated in order to compare their size distribution with the ones obtained in absence of curcumin. Results are shown in Figure 88. Distribution of particles size prepared with curcumin showed a trend similar to those obtained without curcumin. Namely, solid particles showed a peak around 600 nm, whereas particles produced in presence of solvents had higher dimensions with an average diameter slightly higher than 1 μm. This could be due to coalescence of droplets in which phase separation did not take already place.

The dialysis technique (see § 2.5) was applied to study the release of active ingredient from the various types of particles. Samples of the releasing medium were withdrawn and analyzed with UV-visible spectroscopy as widely described in § 2.5. All

types of structure were tested: solid, porous and capsules. Results are shown in Figure 89. Results of curcumin release showed a rather quick rate of release for all the three configurations investigated. Within 170 h from the beginning of the tests a plateau was reached.

Solid particles were able to release the whole amount of ingredient within ~50 h, whereas the 50% release was reached in less than 7 h (~400 min).

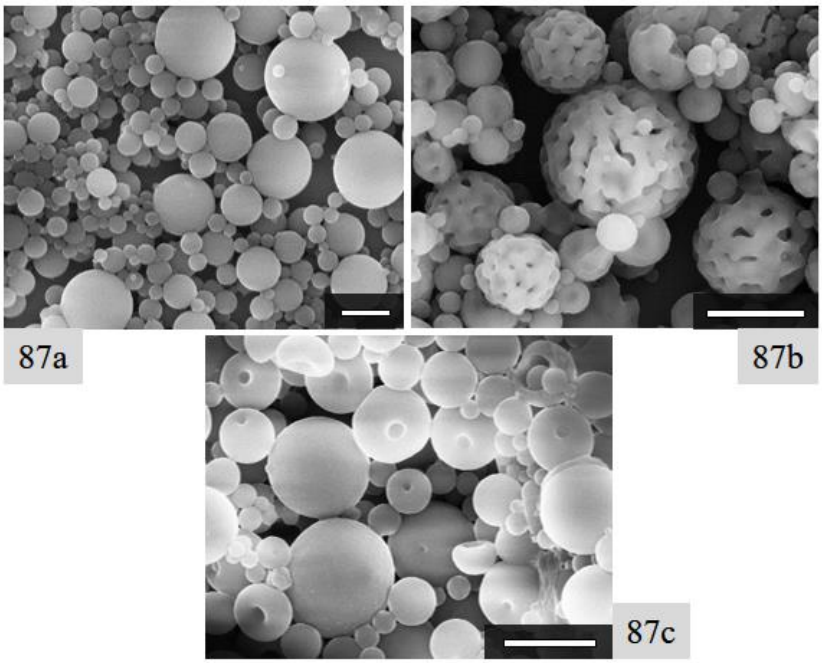

Figure 87. FESEM images of particles produced with formulation (a) L1, (b) L2 and (c) L3. All scale bars refer to 1 µm.

Porous particles, on the other hand, showed slower kinetics. While the initial release was almost as quick as the one from solid particles, a slowdown was observed in the second part of the test. Release of 50% of active ingredient was achieved in ~8.3 h, i.e. larger than that observed by solid particles, while the 90% release was accomplished in more than 67 h. This behavior might be explained by two different phenomena: presence of two mechanisms of release and presence of hexadecane residue in the particles. Two types of release might occur when the active ingredient is partially encapsulated and partially adsorbed on the surface of the particles. On the other hand, a radial difference in structure might also lead to a quicker release of the curcumin in the outer layer of the particle, while the innermost fraction has to go through an additional path of pore diffusion in water.

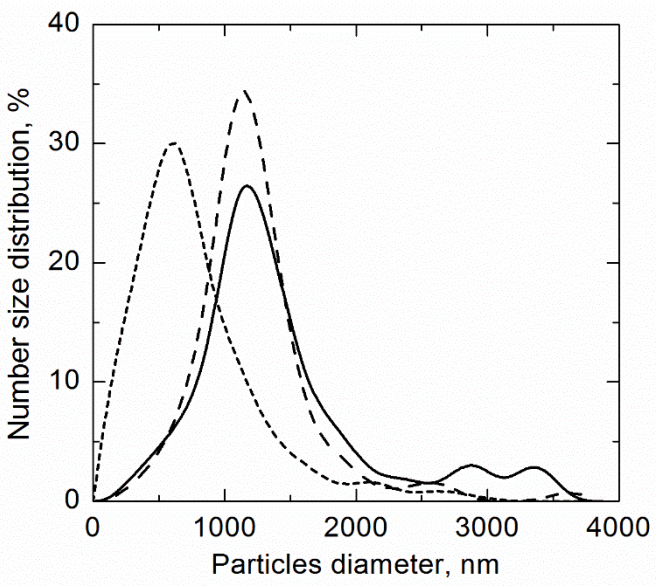

Figure 88. The size distribution curves of samples (----) L1, (– –) L2 and (—) L3.

Furthermore, presence of hexadecane in particles pores can hinder or slow down water intake by the particle and, thus, diminish the swelling rate. Compounds in a less swollen polymeric matrix possess a lower diffusivity, therefore their release is slower. Presence of hexadecane in porous particles was confirmed by DSC analyses in which a melting peak at ~18 °C was detected.

Release from capsules showed a peculiar behavior: active ingredient was released with a rate similar to the one observed in solid particles, but total released amount was significantly different from the theoretical loaded amount. This behavior might be due to different causes: complete degradation of a fraction of curcumin, a strong solvation effect or a strong confinement of curcumin within the capsule core. Kinetics similar to the one of solid particles suggested the presence of diffusion through the polymeric shell. About 35% of the total theoretical curcumin loading was released within 50 h, after which a plateau was reached.

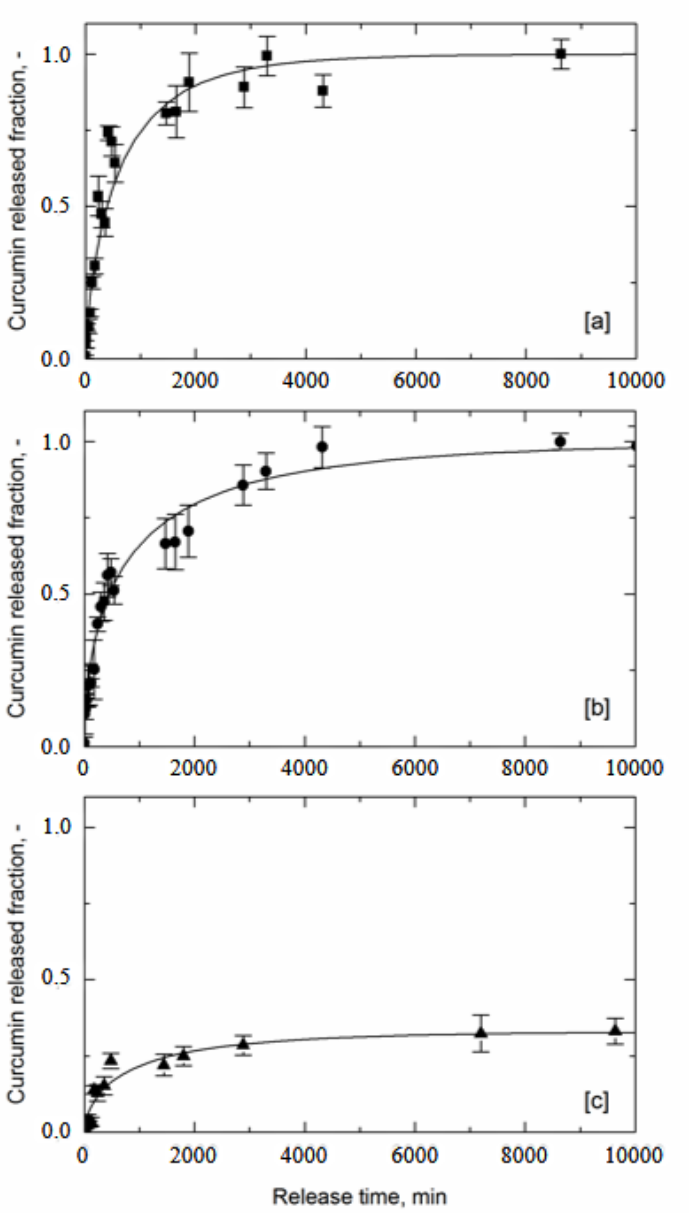

Figure 89. Release curves of curcumin from (a) solid particles, (b) porous particles and (c) capsules. Marks represent experimental data and error bars represent standard deviations, while curves represent the modeled dynamic.

Degradation of curcumin, as already mentioned, can occur in presence of a strong UV source. In the first step, it does not induce a color change but, if complete, color changes to brownish and, thus, the compound is no longer detectable by UV-visible technique at the characteristic wavelenght. In the previous samples, though, a total release of curcumin was detected using the reference peak at ~420 nm, indicating the lack of

complete degradation. Moreover, the sample with capsules, as well as the previous ones, did not show any visible signs of color change. Nonetheless, it might be that degradation of the active compound is limited to the capsule core, where is present a molecule that interacts easily with curcuminoids: 2-ethylhexanol. Many types of alcohols are good solvents of curcumin and, thus, might promote some interactions with these compounds under UV irradiation.

Another explanation for this poor total release is a strong solvation effect, which might block the active ingredient within the capsules core. This, however, should not hinder the complete release of a curcumin fraction but only slow down the release. The solvent, which might be solvating and blocking curcumin, should diffuse, indeed, through the polymeric matrix towards the buffer solution in which it is soluble. Thus, curcumin should be free to be released.

Finally, a strong physical confinement was not reasonable because of the results obtained by the DSC measurement. T_g of capsules samples proved to be much lower than the ones of porous or solid particles. This suggested the presence of a less crosslinked material in which swelling and diffusion should be improved and not hindered.

In the end, complete degradation driven by the presence of 2-ethylhexanol seemed the most likely explanation to the incomplete release of the capsule loading. However, the study was able to prove that aerosol photo-induced polymerization was able to encapsulate and release an active ingredient. Moreover, some differences in the rate of release were observed in samples with different morphologies.

6.3 Conclusions

A study on development of aerosol photo-induced cationic polymerization was carried out. The aim was to produce particles with different morphologies using a technique that has many advantages if compared with water-based syntheses, but whose drawback is the lack of control over the product morphology. The study was mainly focused on two aspects: impact of nitrogen pressure on the size distribution of the product and the development of formulations capable of producing structured particles. Morphologies were analyzed using electron microscopy, while properties of the material were accessed using DSC. Finally, process conversion, as well as solvent residues, were evaluated by FT-IR analyses.

As a general feature, nitrogen pressure was found to slightly affect particles size distribution. Higher pressure in the process led to the production of more monodisperse particles population. Moreover, the mean diameter decreases while increasing nitrogen pressure. This was due to an improved performance of the gas driven nozzle. A drawback of increasing nitrogen pressure is a decreased mean residence time in the photo-reactor.

FT-IR analyses were performed to ensure that a complete monomer conversion was still achieved even with very low residence times.

Different solvents were added to the monomer formulation in order to induce phase separation and control the structuring of particles. Porous particles were produced with a mixture of two solvents able to cause a controlled phase separation. The effect of solvents ratio on morphology was studied. Capsules were produced coupling phase separation with a chain transfer reagent. In such a complex system, both phase separation and chain transfer mechanism were designed in order to contribute to the production of a liquid core and a polymeric shell. A similar approach was attempted using co-polymerization of bi-functional and mono-functional monomers. However, results showed the impossibility to get concurrently a gelation delay and a quick conversion in the photo-reactor. Thus, this approach was abandoned.

Finally, encapsulation of an active ingredient within particles was achieved by simple solvation in the initial formulation. Microscopy analyses confirmed that the presence of an active ingredient did not significantly change the morphology of particles. Release tests were carried out on samples with different morphologies in order to study the effect particles structuring on its release kinetics. Samples were able to release entirely the active ingredient within 4 days.

Aerosol photo-induced polymerization was found capable of continuously generating structured material with a high production rate and an excellent monomer conversion, thus providing promising results in the field of particles manufacturing.

Chapter 7

Experimental investigation of the photo-induced radical aerosol polymerization

7.1 Introduction

After thoroughly investigating the cationic mechanism for particles production using an aerosol photo-reactor, the attention was shifted towards the radical mechanism.

This system has been already studied and interesting works can be found in literature (Akgün *et al.*, 2013; Akgün *et al.*, 2014b). Nonetheless, in the present work, production of structured material using innovative reacting systems was considered. Knowledge coming from studies on cationic system was applied to this field. In the following paragraphs, an overview is provided on the work that has been carried out. The same particle structures obtained by Akgün were pursued (Akgün *et al.*, 2014b), as well as new types of structures that have never been studied with the aerosol technique.

7.2 Materials and Methods

7.2.1 Materials

Different monomers and solvents were used to synthetize polymeric particles by radical polymerization mechanism. In the following tables (Table 30 and Table 31) are presented the complete list of reagents. The reaction was triggered using a commercial photo-initiator, Irgacure 907, supplied by BASF. Butyl-acrylate (BA) was used as mono-functional monomer, while other three multi-functional monomers were used as cross-linkers. The chemical structure of the various monomers is schematized in Figure 90.

Table 30. References for the various monomers used in this work.

Short name	IUPAC name	Purity	Functionalities	Supplier
BA	Butyl-acrylate	99%	1	Sigma Aldrich
HDDA	1,6-hexanediol diacrylate	99%	2	Alfa Aesar
TMPTA	Trimethylolpropane triacrylate	~99%	3	Sigma Aldrich
TMPETA	Trimethylolpropane ethoxylate triacrylate	99%	3	Sigma Aldrich

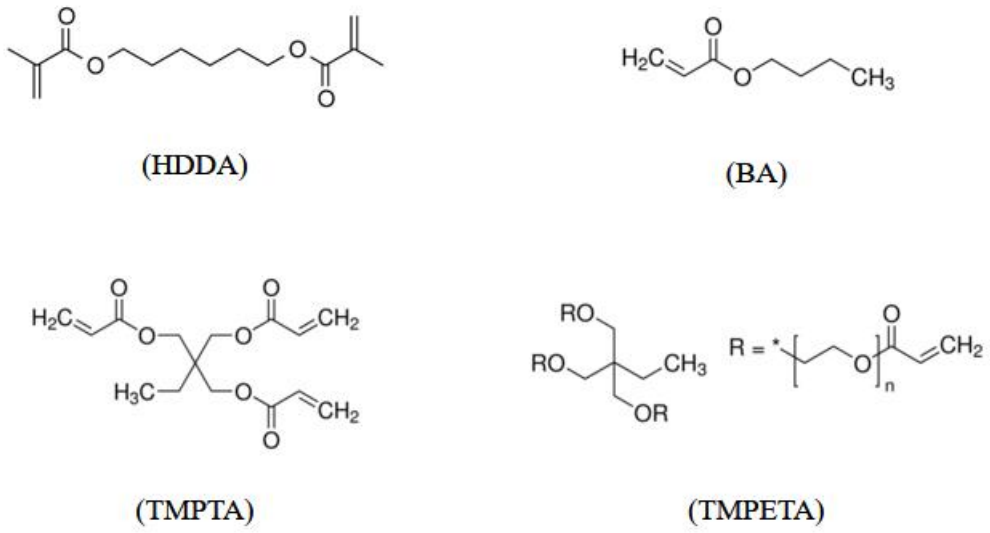

Figure 90. Schematic of the chemical structure of the various monomers used in this work.

Nitrogen gas was used for the generation of the aerosol and was withdrawn from cylinders, which were bought from Air Liquide (Paris, France). Gas purity was higher than 99,999%, being this a crucial parameter for the reaction, which is inhibited by oxygen presence.

Table 31. List of solvents used for the particle synthesis

Short name	IUPAC name	Purity	Supplier
GLY	Propane-1,2,3-triol	>99.5%	Sigma Aldrich
OCT-OH	Ethyl-2-hexanol	99%	Sigma Aldrich
HD	Hexadecane	>99%	Sigma Aldrich
ET-OH	Ethanol	>99.8%	Roth
PR-OH	Propan-1-ol	>99.9%	Sigma Aldrich

7.2.2 Particles synthesis

Synthesis of particles was achieved using the same setup of the cationic synthesis. An homogeneous formulation containing single monomer or their mixture with appropriate solvents was poured into a flask connected to a gas driven nozzle. Gas carrier was nitrogen, supplied at different pressures. The atomized solution flowed through the aerosol photo-reactor where two UV-light sources, each containing three UV lamps, provided the necessary radiation intensity.

Many formulations were tested in order to produce both porous particles and capsules. Different ratios between the mono-functional monomer and cross-linker were used in order to access the impact of crosslinking density on the structure. Higher crosslinking densities, in fact, might hinder mobility of the structure during production of different morphologies. Both bi-functional and tri-functional cross-linkers were adopted to study impact of the functionality number on the ability to obtain a certain structure.

HD and OCT-OH were used as main solvents to study phase separation. Their remarkably different chemical nature was used to access whether a polar or a non-polar solvent was able to induce a controlled phase separation.

As to the production of capsules, differently from cationic mechanism, radical polymerization was not controlled by addition of a reaction interacting solvent. Instead, glycerol (GLY) was added in some formulations as a soft maker (Akgün *et al.*, 2014b). To obtain an initial homogeneous solution, a further solvent was added. Two solvents were adopted for this purpose: ethanol and 1-propanol. Thus, capsules structuring was pursued acting on phase separation of plasticized material and evaporation of volatile

solvents (Akgün *et al.*, 2014b). An overview of the formulations used during synthesis is provided in Table 32.

Table 32. List and recipes of the main formulation sprayed. values represent weight percentage. Ethanol and propanol were added to obtain homogeneity; therefore, their amount was not fixed.

Sample	BA	HDDA	TMPTA	TMPETA	HD	OCT-OH	GLY	ET-OH	PR-OH
R1		100							
R2	50	50							
R3	75	25							
R4	80	20							
R5	80		20						
R6	80			20					
R7	40	10				50			
R8	40	10			50				
R9	48	12			40				
R10	45	15			40				
R11		50			50				
R12		50			45		5		
R13	56		14			30			
R14	47		23			30			
R15	56			14		30			
R16	47			23		30			
R17	40	10			40		10		
R18	37	13			40		10		
R19	50.5	12.5			27		10		X
R20	50.5	12.5				27	10		X
R21	50.5	12.5				27	10	X	
R22	50.5	12.5				17	20		X
R23	47	16				17	20		X
R24	56		14			30		X	
R25	52.6		13.2			28.2	6	X	
R26	50.5		12.5			17	20	X	
R27	50			12.5		27.5	10	X	
R28	50			12.5		17.5	20	X	
R29	50			12.5		17.5	20		X

7.3 Results

7.3.1 Dimension and morphology

As first test, solid full particles were produced using different monomer mixtures. This was useful in order to verify the possibility to copolymerize entirely the mixtures within the mean residence time in the photo-reactor. PI amount was held constant at 1% (w/w). Experiments with pristine BA and 1% PI did not produce any proper material, probably due to a low reaction rate of the mono-functional monomer. Therefore, BA was used only in mixture with HDDA, TMPTA and TMPETA. In Figure 91, some of the results obtained in this study are shown. All productions were carried out using nitrogen overpressure of 1 bar.

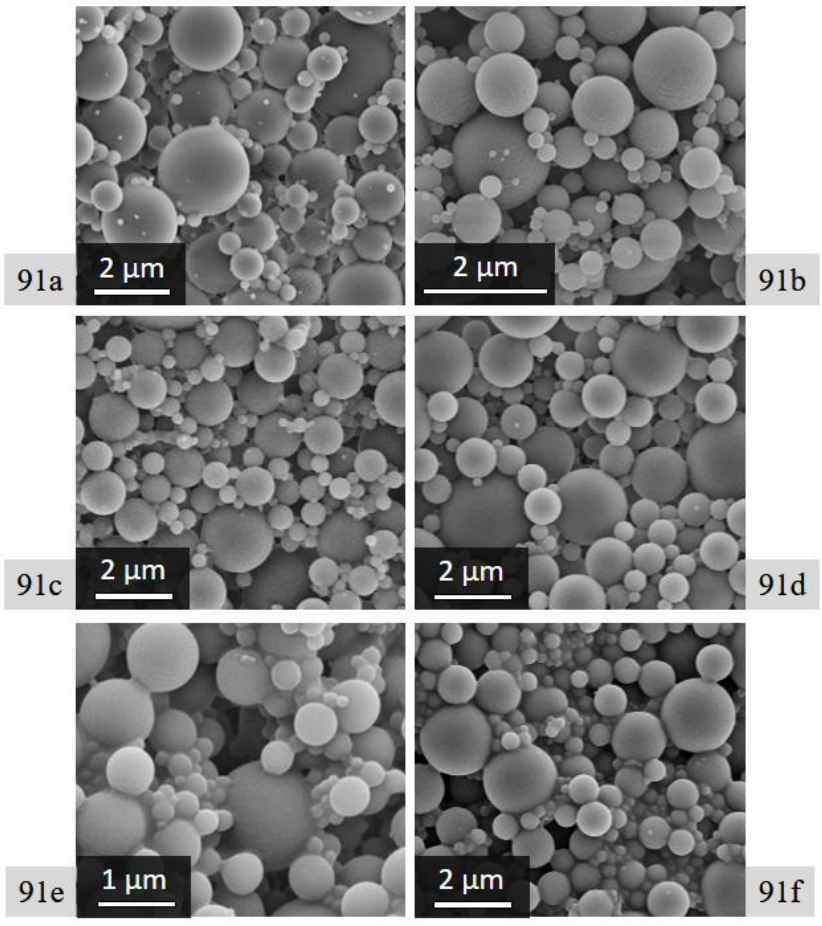

Figure 91. FESEM images of samples prepared with different formulations: (a) R1, (b) R2, (c) R3, (d) R4, (e) R5 and (f) R6.

HDDA was tested as model monomer in order to verify its ability to produce particles when used alone, see Figure 91a. In the following three experiments, HDDA fraction was decreased and BA fraction increased up to 80% (w/w). All tested formulations proved to be suitable for production of solid particles, thus confirming that 20% (w/w) HDDA was enough to obtain distinct non-sticky particles during reactor passage. Moreover, the average size did not significantly change varying monomers ratio.

Tri-functional monomers were also tested in combination with BA. The first one, TMPTA, had a rather low molecular weight and was characterized by functionalities close one another. The second one, TMPETA, was a bigger molecule with MW around 430. Therefore, functionalities were not so close one another and, thus, it was characterized by the production of more flexible materials, with a lower T_g values (Kim *et al.*, 2004). Ratio between the two monomers was held constant at 1:4.

7.3.1.1 Formulation design for the production of porous particles

Once solid particles were prepared, using monomers mixture and 1% (w/w) PI, the study was focused on the production of porous particles. The first experiments were carried out using HD or OCT-OH as solvents. HDDA-BA 1:4 mixture was tested. In Figure 92, results of this preliminary study are shown.

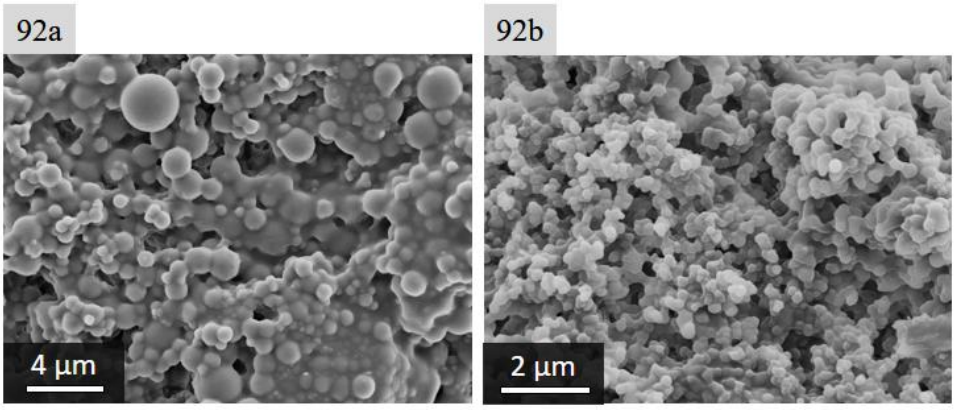

Figure 92. FESEM images of particles obtained formulation (a) R7 and (b) R8.

The particle morphologies observed were significantly different varying the starting formulation. Samples prepared with 50% (w/w) alcohol were sticky and particles appeared merged one into the other, with few distinct particles. However, no porosity could be observed in the sample, see Figure 92a. On the other hand, material prepared with HD appeared in form of small polymer domains weakly attached one another. This situation was similar to the one seen in cationic photo-polymerization when the amount of 2-octanone was too high. Therefore, it might have been caused by a high solvation

effect of hexadecane on the growing copolymer. In must be noticed, in fact, that the monomers involved in the reaction were rather non-polar and could be dissolved in HD.

For these reasons, HD was selected as a promising solvent for phase separation. Further experiments were carried out using different monomer ratios in order to increase crosslinking during reaction and, thus, inducing phase separation in an earlier stage of the process. HDDA amount was then increased and TMPTA/TMPETA were also adopted. In some experiments, solvent amount was lowered in order to facilitate phase separation. In Figure 93, examples of results obtained with HDDA and BA are shown.

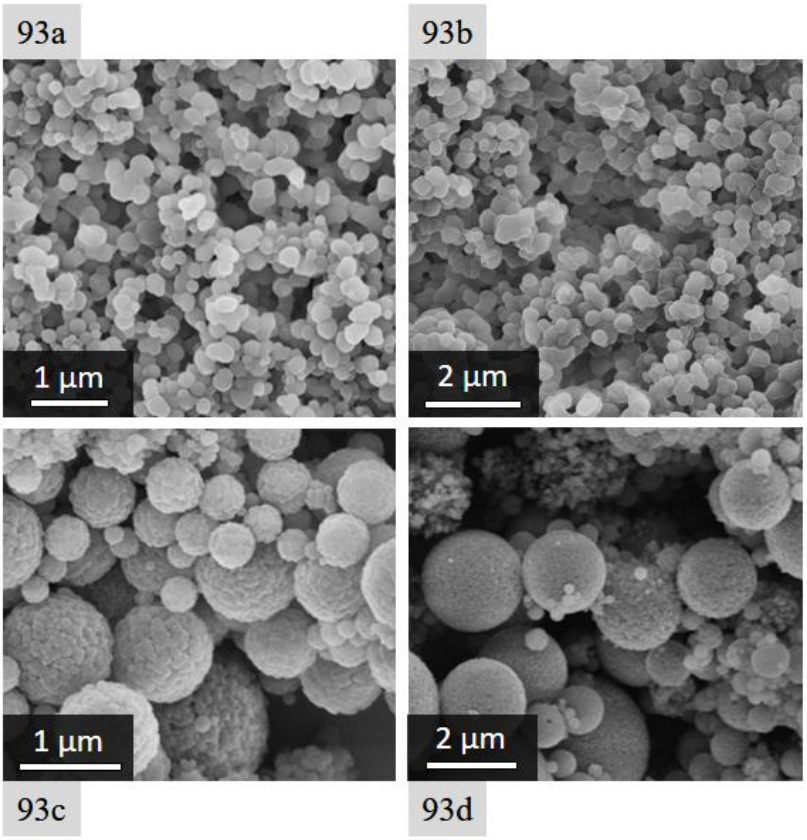

Figure 93. FESEM images of particles obtained with formulation (a) R9, (b) R10, (c) R11 and (d) R12.

The sample prepared with a 4:1 mixture of BA and HDDA, see Figure 93a, did not show any porous structure. The material consisted of small polymeric domain with submicron size. Some of them appeared agglomerate to form clusters with no specific shapes. Apparently, monomer increase from 50% up to 60% (R8 to R9) did not cause any significant improvements in phase separation and each droplet generated many small domains. To increase phase separation, the amount of HDDA was increased up to one fourth of the total monomer amount (R10). Unfortunately, this change did not improve the synthesis from a morphology point of view, see Figure 93b. Probably, presence of BA

in such amount lowered crosslinking density and hindered phase separation. Therefore, pristine HDDA was adopted for porous particles production. HD was used as main solvent while, in formulation R12, 5% of glycerol was added as soft-maker.

Both productions with formulations R11 and R12 appeared successful in obtaining porous material. Porous particles with average size slightly below 1 μm were present in sample obtained from R11. Relatively big domains of polymer material attached one another formed the particles. On the other hand, sample prepared with formulation R12 showed a higher average size, significantly above 1 μm. This was probably due to a higher solution viscosity caused by the presence of glycerol. In contrast, average size of the polymeric domains that formed the spherical particles appeared smaller. In Figure 94 a high magnification FESEM image of a particle of sample R12 is shown. Small domains could easily be seen on the surface of the particle.

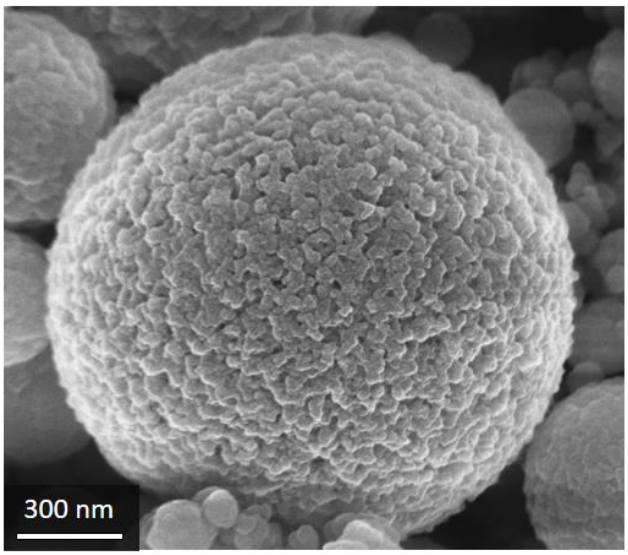

Figure 94. FESEM image at high magnification of a porous particle obtained with formulation R12.

Once HDDA has been carefully studied for production of porous particles and the experimental evidence showed the impossibility to obtain porous spherical particles with BA/HDDA blends, the focus shifted towards monomers with a higher number of functionalities. TMPTA and TMPETA were tested along with BA in different ratios in order to produce porous particles. Examples of results obtained with TMPTA are shown in Figure 95.

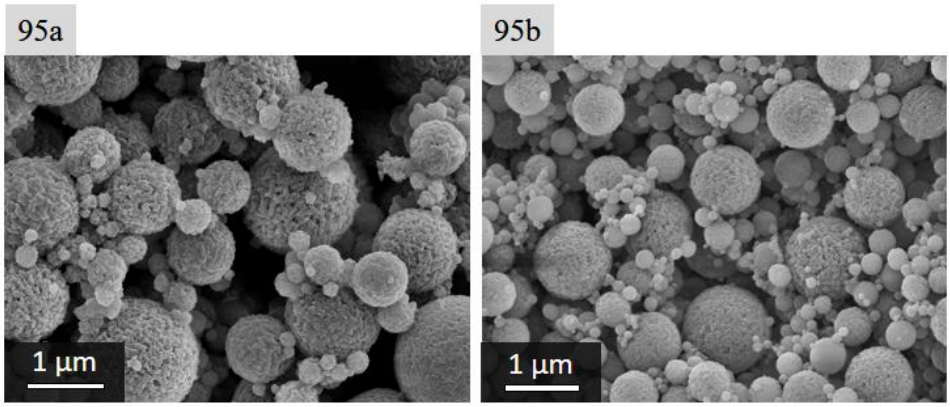

Figure 95. FESEM images of particles obtained with formulation (a) R13 and (b) R14.

Samples were produced initially with a 1:4 ratio between TMPTA and BA, see Figure 95a. The solvent used was OCT-OH since it proved to be more suitable for solvation of the tri-functional monomer. Particles appeared spherical and porosity could be observed on their surface, indicating a good phase separation during reaction. TMPTA led to the production of porous particles also in low amount, while HDDA was not able to produce distinct spherical porous material. This was probably due to the higher crosslinking capability of TMPTA with respect to the bi-functional monomer. A production with higher TMPTA amount was carried out in order to see if a different morphology could be obtained, see Figure 95b. The higher amount of TMPTA did not lead to a significantly different morphology.

The other tri-functional monomer (TMPETA) was also tested to access the impact of molecule mobility and MW on the outcome of the reaction, see Figure 96.

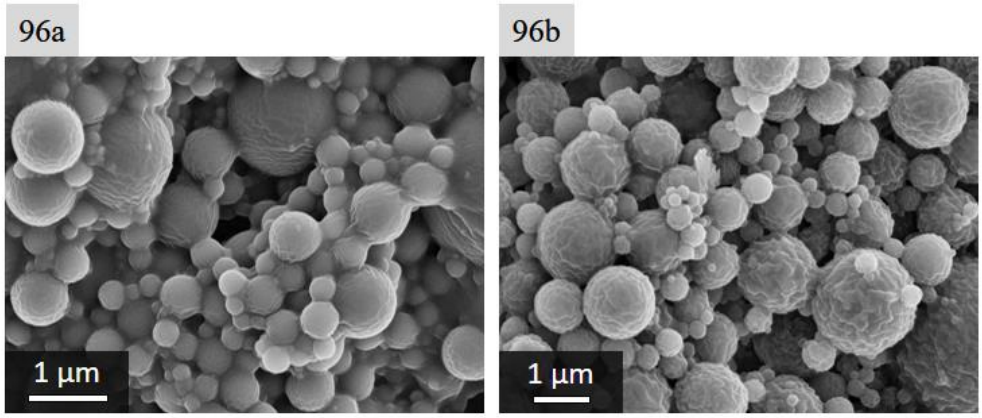

Figure 96. FESEM images of particles obtained with formulation (a) R15 and (b) R16.

Sample prepared with 1:4 ratio between TMPETA and BA appeared as solid particles without surface porosity. Moreover, many particles were attached one another.

The longer and more flexible structure of TMPETA, with respect to TMPTA, might have caused a lower crosslinking density, thus hindering phase separation. Furthermore, side chains of TMPETA are rather polar and could easily be solvated by OCT-OH.

To solve these problems, a production with higher amount of TMPETA was carried out, see Figure 96b. A monomer ratio of 1:3 was not sufficient to cause phase separation during reactor passage. On the other hand, both these two samples were characterized by the presence of superficial roughness. This could be due to the production of a polymeric network that entrapped the solvent within its structure. When evaporation took place, in the FESEM chamber, superficial collapses caused the roughness to appear.

7.3.1.2 Formulation design for the production of capsules

Caps structures, resembling collapsed thin shells have already been produced by radical photo-induced polymerization (Akgün *et al.*, 2014b). In this part of the study, attention was initially focused on production of similar structures with these new monomers and, then, focus shifted towards production of mechanically stable capsules with no collapsing structures.

In all productions, glycerol was added as soft maker in order to maintain a more flexible structure during polymerization, thus helping the production a polymeric shell. With respect to the cationic mechanism, in fact, radical propagation was not controlled by any solvent addition. Growing material was only plasticized by glycerol addition. This has been done because the polymeric structure in this case was rather different. In cationic polymerization, DVE3 constituted the entire polymeric material which, therefore, had a high crosslinking density. In the experiments on radical polymerization, on the other hand, a mixture of mono-functional monomer and cross-linker was used. Thus, crosslinking density was, in general, much lower and a soft maker was sufficient to increase mobility of polymeric molecules. The presence of glycerol, however, led to a poor miscibility of the system. This problem was tackled by adding a further low MW solvent until a homogeneous mixture was achieved. Two different solvents were tested for this purpose: ethanol and 1-propanol.

At first, HDDA-BA mixture was tested in order to obtain caps structures, see Figure 97. In the first two experiments, see Figure 97a and 97b, the total monomer amount was fixed at 50% (w/w), while monomer ratio was varied. The main solvent was hexadecane and 10% (w/w) of glycerol was added. Samples prepared with 1:4 monomer ratio showed the presence of some caps structures as well as low dimension polymeric particles. These little particles were probably, similarly to what observed before, the outcome of a delayed phase separation, which produced multiple polymeric domains in each droplet. Caps dimension, on the other hand, was in agreement with general dimensions of the aerosol droplets, around 0.8-1.2 μm.

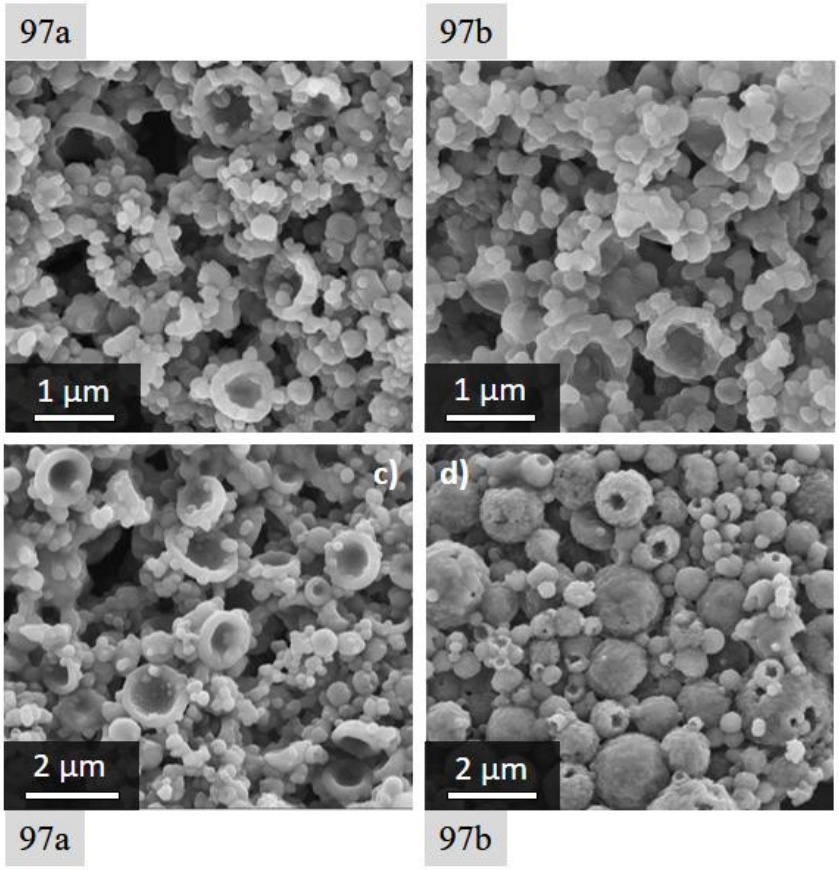

Figure 97. FESEM images of particles obtained with formulation (a) R17, (b) R18, (c) R19 and (d) R20.

In order to boost phase separation and obtain more caps structures, monomer ratio was increased up to 1:3. A higher amount of cross-linker should, indeed, help to induce phase separation earlier, thus solving the previous problem. Unfortunately, as it can be seen in Figure 97b, no significant improvement was obtained. Caps were still present with a similar frequency, while their shape was worse in terms of smoothness. Moreover, the number of agglomerated polymeric domain was similar.

Therefore, another strategy was used to improve the quality of the product. Total monomer amount was increased from 50% up to 63%, see Figure 97c. The formulation, however, did not appear homogeneous at the beginning, so it was necessary to add 1-propanol until homogeneity was reached. Using this approach, the sample appeared richer in caps, which were well defined if compared with the others obtained before. Their dimensions increased a bit, probably due to a higher viscosity of the monomer-rich formulation. The average dimension of caps shifted to 1-1.3 µm. Further experiments were carried out changing the main solvent type. Hexadecane was replaced with 2-ethylhexanol, using the same recipe in terms of monomer ratio and total amount, see

Figure 97d. In addition, in this case, 1-propanol was added to the initial solution to get homogeneity of the formulation. The outcome of the polymerization process was completely different from what previously observed. Most of particles showed a rather spherical shape, with few big holes on the surface. No collapsed caps structures were seen in this sample. The outer part of particles seemed more mechanically stable than that observed in sample prepared with HD. Probably, 2-ethylhexanol was able to subtract a fraction of glycerol and hindered its soft making features. In fact, these two molecules possess a rather similar structure and are quite miscible. On the contrary, HD and glycerol were relatively immiscible. This interesting feature of 2-ethylhexanol was exploited in the following experiments to move towards particles with polymeric shells that avoid collapse during the solvent removal.

In Figure 98a, a modification was implemented to the initial (R20) sprayed solution. 1-propanol, added as good solvent, was replaced with ethanol.

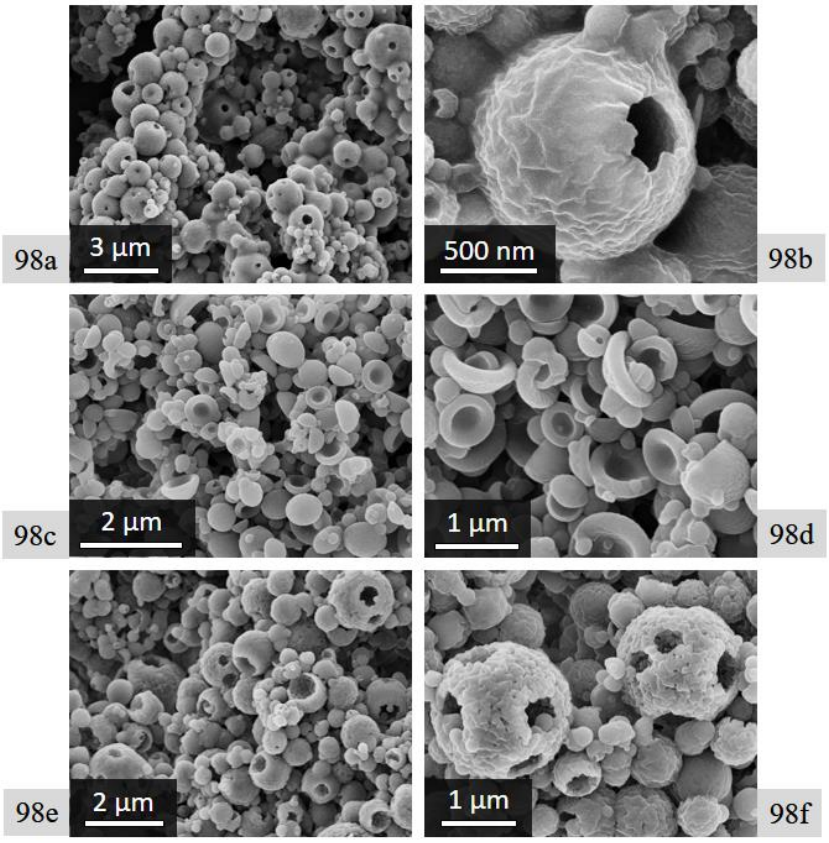

Figure 98. FESEM images of particles obtained with formulation (a) R21 and (b) relative zoom; (c) R22 and (d) relative zoom; (e) R23 and (f) relative zoom.

Ethanol was not only a better solvent for the system, thus requiring lower amounts to homogenize the solution, but it could also quickly evaporate during reactor passage, boosting phase separation.

The sample consisted of almost only spherical particles with size in the range of 1 to 2 μm. On the surface of most of the particles, holes were present, indicating a not complete production of the polymeric shell. In the zoom, see Figure 98b, a rather small spherical capsule is presented. A hole can be observed on its surface and the void core can be seen through the hole.

Maintaining the same ratio between BA and HDDA, an experiment increasing glycerol amount was carried out, see Figure 98c. Results showed that changing the ratio between 2-ethylhexanol and glycerol, production of caps structures was possible. The sample consisted of only caps particles with dimension within the range of 0.5 up to 1.2 μm, which was an excellent result. Probably, a higher amount of glycerol was strongly able to act as soft maker even in presence of 2-ethylhexanol. Therefore, collapsed capsules structures were obtained. Nonetheless, the goal was the production of mechanically stable polymeric shell. To try to tackle this problem, the ratio between the two monomers was changed by increasing the amount of cross-linker, see Figure 98e. However, the production seemed similar to the one in Figure 98a, with a mechanically stable shell which, on the other hand, was not complete. Moreover, as it was possible to see in Figure 98f, the polymeric shells appeared rather porous. Finally, although the production of caps gave excellent results, the BA-HDDA system was considered not suitable for the production of mechanically stable polymeric shells and the attention was shifted towards other types of cross-linkers.

HDDA was replaced with TMPTA or with TMPETA. As first experiment, a formulation similar to R13 was prepared but with addition of ethanol. The general idea was to exploit ethanol evaporation to create a hole within each droplet. As it can be seen in Figure 99a, sample consisted of spherical porous particles with average size below 1 μm.

In some particles, a void volume could be seen in the core, thus indicating a tendency to accumulate more polymeric material in the outer layer of the droplet during polymerization. However, it appeared that crosslinking hindered the possibility to obtain a well-defined core-shell separation. In order to help the structuring of core-shell structures, 6% (w/w) of glycerol was added to the formulation and the experiment was repeated, using ethanol as solvent, see Figure 99b. Sample particles showed the presence of a well-defined core-shell structure. Shells were made of little polymer domains slightly merged one into the other. Thus, porous shells surrounded void volumes. Most of particles observed presented one or more holes in their shells, thus indicating a non-complete shell production. The difference in morphology between these samples and the one before was attributed to glycerol presence that plasticized the forming structure, giving more time before gelation of the structure.

Glycerol amount, then, was further increased to study its effect of the morphology of particles, see Figure 99c. The particles population consisted of numerous caps with dimensions in the range from 0.3 up to 0.8 μm, and few bigger particles with spherical

shape and dimensions above 2 μm. A certain roughness was observed on the surface of these particles and, by observing one broken particle, it was possible to get an insight of their structure, see Figure 99d. The broken particle was a capsule with a ~ 0.8 μm thick polymeric shell and a void core. In particular, the polymeric shell consisted of many polymeric domains attached one another that formed a rather porous structure. These strong differences observed between little and big particles could be due to diffusion during structuring. In fact, in high dimension droplets, polymer must migrate for longer average distances and, at the same time, it reacts and phase separates. An improvement in this technique, therefore, should focus on the polydispersity of the atomized solution.

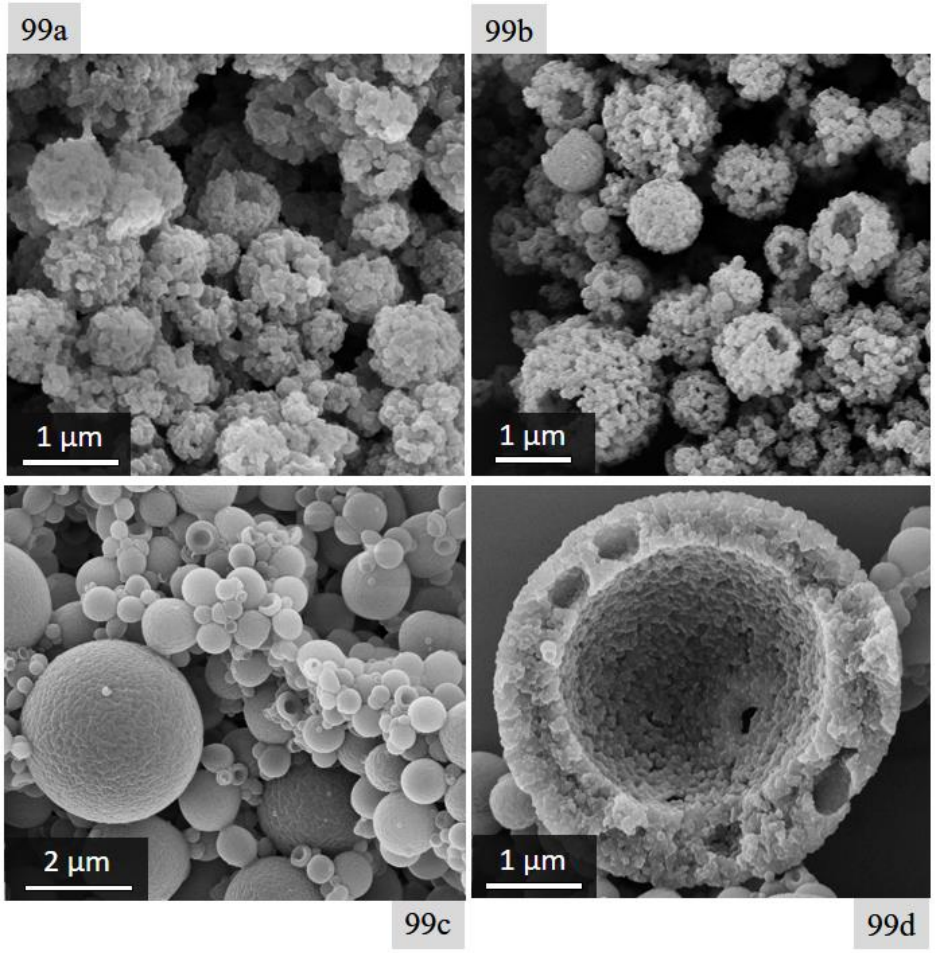

Figure 99. FESEM images of particles obtained with formulation (a) R24, (b) R25 and (c) R26. A zoom of a broken particle from sample R26 is shown in (d).

Capsules production was attempted also using TMPETA as cross-linker. Its more flexible structure seemed even better than TMPTA's one for structuring of capsules. Usually, in fact, one of the aim in capsules production is to obtain polymeric material

flexible throughout polymerization event. Therefore, TMPETA appeared a promising monomer in capsule production. Examples of material produced with TMPETA-BA system and ethanol as solvent are shown in Figure 100.

Experiments were carried out using two different amounts of glycerol as soft maker. Samples prepared with 10% (w/w) glycerol appeared made of core-shell-like structures with non-complete porous shells, see Figure 100a. Particles morphology was similar to the one observed in the optimized formulation with HDDA-BA system. A hollow inner part was surrounded by polymeric shell made of domains attached one another, thus forming a porous-like structure. Most of the particles presented holes on their surface, which made it possible to confirm the hollow structure but also indicated presence of flaws in the structuring process Glycerol amount was increased in order to produce more flexible structures during polymerization and, therefore, to promote the shell formation. An example of sample prepared with 20% (w/w) glycerol is shown in Figure 100b.

Particles, observed by means of FESEM analysis, showed the presence of a better-defined polymeric shell. Most of particles did not show, indeed, macroscopic holes on their surface but only porosity. Few particles, in particular the bigger ones, still showed imperfections and non-continuous shell. This improvement was attributed to a higher amount of glycerol which helped by plasticizing the growing polymer, thus boosting migration of polymeric domains to the outer layer of the droplet and their merging.

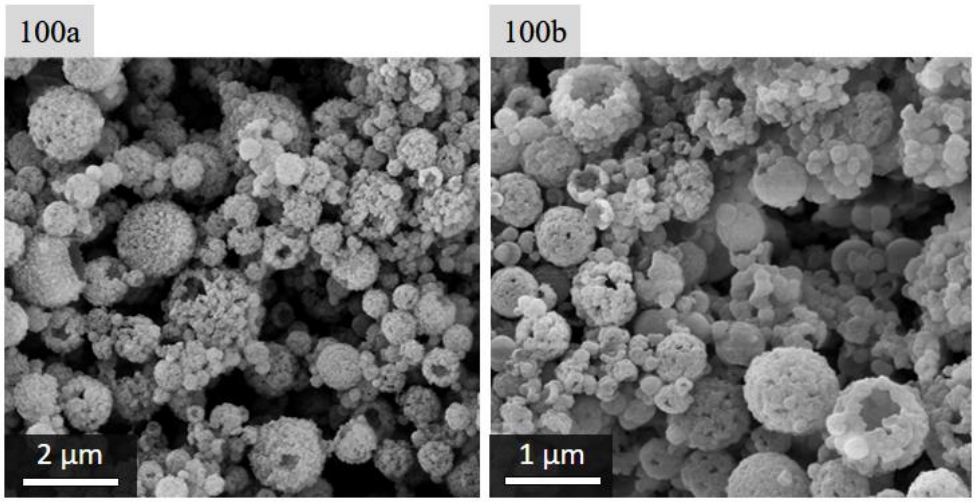

Figure 100. FESEM images of particles obtained with formulation (a) R27 and (b) R28.

1-propanol was also used in TMPETA-BA capsules production, see Figure 101. FESEM images revealed the presence of particles made of porous shells surrounding hollow cores. Shells, however, were poorly continuous, with lots of holes on their surface, thus showing the inner cavities. Glycerol was present in high quantity in the formulation used for the production, but most of particles shells appeared non-complete.

This could be due to presence of 1-propanol instead of ethanol, which, evaporating, could promote a better phase separation, therefore providing more time for shell production.

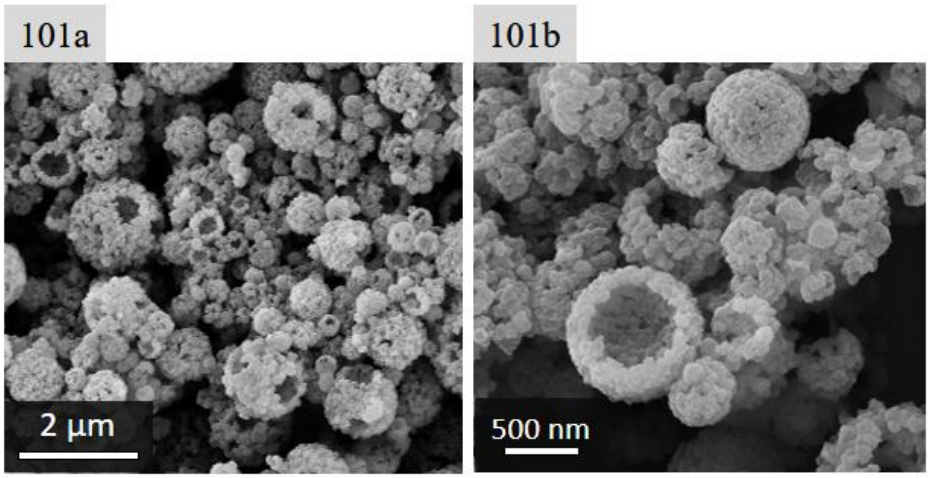

Figure 101. FESEM image of (a) particles obtained with formulation R29 and (b) high magnification scan of few hollow particles of the same sample.

In Figure 101b a high magnification FESEM image of sample prepared with 20% glycerol and using 1-propanol is provided. It could easily be seen that there were particles with holes on their surface and others with complete shell. This high magnification scan also provided an insight on the shells structure which is composed by lots of 30-50 nm polymeric domains attached one another.

7.3.2 Evaluation of monomer conversion during polymerization

Process conversion was evaluated by means of DSC analyses to verify that no monomer residues were present in the final product. Moreover, a significant part of the study was focused on the variation of monomers ratio, therefore it was necessary a proof that cross-linker amount was enough to obtain a complete monomer conversion.

As first experiments, FT-IR spectra of pure monomers were acquired, see Figure 102. In all spectra it was possible to see the presence of some characteristics peaks. Peak at ~1740 cm^{-1} is characteristic of C=O stretching, whereas peak at ~1630 cm^{-1} indicates the presence of C=C stretching. These to peaks were used to evaluate conversion during reactor passage, similarly to what has been done in the section on cationic mechanism.

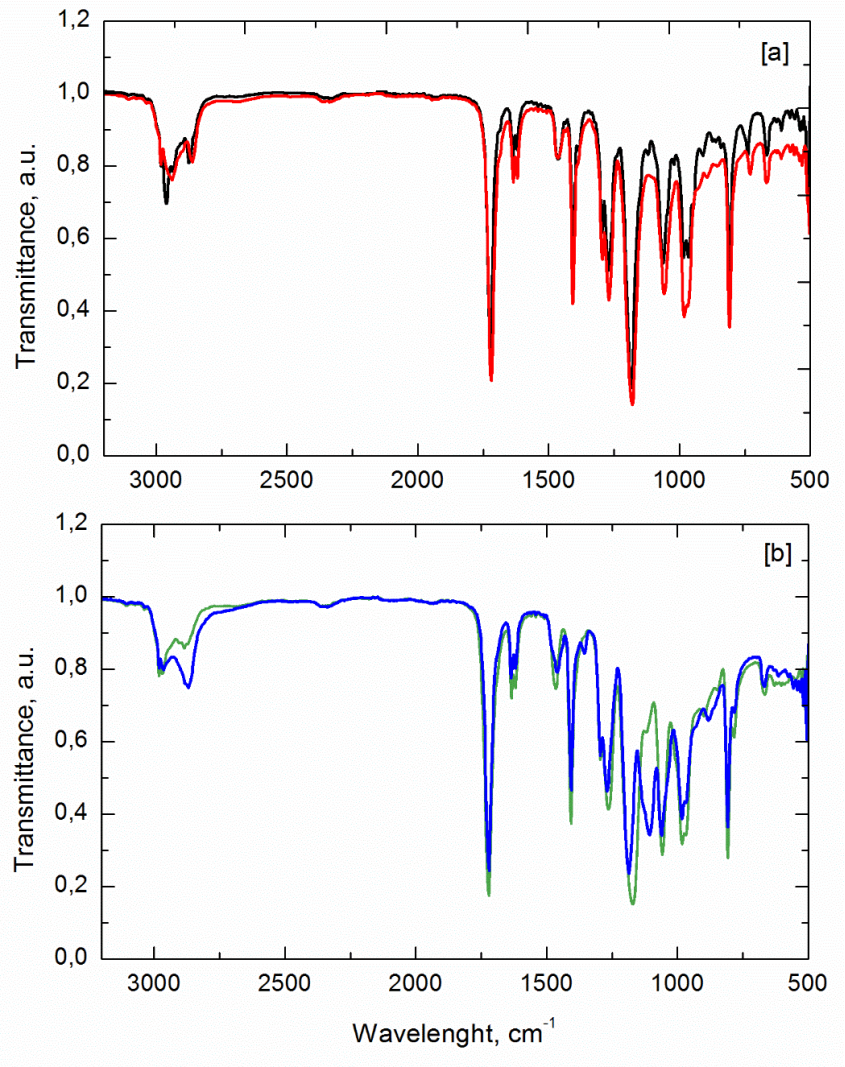

Figure 102. FT-IR spectra of (a) pure (—) BA, (—) HDDA and (b) (—) TMPTA, (—) TMPETA.

Samples were also analyzed after the reaction step to calculate monomer conversion. In Figure 103, some results obtained on mixtures of HDDA and BA with different ratios are reported.

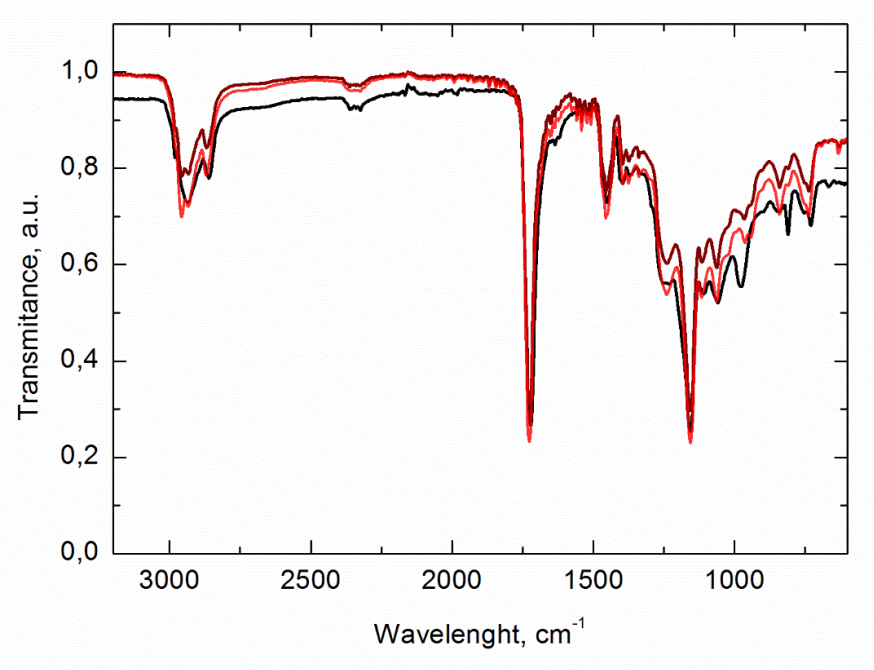

Figure 103. FT-IR spectra of particles obtained with different monomer mixtures: (—) 100% HDDA, (—) 1:1 HDDA:BA and (—) 1:4 HDDA:BA.

It could easily be seen in Figure 103 that the C=C stretching peak disappeared after reactor passage in all samples, thus confirming a complete monomer conversion.

Evaluation of monomer conversion was also carried out on samples obtained with the addition of solvents. In Figure 104 are reported FT-IR spectra on the preliminary samples for porous particles that were produced with addition of hexadecane or 2-ethylhexanol.

In both samples with HD and OCT-OH the C=C peak disappeared during reaction, thus confirming a good monomer conversion. Sample prepared with OCT-OH still showed the characteristic broad peak of the OH group at ~3400 cm^{-1}. These results pointed out that, even if particles seemed sticky, especially in case of OCT-OH presence, see Figure 92a, the monomer was fully converted.

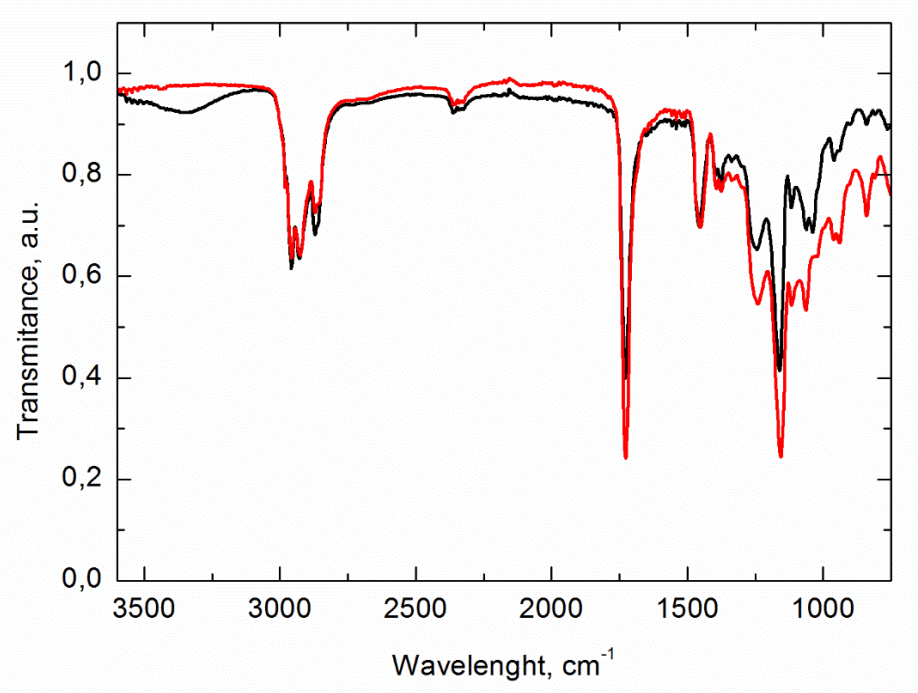

Figure 104. FT-IR spectra of particles obtained with 10% HDDA – 40% BA and different solvent: (—) 50% OCT-OH and (—) 50% HD.

FT-IR evaluation was carried out also on other samples of porous particles obtained with the HDDA-BA monomeric system, see Figure 105. Samples produced with HDDA-BA mixtures, R9 and R10, showed the absence of the C=C peak and were, therefore, completely polymerized. On the other hand, samples prepared with 100% HDDA, R11 and R12, showed the presence of a small lump at ~1640 cm^{-1}, partially overlapped with the intense C=O peak at ~1740 cm^{-1}. This suggested the presence of a small amount of non-reacted monomer, which happens quite frequently in gelified systems, in which monomer diffusion is hindered. Although it was difficult to evaluate the exact conversion, since there was overlapping of the two peaks, a preliminary evaluation decoupling the two peaks gave a 94-95% of conversion, which was still very high.

In Figure 106 are provided two examples of FT-IR spectra of samples with caps or capsules structure. In both samples it could be seen the presence of the OH broad peak given by the presence of glycerol, ethanol or propanol and, in sample R21, 2-ethylhexanol. The higher intensity of the OH peak in sample R19 might be because of ethanol evaporation in sample R21, while propanol in R19 did not evaporate completely. C=C residual peak is very low in both samples and it can be seen on the side of the intense C=O peak.

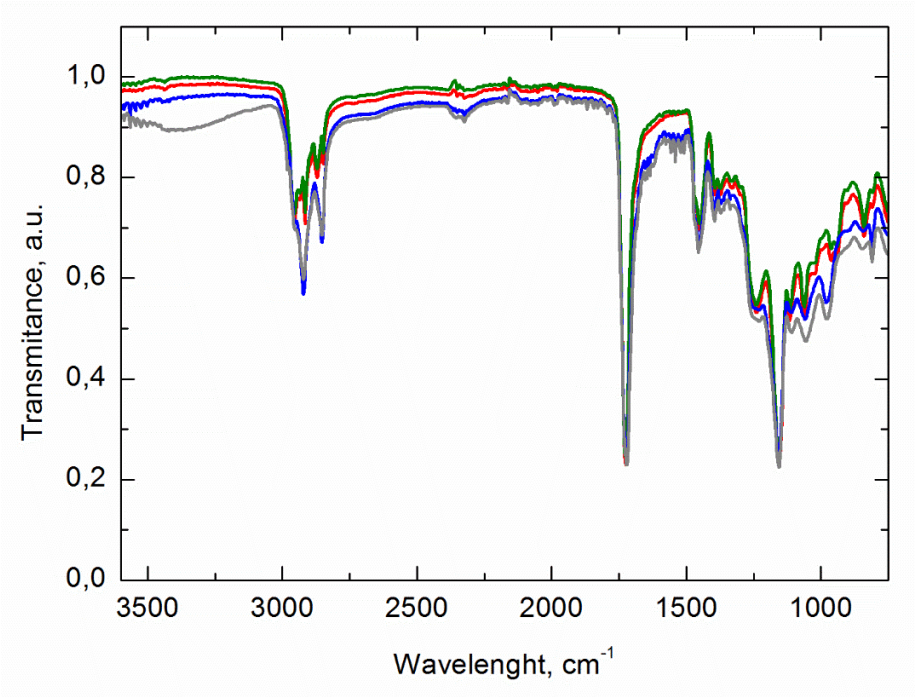

Figure 105. FT-IR spectra of particles obtained with different monomer mixtures: (—) R9, (—) R10, (—) R11 and (—) R12.

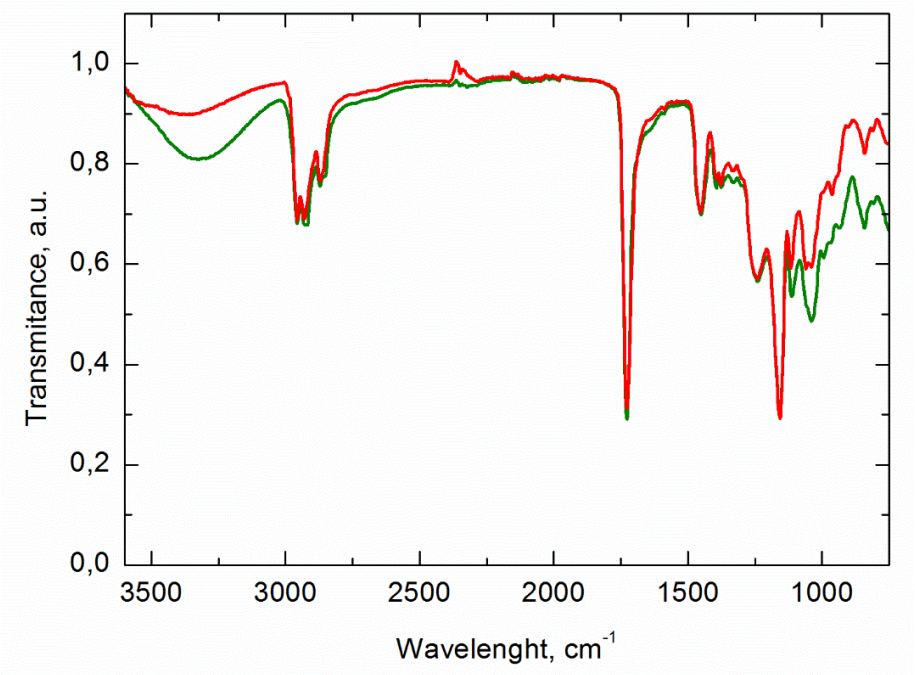

Figure 106. FT-IR spectra of particles obtained with different monomer mixtures: (—) R19, (—) R21.

Productions with TMPETA and BA were analyzed with FT-IR and an example is given in Figure 107. Results of samples consisting of core-shell structures with a porous polymeric shell confirmed that a good monomer conversion was achieved. A small lump on the C=O peak side was detected, indicating a little C=C peak, but monomer conversion was still higher than 95% in all samples. OH broad peak was detected in these samples and it was caused by glycerol, 2-ethylhexanol and, alternatively, ethanol or propanol.

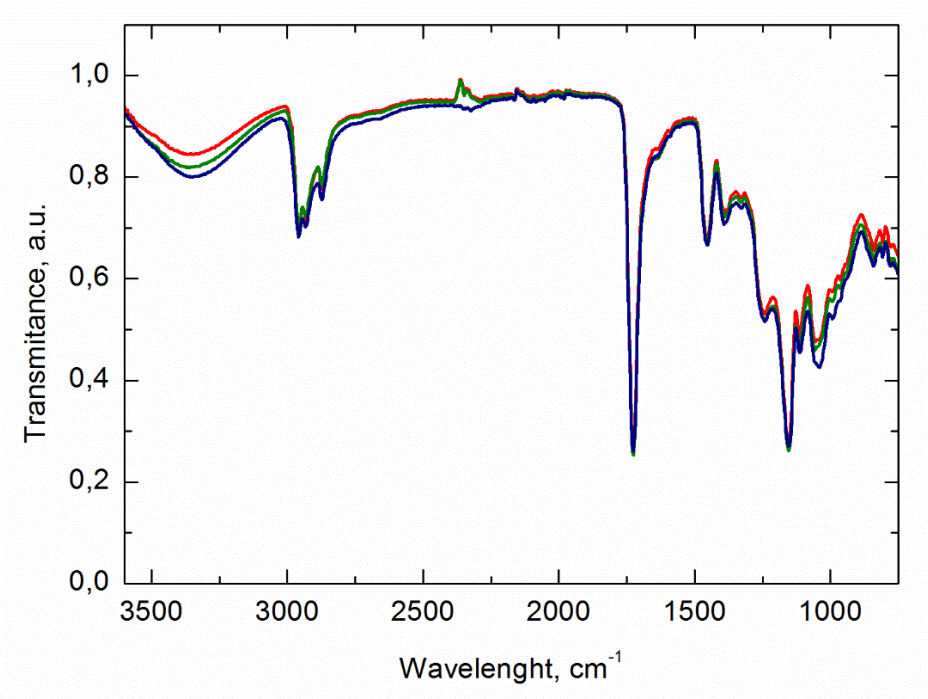

Figure 107. FT-IR spectra of particles obtained with different monomer mixtures: (—) R27, (—) R28 and (—) R29.

All evaluated monomer conversions of samples are reported in Table 33.

Table 33. The monomer conversion for the various aerosol polymerization tests carried out.

Sample	C=C conversion, %	Sample	C=C conversion, %
R1	96	R16	98
R2	98	R17	98
R3	99	R18	98
R4	98	R19	97
R5	98	R20	99
R6	99	R21	98
R7	97	R22	99
R8	98	R23	97
R9	99	R24	98
R10	99	R25	97
R11	94	R26	97
R12	95	R27	97
R13	99	R28	98
R14	98	R29	98
R15	98		

It can be easily seen that almost complete conversion was obtained in most of the samples. The only samples that showed a slightly lower conversion were the ones obtained with high amounts of cross-linker and low amount, or zero, mono-functional monomer.

7.4 Conclusions

Radical polymerization mechanism was studied to produce microparticles with a designed and well-defined structure. The initial formulation was atomized and polymerization was then triggered by UV-light during photo-reactor passage. A controlled phase separation was induced in order to obtain different structures.

Different formulations were tested, using various solvents as phase separators or as soft maker. Recipes were optimized and many types of particles were produced: porous particles, caps, capsules with a porous shell. In particular, it was the first time that polymeric porous shell particles were synthetized in an aerosol photo-reactor. Moreover, properties of the obtained material were varied by changing the ratio between monomer and cross-linker. Therefore, samples were produced with quite heterogeneous features in terms of thermal behavior and this can be exploited in many application fields, making this technique interesting for various uses.

In addition, reaction process proved to be fast enough to obtain a fully cured material during reactor passage. This was almost independent of the type of formulation that was used.

Chapter 8

General conclusions

In this work, two different polymerization techniques for the production of micro and nanoparticles were studied: miniemulsion and aerosol polymerization. Both techniques were developed in order to fit the purposes of this project, namely the production of particles with peculiar structures, able to be adopted as drug releasing devices. Reaction triggering was induced by UV-light exposure using photo-initiator compounds. They are able to decompose upon UV exposure, thus forming reactive species. This type of triggering is interesting for its low energy consumption and the possibility to obtain a fully cured material within few minutes or, in some cases, even seconds. Radical and cationic reaction mechanisms were investigated and applied to both miniemulsion and aerosol polymerization. Advantages and drawbacks of each polymerization mechanism were identified and exploited to obtain the best outcome in terms of product morphology.

Miniemulsion was developed in order to obtain capsules with a liquid core in which an active ingredient could be solubilized. Miniemulsion of oil-in-water was prepared, applying mechanical stirring followed by ultrasounds, and droplets were used as templates on which polymeric shells were grown. In order to limit the reaction within a confined area, namely droplets surface, PI and monomers were solubilized in two different phases. Therefore, the reaction could be triggered only at the oil-water interface and the technique was called interfacial miniemulsion polymerization.

Synthesis was optimized upon both its formulation and process performances. Formulations with different amounts and types of surfactants were tested as well as various amounts of dispersed phase. Process parameters whose impact was studied were two: time of ultrasounds and UV exposure time. The latter was found to have a small impact within a certain range in which the reaction of droplets coverage is completed and the further reaction of crosslinking between shells of different capsules has not started yet. On the other hand, time of ultrasounds application was found to have a strong impact for short time intervals, while for longer exposure times the effect was negligible. Moreover, in the case of radical polymerization mechanism, different monomers were tested, both with one and two functionalities. Finally, co-polymerization was achieved in order to gain control over the properties of the polymeric shells. During synthesis of nanocapsules by interfacial miniemulsion polymerization, an active ingredient was encapsulated and its release kinetics was studied under controlled conditions. Release profiles confirmed the possibility, to some extent, to design release properties of the shell by changing monomers ratio in the synthesis process.

Miniemulsion polymerization was found to be interesting under many aspects, in particular for its flexibility under different process conditions. The presence of two non-miscible phases enabled the solvation of the necessary components while keeping them separated. Therefore, structuring of nanocapsules was possible in different conditions. On the other hand, one of the major drawbacks of this technique was the production of an extremely diluted aqueous suspension and the resulting difficulties in purification of the product in those cases when water must be removed.

Aerosol photo-polymerization was studied because it is able to tackle the issues present in miniemulsion. It does not need a liquid medium/dispersant; therefore, purification of the product is rather simple if compared to liquid suspension techniques. Moreover, it usually does not need surfactant to control droplets size and this is another point of interest for systems that require high purity. Finally, aerosol technique is continuous and, thus, it is characterized by an easier scalability and control over the homogeneity of the product. As a drawback, on the other hand, it is characterized by a certain difficulty in controlling the product morphology. In this case, it is usually not possible to start reaction in an already phase separated system; therefore, structuring and reaction take place at the same time. For this reason, the study was focused on the development of monomer/solvents formulations capable of react and phase separate in order to obtain a fully cured material with a designed morphology. The process parameter to be varied was the nitrogen overpressure of the pneumatic nozzle. It is a crucial parameter for the control of droplets mean diameter and size distribution. Impact of nitrogen overpressure on both size and morphology of particles was studied and results showed that an increase in pressure led to a slightly lower mean diameter and to an improvement in monodispersity of particles population. This was a key effect since particles populations were generally really polydisperse and dimensions were higher than

the ones that could be obtained by miniemulsion polymerization. On the other hand, it did not cause any significant changes in particles morphology.

The cationic mechanism of polymerization was the first applied to aerosol polymerization and a bi-functional monomer was used. Formulations were designed for production of two main morphologies: porous particles and capsules. These two morphologies were pursued inducing a phase separation followed, in case of capsules, by a migration of the polymeric material to the outer layer of the droplet. In the first part of the work, a preliminary evaluation of transport phenomena involving oligomer molecules was carried out using MD simulations. This study pointed out the differences in diffusivity of growing oligomer molecules in various types of solvents, thus suggesting that one of the controlling mechanisms of particles structuring might be diffusion. Moreover, evidence from simulation work confirmed the presence of tunable phase separation by varying solvents ratios. With respect to the experimental work, on the other hand, formulations for porous particles production were investigated, thus studying thoroughly phase separation during reaction. It was possible to demonstrate that different porous morphologies were possible by designing an appropriate solvent mixture.

Formulations for production of polymeric capsules were developed exploiting a feature of cationic polymerization mechanism, namely the possibility to induce a chain transfer mechanism, which is capable to delay gelation of the polymeric matrix. A chain transfer reagent, such as an alcohol, was added to the formulation and it induced a lower crosslinking in the network. Thus, growing polymer was able to migrate towards the outer layer of the droplets, forming a shell. Formulations were optimized and the effects of different solvent ratios was studied. Molecular dynamics simulations were carried out in order to study the impact of formulation on compounds diffusion. Although MD could not simulate the presence of chain transfer mechanism, it gave some hints about the role that solvent ratios played on the diffusivity. Moreover, it simulated, to some extent, the behavior of the solvated molecule and how it tended to collapse on itself causing phase separation in the system. Production of microcapsules was also attempted by using a blend of two monomers, one mono-functional and the other bi-functional. The consequent decrease in functionalities should have led to a lower crosslinking and, thus, to an easier structuring. Unfortunately, the resulting lower reaction rate caused an over-delayed phase separation and this pathway was abandoned.

Particles with different morphologies were tested for drug releasing properties. Encapsulation of an active ingredient was carried out during particles production and followed by release in controlled conditions. Slight differences in release rate were observed between solid, porous particles and capsules.

As a further research work, radical mechanism was applied to aerosol polymerization, expanding a previous work, one of the first on structuring of polymeric particles obtained by aerosol technique (Akgün *et al.*, 2014b). Various monomers were used with different numbers of functionalities, ranging from one up to three. At the

beginning, porous particles were obtained with combinations of monomers. The study was then focused on the production of mechanically stable capsules. In the previous work (Akgün *et al.*, 2014b), collapsed structures, called "caps", were obtained. With a mixture of mono- and bi-functional monomers, it was possible to produce capsules that did not collapse upon solvent removal. On the other hand, using mono- and tri-functional monomers coupled with a soft maker, non-collapsing capsules with porous shells were obtained. Both these two structures were actually not flawless, presenting holes in the shells, results of a non-complete shell production. However, the morphology was improved modifying the initial formulation.

This work, whose aim was the development of two rather conceptually different ways to produce structured polymeric particles, led to the design of materials with quite similar characteristics. Pros of miniemulsion were exploited in order to produce monodisperse populations of nanocapsules and to encapsulate an active ingredient. Design of nanocapsules dimensions was successful within a certain range by varying some process parameters. Drawbacks of this technique were tackled implementing photo-polymerization in another experimental setup, namely an aerosol reactor. The produced material, in powder form, was optimized in terms of morphology and size distribution, the two main drawbacks of aerosol technique.

Abbreviations

2OCT	2-octanone
AIBN	azobisisobutyronitrile
ATR	attenuated total reflectance
BA	butyl acrylate
CFD	computational fluid dynamics
CTM	chain transfer mechanism
CTR	chain transfer reagent
DLS	dynamic light scattering
DSC	differential scanning calorimetry
DVE3	divinylether tri-ethylenglycol
EM	energy minimization
ET-OH	ethanol
FESEM	field emission scatting electron microscope
FT-IR	Fourier transform infrared miscroscopy
GLY	glicerol
HD	hexadecane
HDDA	1,6-hexanediol diacrylate
LED	light-emitting diode
MD	molecular dynamics
MP	microparticle
MSD	mean square displacement
MW	molecular weight, dalton
NP	nanoparticle

NPT	ensemble with number of atoms, pressure and temperature constant
NVT	ensemble with number of atoms, volume and temperature constant
OCT-OH	2-ethylhexanol or iso-octanol
OPLS	optimized potential for liquid simulations
OPLS-AA	optimized potential for liquid simulations – all atoms
PBS	phosphate buffer saline
PCL	poly-ε-caprolactone
PDI	polydispersity index
PEG	polyethylenglycol
PEGDA	poly(ethylene glycol) diacrylate
PEGMEMA	poly(ethylene glycol) methyl methacrylate
PI	photo-initiatior
PLA	polylactic acid
PLGA	poly(lactic-co-glycolic acid)
PROP-OH	1-propanol
PTFE	polytetrafluoroethylene
PVP	polyvinylpyrrolidone
SDS	sodium dodecyl sulfate
TAS-HFA	triarylsulfonium hexafluoroantimoniate
TEM	transmission electron microscope
TMPETA	trimethylolpropane triacrylate
TMPTA	trimethylolpropane ethoxylate triacrylate
US	ultrasounds
UV	ultraviolet
UV-vis	ultraviolet & visible spectrum

List of Symbols

Ca	capillary number, -
D	diffusivity, m^2/s
D_{max}	maximum nanocapsules diameter as evaluated from TEM analysis, nm
D_{min}	minimum nanocapsules diameter as evaluated from TEM analysis, nm
k	release parameter of the Weibull equation, -
k_B	Boltzmann constant, J/K
N	number of atoms in the simulation box, -
n	number of components in the mixture in Kendall & Monroe eq., -
N_a	total number of atoms in Kendall & Monroe eq., -
P	box pressure, bar
R	radius in Stokes-Einstein equation, m
$R_{A/K}$	alcohol/ketone ratio, -
R_g	radius of gyration, nm
$R_{K/HD}$	ketone/hexadecane ratio, -
T	absolute temperature, K
t	simulation time, s
T_g	glass transition temperature, °C
V	box volume, m^3
x_i	position of the i-esim atom in R_g definition
x_{mean}	position of the center of mass in R_g definition
y_i	mass fraction of i-esim component in Kendall & Monroe eq., -

Greek letters

α	Flory's parameter, -
η	dynamic viscosity in Stokes-Einstein equation, Pa*s
θ	release parameter of the Weibull equation, -
μ_i	dynamic viscosity of the i-esim component in Kendall & Monroe eq., Pa*s
μ_{mix}	dynamic viscosity of the mixture in Kendall & Monroe eq., Pa*s
π	pi=3,14159…
φ	fraction of active ingredient release (Weibull equation). -
Ω	shape factor, -

List of Figures

Figure 19. DLS evaluation of the nanocapsules diameter vs UV exposure time. Samples were prepared from Resin A and sonicated for 10 min. Markers refer to the mean values and error bars refer to the standard deviations.

Figure 20. DLS evaluation of nanocapsules diameter vs SDS concentration. Vertical line represent CMC of SDS in water at 25 °C. Samples were prepared with Resin A, sonicated for 10 min and exposed to UV light for 10 min. Markers refer to the mean values and error bars refer to the standard deviations.

Figure 21. The average size of the NCs (as observed by DLS) as a function of the time of sonication. Results refer to the NCs with (■) and without (○)curcumin. Samples were prepared from Resin A and irradiated for 10 minutes. Markers refer to the mean values and error bars refer to the standard deviations.

Figure 22. (a) TEM micrograph and (b) FESEM image of nanocapsules prepared with 15 min sonication, 10 min UV exposure and Resin A. The sample was prepared with curcumin.

Figure 23. Nanocapsules dimensions vs sonication time as observed by (■) DLS and (○) TEM. Samples were prepare with Resin A, using 10 min of UV exposure and curcumin in the dispersed phase. Markers refer to the mean values and error bars refer to the standard deviations.

Figure 24. Nanocapsules shape factor vs sonication time. Samples prepared with Resin A, using 10 min of UV exposure and curcumin in the dispersed phase. Markers refer to the mean values and error bars refer to the standard deviations.

Figure 25. TEM micrograph of nanocapsule prepared with 15 min sonication, 10 min UV exposure and Resin B. The sample was prepared with curcumin.

Figure 26. TEM micrograph of nanocapsule prepared with 15 min sonication, 10 min UV exposure and Resin C. The sample was prepared with curcumin.

Figure 27. The average size of the NCs (as observed by TEM) as a function of the time of sonication. Results refer to the NCs prepared with (Δ) Resin B and with (■) Resin C. Samples were irradiated for 10 minutes. Markers refer to the mean values and error bars refer to the standard deviations.

Figure 28. Nanocapsules shape factor vs sonication time. Samples prepared with Resin (♦) B and (◊) C, using 10 min of UV exposure and curcumin in the dispersed phase. Markers refer to the mean values and error bars refer to the standard deviations.

Figure 29. TEM micrograph of nanocapsule prepared with 15 min sonication, 10 min UV exposure and mixture of resins: 20% Resin A and 80% Resin B. The sample was prepared with curcumin.

Figure 30. Upper graph: nanocapsules dimensions vs percentage of Resin B as observed by TEM. Lower graph: Percent standard deviation of nanocapsules dimensions vs percentage of

Resin B. Samples were prepare with Resin A and B, using 15 min sonication, 10 min of UV exposure and curcumin in the dispersed phase.

Figure 31. The average size of the NCs (as observed by DLS) as a function of the time of sonication. With respect to Table 4 experiments: (■) M1, (Δ) M3, (▼) M5, (○) M7 and (♦) M9. Samples were irradiated for 10 minutes. Markers refer to the mean values and error bars refer to the standard deviations.

Figure 32. DSC scan of dried sample prepared with Resin A, using 15 min sonication and 10 min UV exposure.

Figure 33. Release curves with nanocapsules obtained from different resins: (■) 100% Resin A, (●) 50% Resin A and 50% resin B, (◊) 100% Resin B. Samples obtained with 15 min sonication and 10 min UV exposure. Markers refer to the mean values and error bars refer to the standard deviations.

Figure 34. Diameter of nanocapsules, as evaluated with (♦) DLS and (■) TEM, according to hexadecane amount. Samples prepared with 15 min sonication time and 10 min UV exposure. Markers refer to the mean values and error bars refer to the standard deviations.

Figure 35. (a)TEM micrograph and (b) FESEM image of nanocapsule prepared with 15 min sonication and 10 min UV exposure.

Figure 36. Diameter of nanocapsules, as evaluated with (♦) DLS and (▲) TEM, according to sonication time. Samples prepared with 10 min UV exposure. Markers refer to the mean values and error bars refer to the standard deviations.

Figure 37. DSC scan of sample prepared with DVE3, using 15 min sonication time and 10 min UV exposure time. Transformations are highlighted in the graph.

Figure 38. Schematics of molecules building.

Figure 39. Example of result from Gromacs' *msd* calculation.

Figure 40. Example of R_g dynamic during simulation time.

Figure 41. Radius of gyration vs. oligomer MW and the formulation type: (▼) S4, (▲) S3, (●) S2 and (■) S1. Markers refer to mean values and error bars to standard deviations.

Figure 42. A values vs. solvent ratio. Markers refer to mean values and error bars to standard deviations.

Figure 43. Comparison between α and relative morphologies: (a) S1, (b) S2, (c) S3 and (d) S4.

Figure 44. Diffusivity of oligomers vs. formulation solvents ratio and their molecular weight: (■) 808, (●) 1616, (▲) 3232 and (▼) 6464 Daltons. Markers refer to mean values and error bars to standard deviations.

Figure 45. (a) Radius of gyration vs. oligomer MW and formulation type: (■) S3, (▼) S5 and (▲) S7. (b) α according to monomer concentration. Markers refer to mean values and error bars to standard deviations.

Figure 46. (a) Viscosity vs. monomer concentration. (b) Diffusivity of oligomers according to monomer concentration and MW: (■) 800, (▼) 1600, (▲) 3200 and (●) 6400 Daltons. Markers refer to mean values and error bars to standard deviations.

Figure 47. FESEM images of particles obtained using $R_{K/HD}$=1, with (a) 70% and (b) 60% monomer.

Figure 48. (a) Radius of gyration Radius of gyration vs. oligomer MW and formulation type: (▲) S8, (■) S9 and (●) S10. (b) α vs. solvents ratio. Markers refer to mean values and error bars to standard deviations.

Figure 49. Comparison between α and relative morphologies. Samples prepared using formulation (a) S8, (b) S9 and (c) S10.

Figure 50. Diffusivity of oligomers vs. $R_{A/K}$ in the formulation and molecular weight: (■) 800, (▼) 1600, (▲) 3200 and (●) 6400 Daltons. Markers refer to mean values and error bars to standard deviations.

Figure 51. (a) Radius of gyration vs. oligomer MW and formulation type: (■) S10, (▲) 11 and (●) S12. (b) α vs. solvents ratio. Markers refer to mean values and error bars to standard deviations.

Figure 52. Comparison between α and relative morphologies. Samples prepared using formulation (a) S10 and (b) S12.

Figure 53. Diffusivity of oligomers vs. $R_{K/HD}$ in the formulation and molecular weight: (■) 800, (▼) 1600, (▲) 3200 and (●) 6400 Daltons. Markers refer to mean values and error bars to standard deviations.

Figure 54. Comparison between (■) R_g and (●) MSD method for diffusivity calculation. Diffusivities of the 6400 dalton MW oligomer are reported according to $R_{K/HD}$ in case of porous particles. Markers refer to mean values and error bars to standard deviations.

Figure 55. Comparison between (■) R_g and (●) MSD method for diffusivity calculation. Diffusivities of the 6400 dalton MW oligomer are reported according to $R_{A/K}$ in case of capsules. Markers refer to mean values and error bars to standard deviations.

Figure 71. FESEM images of samples prepared with formulation (a) C19 and (b) C20. All scale bars refer to 1 µm.

Figure 72. FESEM images of samples prepared with formulation (a) C21, (b) C22, (c) C23 and (d) C24. All scale bars refer to 2 µm.

Figure 73. FESEM images of particles obtained using 80% of DVE3 and 20% of (a) VE2 and (b) EHVE. All scale bar refer to 2 µm.

Figure 74. Size distribution of samples obtained using 80% of DVE3 and 20% of (---) VE2 and (—) EHVE.

Figure 75. FESEM images of samples prepared with formulation (a) CP3 and (b) CP4. Scale bars refer to 2 µm.

Figure 76. DSC scan of samples prepared with formulation P3.

Figure 77. FT-IR spectrum of pure DVE3.

Figure 78. FT-IR spectra pure solvents: (a) hexadecane, (b) 2-octanone and (c) 2-ethylhexanol.

Figure 79. FT-IR spectra of DVE3 plus 1% PI (—) before and (—) after reactor passage.

Figure 80. FT-IR spectra of formulations with 70% DVE3 and different amounts of 2-octanone: (—) 12.5%, (—) 15%, (—) 20%, (—) 25% and (—) 30%.

Figure 81. Calibration curve for detection of 2-octanone.

Figure 82. FT-IR spectra of (—) formulation P4 and (—) polymeric material obtained in the reactor outlet.

Figure 83. FT-IR spectra of (—) formulation P7 film and of film after (—) 15 s, (—) 30 s and (—) 60 s of UV irradiation.

Figure 84. FT-IR spectrum of (---) formulation with 70% DVE3, 20% 2-octanone, 3% 2-ethylhexanol and 7% hexadecane. FT-IR spectra of reacted material at (—) 0 min, (—) 5 min, (—) 10 min, (—) 15 min and (—) 30 min after production.

Figure 85. FT-IR spectra of (---) formulation (75% DVE3 – 15% 2-octanone – 10% 2-ethylhexanol) film and of film after (—) 15 s and (—) 30 s of UV irradiation.

Figure 86. FT-IR spectra of (---) formulation C18 and (—) the relative material obtained after reactor passage.

Figure 87. FESEM images of particles produced with formulation (a) L1, (b) L2 and (c) L3. All scale bars refer to 2 µm.

Figure 105. FT-IR spectra of particles obtained with different monomer mixtures: (—) R9, (—) R10, (—) R11 and (—) R12.

Figure 106. FT-IR spectra of particles obtained with different monomer mixtures: (—) R19, (—) R21.

Figure 107. FT-IR spectra of particles obtained with different monomer mixtures: (—) R27, (—) R28 and (—) R29.

List of Tables

References

Ahlrichs, P.; Dünweg, B. (1999). Simulation of a single polymer chain in solution by combining lattice Boltzmann and molecular dynamics. J Chem Phys, 111, 8225-8239.

Akgün, E.; Hubbuch, J.; Wörner, M. (2013). Perspectives of aerosol-photopolymerization: nanoscale polymer particles. Chem Eng Sci, 101, 248-252.

Akgün, E.; Hubbuch, J.; Wörner, M. (2014a). Perspectives of aerosol-photopolymerization: organic-inorganic hybrid nanoparticles. Coll Polym Sci, 292, 1241-1247.

Akgün, E.; Hubbuch, J.; Wörner, M. (2014b). Perspectives of aerosol-photopolymerization: nanostructured polymeric particles. Macromol Mater Eng, 299, 1316-1328.

Akgün, E.; Muntean, A.; Hubbuch, J.; Wörner, M.; Sangermano, M. (2015). Cationic aerosol photopolymerization. Macrom Mat Eng, 300, 136-139.

Alder, B. J.; Wainwright, T. E. (1959). Studies in molecular dynamics. I. General method. J Chem Phys, 31, 459-466.

Allen, N. S. (1996). Photoinitiators for UV and visible curing of coatings: mechanisms and properties. J Photochem Photobiol A Chem, 100, 101-107.

Ansari, M. J.; Ahmad, S.; Kohli, K.; Ali, J.; Khar, R. K. (2005). Stability-indicating HPTLC determination of curcumin in bulk drug and pharmaceutical formulations. J Pharm Biomed Anal, 39, 132-138.

Asua, J. M. (2002). Miniemulsion polymerization. Prog Polym Sci, 27, 1283-1346.

Barzegar-Jalali, M., Adibkia, K., Valizadeh, H., Shadbad, M. R. S., Nokhodchi, A., Omidi, Y., ... & Hasan, M. (2008). Kinetic analysis of drug release from nanoparticles. J Pharm Pharmaceut Sci, 1, 167-177.

Bazzano, M.; Latorre, D.; Pisano, R.; Sangermano, M; Woerner, M. (2017). Nano-structured polymeric microparticles produced via cationic aerosol photopolymerization. J Photochem Photobiol A Chem, 346, 364-371.

Bazzano, M.; Pisano, R.; Brelstaff, J.; Spillantini, M. G.; Sidoryk-Wegrzynowicz, M.; Rizza, G.; Sangermano, M. (2016). Synthesis of polymeric nanocapsules by radical UV- activated interface- emulsion polymerization. J Polym Sci A Polym Chem, 54, 3357-3369.

Biskos, G.; Vons, V.; Yurteri, C. U.; Schmidt-Ott, A. (2008). Generation and sizing of particles for aerosol-based nanotechnology. KONA Powder Part J, 26, 13-35.

Blomberg, S.; Ostberg, S.; Harth, E.; Bosman, A. W.; Van Horn, B.; Hawker, C. J. (2002). Production of crosslinked, hollow nanoparticles by surface-initiated living free-radical polymerization. J Polym Sci A Polym Chem, 40, 1309-1320.

Brown, W. H.; Poon, T. (2014). Introduction to organic chemistry. John Wiley & Sons.

Capek, I. (2001). Microemulsion polymerization of styrene in the presence of a cationic emulsifier. Adv Colloid Interface Sci, 92, 195-233.

Carpenter, A. W.; de Lannoy, C. F.; Wiesner, M. R. (2015). Cellulose nanomaterials in water treatment technologies. Environ Sci Technol, 49, 5277-5287.

Champion, J. A.; Walker, A.; Mitragotri, S. (2008). Role of particle size in phagocytosis of polymeric microspheres. Pharm Res, 25, 1815-1821.

Chemtob, A.; Kunstler, B.; Croutxé-Barghorn, C.; Fouchard, S. (2010). Photo-induced miniemulsion polymerization. Coll Polym Sci, 288, 579-587.

Chiappone, A.; Gerbaldi, C.; Roppolo, I.; Garino, N.; Bongiovanni, R. (2015). Degradable photopolymerized thiol-based solid polymer electrolytes towards greener Li-ion batteries. Polymer, 75, 64-72.

Chicoma, D. L.; Carranza, V.; Giudici, R. (2013). Synthesis of core.shell particles of polystyrene and poly (methyl methacrylate) using emulsion photopolymerization. Macromol Symp, 324, 124-133.

Crabb, G. (1833). Universal Technological Dictionary, Or Familiar Explanation of the Terms Used in All Arts and Sciences, Containing Definitions Drawn from the Original Writers and Illustrated by Plates, Epigrams, Cuts, &c. (Vol. 1). Baldwin and Cradock.

Crivello, J. V. (1984). Cationic polymerization—iodonium and sulfonium salt photoinitiators. In Initiators—poly-reactions—optical activity. Adv Polym Sci, 62, 1-48. Springer, Berlin, Heidelberg

Decker, C. (2002). Kinetic study and new applications of UV radiation curing. Macromol Rapid Commun, 23, 1067–1093.

Dendukuri, D.; Doyle, P. S. (2009). The synthesis and assembly of polymeric microparticles using microfluidics. Adv Mat, 21, 4071-4086.

Dendukuri, D.; Tsoi, K.; Hatton, T. A.; Doyle, P. S. (2005). Controlled synthesis of nonspherical microparticles using microfluidics. Langmuir, 21, 2113-2116.

dos Santos Silva, M.; Cocenza, D. S.; Grillo, R.; de Melo, N. F. S.; Tonello, P. S.; de Oliveira, L. C.; Cassimiro, D. L.; Rosa, A. H.; Fraceto, L. F. (2011). Paraquat-loaded alginate/chitosan nanoparticles: preparation, characterization and soil sorption studies. J Haz Mat, 190, 366-374.

Drexler, K. E. (1986). Engines of Creation: The Coming Era of Nanotechnology.

Drexler, K. E. (1992). Nanosystems: molecular machinery, manufacturing, and computation. John Wiley & Sons, Inc.

Ebewele, R.O. (2000). Polymer Science and Technology. CRC Press, Boca Raton.

Eerikäinen, H.; Kauppinen, E. I. (2003). Preparation of polymeric nanoparticles containing corticosteroid by a novel aerosol flow reactor method. Int J Pharm, 263, 69-83.

Einstein, A. (1956). Investigations on the Theory of the Brownian Movement. Courier Corporation.

Esen, C.; Kaiser, T.; Borchers, M. A.; Schweiger, G. (1997). Synthesis of spherical microcapsules by photopolymerization in aerosols. Colloid Polym Sci, 275, 131-137.

Esen, C.; Schweiger, G. (1996). Preparation of monodisperse polymer particles by photopolymerization. J Colloid Interf Sci, 179, 276-280.

Feynman, R. P. (1960). There's plenty of room at the bottom. Engineering and science, 23, 22-36.

Flory, P. J. (1953). Principles of polymer chemistry. Cornell University Press.

Fouassier, J. P. (2012). Photoinitiators for Polymer Synthesis: Scope, Reactivity, and Efficiency. John Wiley & Sons.

Gao, Z.; Grulke, E. A.; Ray, A. K. (2007). Synthesis of monodisperse polymer microspheres by photopolymerization of microdroplets. Colloid Polym Sci, 285, 847-854.

Gaucher, G.; Asahina, K.; Wang, J.; Leroux, J-C. (2009). Effect of poly(N-vinyl-pyrrolidone)-block-poly(D,L-lactide) as coating agent on the opsonization, phagocytosis, and pharmacokinetics of biodegradable nanoparticles. Biomacr, 10, 408-416.

Gaudin, F., & Sintes-Zydowicz, N. (2008). Core–shell biocompatible polyurethane nanocapsules obtained by interfacial step polymerisation in miniemulsion. Colloids Surf A Physicochem Eng Asp, 331, 133-142.

Gelin, B. R., & Karplus, M. (1975). Sidechain torsional potentials and motion of amino acids in proteins: bovine pancreatic trypsin inhibitor. Proc Natl Acad Sci, 72, 2002-2006.

Godawat, R.; Jamadagni, S. N.; Garde, S. (2010). Unfolding of hydrophobic polymers in guanidinium chloride solutions. J Phys Chem B, 114, 2246-2254.

Hauser, E. A.; Perry, E. (1948). Emulsion Polymerization of Styrene. J Phys Chem , 52, 1175–1186.

Hirschfelder, J.; Eyring, H.; Topley, B. (1936). Reactions involving hydrogen molecules and atoms. J Chem Phys, 4, 170-177.

Hoijemberg, P. A.; Chemtob, A.; Croutxé-Barghorn, C.; Poly, J.; Braun, A. M. (2011). Radical photopolymerization in miniemulsions. Fundamental investigations and technical development. Macromol, 44, 8727-8738.

Jia, H.; Zhu, G.; Wang, P. (2003). Catalytic behaviors of enzymes attached to nanoparticles: the effect of particle mobility. Biotechnol Bioeng, 84, 406-414.

John, B.; Sachs, C. C. (1951). U.S. Patent No. 2,548,685. Washington, DC: U.S. Patent and Trademark Office.

Jorgensen, W. L.; Maxwell, D. S.; Tirado-Rives, J. (1996). Development and testing of the OPLS all-atom force field on conformational energetics and properties of organic liquids. J Am Chem Soc, 118, 11225-11236.

Kaminski, G. A.; Friesner, R. A.; Tirado-Rives, J.; Jorgensen, W. L. (2001). Evaluation and reparametrization of the OPLS-AA force field for proteins via comparison with accurate quantum chemical calculations on peptides. J Phys Chem B, 105, 6474-6487.

Karplus, M. (2003). Molecular dynamics of biological macromolecules: a brief history and perspective. Biopolymers, 68, 350-358.

Kendall, J.; Monroe, K. P. (1917). The viscosity of liquids. ii. the viscosity-composition curve for ideal liquid mixtures. 1. J Am Chem Soc, 39, 1787-1802.

Kim, S. I.; Kim, H. S.; Na, S. H.; Moon, S. I.; Kim, Y. J.; Jo, N. J. (2004). Electrochemical characteristics of TMPTA-and TMPETA-based gel polymer electrolyte. Electrochim Acta, 50, 317-321.

Kobayashi, I.; Vladisavljević, G. T.; Uemura, K.; Nakajima, M. (2011). CFD analysis of microchannel emulsification: Droplet generation process and size effect of asymmetric straight flow-through microchannels. Chem Eng Sci, 66, 5556-5565.

Kumar, S.; Bhanjana, G.; Sharma, A.; Sidhu, M. C.; Dilbaghi, N. (2014). Synthesis, characterization and on field evaluation of pesticide loaded sodium alginate nanoparticles. Carbohydr Polym, 101, 1061-1067.

Kumari, A.; Yadav, S. K.; Yadav, S. C. (2010). Biodegradable polymeric nanoparticles based drug delivery systems. Coll Surf B, 75, 1-18.

Landfester, K. (2001). The generation of nanoparticles in miniemulsions. Adv Mat, 13, 765-768.

Landfester, K. (2003). Miniemulsions for nanoparticle synthesis. Colloid chemistry II, 75-123, Springer Berlin Heidelberg.

LaVan, D. A.; Lynn, D. M.; Langer, R. (2002). Moving smaller in drug discovery and delivery. Nat Rev Drug Discov, 1, 77–84.

Levenson, M. D.; Viswanathan, N. S.; Simpson, R. A. (1982). Improving resolution in photolithography with a phase-shifting mask. IEEE Trans Electron Devices, 29, 1828-1836.

Lide, D.R. (2007). CRC Handbook of Chemistry and Physics, 88th ed. CRC Press/Taylor & Francis Group, Boca Raton (USA).

Lin, Y. H.; Chung, C. K.; Chen, C. T.; Liang, H. F.; Chen, S. C.; Sung, H. W. (2005). Preparation of nanoparticles composed of chitosan/poly-γ-glutamic acid and evaluation of their permeability through Caco-2 cells. Biomacr, 6, 1104-1112.

Liu, B.; Wang, Y.; Yang, F.; Wang, X.; Shen, H.; Cui, H.; Wu, D. (2016). Construction of a controlled-release delivery system for pesticides using biodegradable PLA-based microcapsules. Coll Surf B, 144, 38-45.

Liu, Y.; Tong, Z.; Prud'homme, R. K. (2008). Stabilized polymeric nanoparticles for controlled and efficient release of bifenthrin. Pest Manag Sci, 64, 808-812.

Luan, J.; Wang, S.; Hu, Z.; Zhang, L. (2012). Synthesis techniques, properties and applications of polymer nanocomposites. Curr Org Synth, 9, 114-136.

Metatla, N.; Soldera, A. (2006). Computation of densities, bulk moduli and glass transition temperatures of vinylic polymers from atomistic simulation. Mol Simul, 32, 1187-1193.

Minko, S. (2008). Grafting on solid surfaces:"Grafting to" and "grafting from" methods. Polymer surfaces and interfaces, 215-234. Springer Berlin Heidelberg.

Mittal, K. L. (Ed.). (2005). Polyimides and other high temperature polymers: synthesis, characterization and applications (Vol. 3). CRC Press.

Mora-Huertas, C. E.; Fessi, H.; Elaissari, A. (2010). Polymer-based nanocapsules for drug delivery. Int J Pharm, 385, 113-142.

Morales, M. E.; Gallardo, L. V.; Calpena, A. C.; Domenech, J.; Ruiz, M. A., (2004). Comparative study of morphine diffusion from sustained release polymeric suspensions. J Control Release, 95, 75-81.

Müller, M.; Smith, G. D. (2005). Phase separation in binary mixtures containing polymers: A quantitative comparison of single- chain- in- mean- field simulations and computer simulations of the corresponding multichain systems. J Polym Sci Pol Phys, 43, 934-958.

Owens, D. E.; Peppas, N. A. (2006). Opsonization, biodistribution, and pharmacokinetics of polymeric nanoparticles. Int J Pharm, 307, 93-102.

Papadopoulou, V.; Kosmidis, K.; Vlachou, M.; Macheras, P. (2006). On the use of the Weibull function for the discernment of drug release mechanisms. Int J Pharm, 309, 44–50.

Palmer, B. J. (1994). Transverse-current autocorrelation-function calculations of the shear viscosity for molecular liquids. Phys Rev E, 49, 359.

Paradossi, G.; Finelli, I.; Natali, F.; Telling, M. T.; Chiessi, E. (2011). Polymer and water dynamics in poly (vinyl alcohol)/poly (methacrylate) networks. A molecular dynamics simulation and incoherent neutron scattering investigation. Polymers, 3, 1805-1832.

Piradashvili, K.; Alexandrino, E. M.; Wurm, F. R.; Landfester, K. (2015). Reactions and polymerizations at the liquid–liquid interface. Chem Rev, 116, 2141-2169.

Prucker, O.; Schimmel, M.; Tovar, G.; Knoll, W.; Rühe, J. (1998). Microstructuring of molecularly thin polymer layers by photolithography. Adv Mat, 10, 1073-1077.

Ramisetty, K. A.; Pandit, A. B.; Gogate, P. R. (2015). Ultrasound assisted preparation of emulsion of coconut oil in water: Understanding the effect of operating parameters and comparison of reactor designs. Chem Eng Process Intensif, 88, 70-77.

Raula, J.; Eerikäinen, H.; Kauppinen, E. I. (2004). Influence of the solvent composition on the aerosol synthesis of pharmaceutical polymer nanoparticles. Int J Pharm, 284, 13-21.

Reynolds, W.B. (1949). Emulsion polymerization. J Chem Educ, 26, 135-138.

Sangermano, M. (2012). Advances in cationic photopolymerization. Pure Appl Chem, 84, 2089-2101.

Sastre, R. L.; Olmo, R.; Teijón, C.; Muñíz, E.; Teijón, J. M.; Blanco, M. D. (2007). 5-Fluorouracil plasma levels and biodegradation of subcutaneously injected drug-loaded microspheres prepared by spray-drying poly (D, L-lactide) and poly (D, L-lactide-co-glycolide) polymers. Int J Pharm, 338, 180-190.

Schork, F. J.; Luo, Y.; Smulders, W.; Russum, J. P.; Butté, A.; Fontenot, K. (2005). Miniemulsion polymerization. Adv Polym Sci, 175, 129-255.

Shaban, M.; SA, A. R.; Ahadian, M. M.; Tamsilian, Y.; Weber, A. P. (2016). Facile synthesis of cauliflower-like hydrophobically modified polyacrylamide nanospheres by aerosol-photopolymerization. Eur Polym J, 83, 323-336.

Sherrington, D.C., 1998. Preparation, structure and morphology of polymer supports. Chem Commun, 21, 2275-2286.

Sinha, V. R.; Trehan, A. (2003). Biodegradable microspheres for protein delivery. J Control Release, 90, 261–280.

Steven, L.; Mueller, F. W. (1962). U.S. Patent No. 3,050,390. Washington, DC: U.S. Patent and Trademark Office.

Tamai, T.; Watanabe, M.; Teramura, T.; Nishioka, N.; Matsukawa, K. (2009). Metal nanoparticle/polymer hybrid particles: the catalytic activity of metal nanoparticles formed on the surface of polymer particles by UV- irradiation. Macromolecular symposia, 282, 199-204. WILEY- VCH Verlag.

Tamai, Y.; Tanaka, H.; Nakanishi, K. (1996). Molecular dynamics study of polymer− water interaction in hydrogels. 1. Hydrogen-bond structure. Macromol, 29, 6750-6760.

Tønnesen, H. H. (1992). Chemistry of curcumin and curcuminoids. ACS Symposium Series, 506, 143-153.

Tønnesen, H. H.; Másson, M.; Loftsson, T. (2002). Studies of curcumin and curcuminoids. XXVII. Cyclodextrin complexation: solubility, chemical and photochemical stability. Int J Pharm, 244, 127-135.

Toumey, C. P. (2008). Reading Feynman into nanotechnology: A text for a new science. Techné: Research in Philosophy and Technology, 12, 133-168.

Tsunooka, M.; Tanaka, M. (1978). Photochemical reactions of high polymers. XVII. Micellar effect on the photopolymerization of methyl methacrylate with ferrocene-carbon tetrachloride. J Polymer Sci C: Polymer Lett, 16, 119-120.

Vadalia, H. C.; Lee, H. K.; Myerson, A. S.; Levon, K. (1994). Thermally induced phase separation in ternary crystallizable polymer solutions. J Membrane Sci, 89, 37-50.

Valavala, P. K.; Clancy, T. C.; Odegard, G. M.; Gates, T. S. (2007). Nonlinear multiscale modeling of polymer materials. Int J Solids Struct, 44, 1161-1179.

Vert, M.; Doi, Y.; Hellwich, K-H.; Hess, M.; Hodge, P.; Kubisa, P.; Rinaudo, M.; Schué, F. (2012). Terminology for biorelated polymers and applications (IUPAC Recommendations 2012). Pure Appl Chem, 84, 377-410.

Vorderbruggen, M. A.; Wu, K.; Breneman, C. M. (1996). Use of cationic aerosol photopolymerization to form silicone microbeads in the presence of molecular templates. Chem Mater, 8, 1106-1111.

Wang, Z.; Leung, M. H.; Kee, T. W.; English, D. S. (2009). The role of charge in the surfactant-assisted stabilization of the natural product curcumin. Langmuir, 26, 5520-5526.

Ye, W.; Leung, M. F.; Xin, J.; Kwong, T. L.; Lee, D. K. L.; Li, P. (2005). Novel core-shell particles with poly (n-butyl acrylate) cores and chitosan shells as an antibacterial coating for textiles. Polym, 46, 10538-10543.

Ye, W.; Xin, J. H.; Li, P.; Lee, K. L. D.; Kwong, T. L. (2006). Durable antibacterial finish on cotton fabric by using chitosan- based polymeric core- shell particles. J Appl Pol Sci, 102, 1787-1793.

Zhao, C. X. (2013). Multiphase flow microfluidics for the production of single or multiple emulsions for drug delivery. Adv Drug Deliv Rev, 65, 1420-1446.

Published works

Works published during PhD period regarding PhD topics:

Bazzano, M.; Pisano, R.; Brelstaff, J.; Spillantini, M. G.; Sidoryk-Wegrzynowicz, M.; Rizza, G.; Sangermano, M. (2016). Synthesis of polymeric nanocapsules by radical UV-activated interface-emulsion polymerization. *J Polym Sci A Polym Chem*, **54**, 3357-3369.

Bazzano, M.; Latorre, D.; Pisano, R.; Sangermano, M; Woerner, M. (2017). Nano-structured polymeric microparticles produced via cationic aerosol photopolymerization. *J Photochem Photobiol A Chem*, **346**, 364-371.

Works published during PhD period on other topics:

Bazzano, M.; Barolo, C.; Buscaino, R.; D'Agostino, G.; Ferri, A.; Sangermano, M.; Pisano, R. (2016). Controlled atmosphere in food packaging using ethylene-α-cyclodextrin inclusion complexes dispersed in photocured acrylic films. *Ind Eng Chem Res*, **55**, 579-585.

Capozzi, L.C.; Bazzano, M.; Cavallero, M.C.; Barolo, C.; Buscaino, R.; Ferri, A.; Sangermano, M.; Vallauri, D.; Pisano, R. (2016). Polymeric supports for controlled release of ethylene for food industry. *Int Polym Proc*, **31**, 570-576.

Capozzi, L.C.; Bazzano, M.; Sangermano, M.; Pisano, R. (2017). Inclusion complexes dispersed in polystyrene-based labels for fruit ripening on demand. *Int J Food Sci Tech*, DOI 10.1111/ijfs.13596.

Proceedings & conference acts:

Pisano, R.; Bazzano, M.; Capozzi, L. C.; Ferri, A.; Sangermano, M. (2015, December). Controlled release of ethylene via polymeric films for food packaging. In AIP Conference Proceedings (Vol. 1695, No. 1, p. 020009). AIP Publishing.

Bazzano, M.; Pisano, R.; Woerner, M.; Sangermano, M. (2017, April). Structured polymeric microparticles via aerosol cationic photopolymerization. ACS 253rd Meeting, San Francisco (CA).